JOURNAL OF THE GEORGIAN CERAMISTS' ASSOCIATION

INTERNATIONAL JOURNAL OF CERAMICS, COMPOSITES, SCIENCE AND ADVANCED TECHNOLOGIES

Scientific, technical and industrial illustrated, registered, referral magazine

Vol. 27. 1(53).2025

Guidelines for submitting an article to the journal

- It is necessary to submit, one hardcopy of the article, as well as an electronic versionin English language, to editorial office.

- The length of the article is not limited to pages (including tables and images with appropriate numbering). Interval 1.5. Program-Sylfaen. Font size 12, the article must be accompanied by an abstract in Georgian of no more than 300 words.

- The article should use International System of Units (SI), as well as those units that are equated to this system.

- Mathematical and chemical formulas should be clearly indicated so that the difference between Capital (upper case) and Nuskhuri (Georgian script AD 800-1100) (lower case) letters, quality coefficient and co-multiplier can be easily discerned. All letter designations in the text of the article and formula are subject to decoding. Different concepts can not be represented by the same symbol.

- The literary source should be indicated at the end of the article as follows: for a book - indicating the author, title, title of publication, place of publication, year of publication and total number of pages;

  for a journal - indicating the author of the article, the name of the journal, year of publication, volume, number, beginning and end pages of the article;

  Foreign surnames, the title of the book and journal must be in the original language without abbreviation, it is not allowed to refer to unpublished work.

- When using a copyright certificate, it is necessary to refer to the bulletin of the invention (where the formula of the invention is published) indicating the number and year of publication.

- Pictures and drawings should be presented only in text in one copy in computerized form, they should not be overloaded with details and inscriptions. The position must be indicated by numbers and decoded by inscriptions under the picture;

- The article must be signed by one of the authors. It is necessary to indicate place of work, position, scientific degree, and telephone number.

- The publishing fee for foreign authors not residing in Georgia makes up 100 euros. It's free for authors residing in Georgia.

C O N T E N T S

REDUCED ELECTRICAL CONDUCTIVITY AND OTHER THERMOELECTRIC CHARACTERISTICS OF N- Si_xGe_{1-x} ALLOY AT ROOM TEMPERATURE

G. Kakhniashvili[1], Z. Adamia[2], I. Nakhutsrishvili[1]

[1] Institute of Cybernetics of Georgian Technical University, Anjaparidze 6, 0186 Tbilisi

[2] Sukhumi State University, Politkovskaia 61, 0186 Tbilisi

E-mail: iraklinakhutsrishvili52@gmail.com

Resume: *Goal.* The paper presents data on the reduced electrical conductivity, as well as on the dependences of the concentration and mobility of charge carriers on the composition of the N-type alloy Si_xGe_{1-x}. The values of the ratio of the effective mass to the rest mass of an electron vary in the range of (0.67–1.47), and the weighted mobility – in the range of (29.6 – 112.3) $cm^2/V \cdot s$. The corresponding calculations are carried out for room temperature. The scattering parameter of charge carriers is discussed in the paper. *Method.* SiGe samples were produced by vacuum hot pressing of powders obtained from zone melting ingots. Bulk Si and Ge wastes were crushed with a steel rod and sifted through a sieve with 0.2 mm cells. Then it was loaded into the mill chamber REK PM-100 SM and crushed for 20-25 hours. The granulometric composition of the powder was estimated using a Nikon optical microscope and a DRON-3M X-ray diffractometer. *Result.* ZT can be calculated using σ'' in combination with the universal electrical conductivity (σ'): from definitions of universal and reduced electricasl conductivities it is clear that

$$\sigma''/\sigma'=(k_B/q_e)^4 B_E T/\lambda_L \cong 5.512 \cdot 10^{-17}$$
$$(ZT/B_S)[(\lambda_E/\lambda_L)+1].$$

Thus, from relation to σ''/σ' it is possible to predict the figure of merit. Note that for N-Si_xGe_{1-x} of all the studied compositions at room temperature ZT is hundredths. But at $1073°K$ $ZT \cong 0.8$. *Conclusion.* Some thermoelectric characteristics of N-type SiGe alloy were investigated. It is shown that using reduced electrical conductivity it is possible to calculate the figure of merit of a material. The values of the ratio of the effective mass to the rest mass of an electron vary in the range of (0.67–1.47), and the weighted mobility – in the range of (29.6 – 112.3) $cm^2/V \cdot s$. The calculation of the scattering parameter shows that $A \approx 3$ which means that polar scattering of optical phonons takes place

Key words: SiGe alloy, thermoelectric characteristics, room temperature.

1. INTRODUCTION

For the energy supply of humanity, along with other methods of direct energy conversion, there is the thermoelectric effect, which consists of obtaining an electric potential using a temperature difference. At present the most widely used thermoelectric materials are semiconductor compounds and alloys, in particular the system silicon-germanium. Si and Ge form an alloy that has been used in spacecraft generators since the second half

of the last century until recently [1-4]. This thermoelectric material is also used in many other areas of science and technology: coolers, sensors, thin-film transistors, batteries, solar cells, photodetectors, nuclear radiation detectors, thermal neutron monochromators and X-ray diffractometry devices [5-16].

SiGe is characterized by a fairly high electrical conductivity (σ), which increases its figure of merit $ZT=\sigma S^2 T/k$ (S – Seebeck coefficient, T – absolute temperature, $k=k_E+k_L$ – thermal conductivity, the sum of its electron and lattice components).

Specific electrical conductivity of materials depends on two main parameters – on the concentration of charge carriers (n) and their drift mobility (μ_d): $\sigma=q_e n\mu$ (q_e – elementary charge). For many alloys and compounds, the electrical conductivity differs from σ of the individual components. The electrical conductivity of materials also depends on their state. For example, at (298-300)°K for crystalline SiGe $\sigma\cong2.5\cdot10^5$ Sm·m^{-1}, for nanostructured SiGe $\cong (1.5-5)\cdot10^4$ Sm·m^{-1} [17,18], and for polycrystalline SiGe thin film $\cong 2.4\cdot10^4$ Sm·m^{-1} [19], respectively. When doping SiGe with tantalum carbide nanoparticles $\sigma\cong(1-2)\cdot10^5$ Sm·m^{-1} [20], for SiGe by silicon-molibdenum addition $\cong (0.6-1.8)\cdot10^5$ Sm·m^{-1} [21], and for SiGe by aurum addition$\cong 1\cdot10^5$ Sm·m^{-1} [22].

The concepts of reduced[1] electrical conductivity is introduced in the theory of thermoelectricity. Let's denote this by

σ'': $\sigma''=(k_B/q_e)^2 T\sigma/k_L\cong7.425\cdot10^{-9}\sigma T/k_L$

(k_B – Boltzmann's constant) [23]. That is, in addition to specific electrical conductivity, this also depends on other important thermoelectric parameters.

This paper presents data on the temperature dependence of the reduced electrical conductivity, as well as on the dependencies of the concentration and drift mobility of charge carriers on composition of alloy N-Si$_x$Ge$_{1-x}$[2]: x=0.7, 0.72, 0.76, 0.8 and 0.83. The calculation of the effective masses (m*) and weighted mobilities (μ_w) of electrons at room temperature was carried out.

2. MAIN PART

SiGe samples were produced by vacuum hot pressing of powders obtained from zone melting ingots. Bulk Si and Ge wastes were crushed with a steel rod and sifted through a sieve with 0.2 mm cells. Then it was loaded into the mill chamber REK PM-100 SM and crushed for 20-25 hours. The granulometric composition of the powder was estimated using a Nikon optical microscope and a DRON-3M X-ray diffractometer. The dispersed SiGe alloy powder obtained in this mode consisted of grains of constituent elements with sizes of 60-80 nm. The resulting powder was pressed in a high-temperature vacuum induction pressure chamber at temperatures of (1200-1320)°C and a pressure of 480 kg cm^{-2} for 20-30 minutes. The matrix and punches were made of high-strength graphite. Profiled samples in the form of rectangular parallelepipeds measuring 10x10x20 mm were cut out from the obtained briquettes on a diamond-disc cutting device.

For N-type conductivity, phosphorus was used as a dopant. The concentration of charge carriers was $3.2\cdot10^{20}$ cm^{-3}. Data on specific electrical and thermal conductivities are taken from [26] (σ was determined by measuring of resistivity: $\rho=1/\sigma$).

3. Results and Discussion

First, we present the typical temperature dependences of reduced electrical conductivity for n-type Si_xGe_{1-x} (Fig.1). It differs significantly from the data obtained for $P-Si_xGe_{1-x}$ [27]. In this case the temperature dependences of σ'' have the shape of a "distorted" inverted parabola i.e. have a maximum.
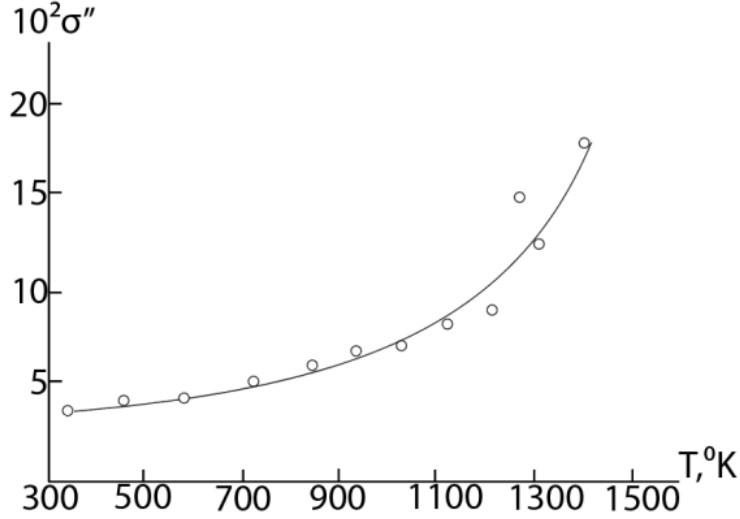
Fig. 1 Temperature dependence of σ'' for N-Si₀.₇Ge₀.₃
(For other alloy compositions, the type of dependences is the same,
only shifted in the direction of the ordinate axis.)

ZT can be calculated using σ'' in combination with the universal electrical conductivity (σ') [(3)]: from definitions of universal and reduced electricasl conductivities it is clear that

$$\sigma''/\sigma' = (k_B/q_e)^4 B_E T/k_L \cong 5.512 \cdot 10^{-17} (ZT/B_S)[(k_E/k_L)+1].$$

Thus, from relation to σ''/σ' and taking into account $k_L \approx k$ it is possible to predict of figure of merit. Note that for $N-Si_xGe_{1-x}$ of all the studied compositions at room temperature ZT is hundredths. But at 1073°K ZT≅0.8 [29].

Let us consider the effective masses (m^*), drift and weighted mobilities (μ_d, μ_W) of $N-Si_xGe_{1-x}$ at room temperature and their dependence on the alloy composition. For this, we will use the formulas known from the literature [30,31], which for 298°K and the concentration specified above ($n \cong 3.2 \cdot 10^{20} cm^{-3} = 3.2 \cdot 10^{26} m^{-3}$) will take the following form:

$$m^*/m_0 \cong 1.656 \left\{ \frac{3\left[e^{(S_r-2)}-0.17\right]^{2/3}}{1+e^{-5(S_r-S_r^{-1})}} + \frac{S_r}{1+e^{5(S_r-S_r^{-1})}} \right\} \tag{1}$$

and

$$\mu_W \cong 3.276 \cdot 10^3 \sigma \left\{ \frac{e^{(S_r-2)}}{1+e^{-5(S_r-1)}} + \frac{0.304 S_r}{1+e^{5(S_r-1)}} \right\} \quad (\tag{2}$$

(m_0 - electron rest mass, $\mu_W/\mu_d = (m^*/m_0)^{3/2}$).

The dependencies under consideration are shown in Figs 2 and 3. These results are close to the literature data [32,33].

Fig.2 Dependence $m^*/m_0 - x$ in N-Si_xGe_{1-x}

Fig. 3 Dependences $\mu_d - x$ (o) and $\mu_W - x$ (Δ) in N-Si_xGe_{1-x}

The thermoelectric properties of materials are essentially determined by the mechanism of scattering of charge carriers [34,35]. There is a relationship between the scattering parameter (A), temperature, Seebeck coefficient, effective mass and concentration of charge carriers [36], which at the considered temperature and concentration will take the form:

$$A \cong 1.16 \cdot 10^4 S + 2.545 - \ln(m^*/m_0)^{3/2} \cong 1.16 \cdot 10^4 S + 2.545 - \ln(\mu_W/\mu_d). \tag{3}$$

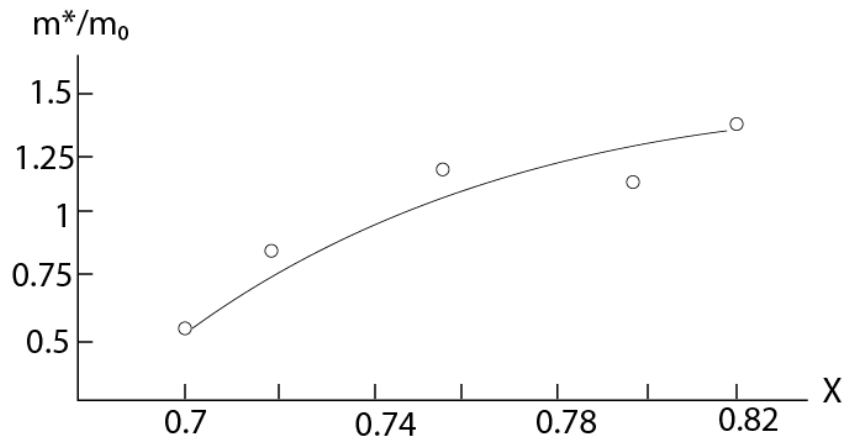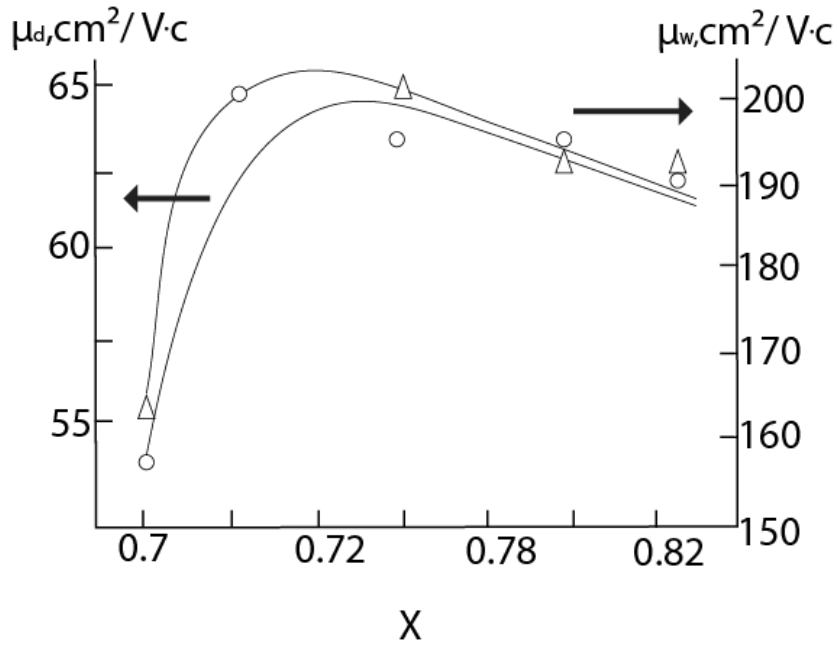Here, the constant A is determined by the scattering mechanism of charge carriers and takes the following values:[1] (acoustic-phonon scattering), [2] (polar optical-phonon scattering), [3] (scattering by ionized impurities). (Strictly speaking, the scattering parameter is denoted by the letter r, is included in formulas as r+2.5 (instead of A) and takes the values -0.5, 0.5 or 1.5.)

The calculation shows that for N-type samples A ≈ 3. This means that polar scattering of optical phonons takes place. For comparison, the calculation was also performed for the P-type. In this case, A≈2 (acoustic-phonon scattering).

mass of an electron vary in the range of (0.67–1.47), and the weighted mobility – in the range of (29.6 – 112.3) cm^2/V·s. The calculation of the scattering parameter shows that A ≈ 3 which means that polar scattering of optical phonons takes place.

3. CONCLUSION

Some thermoelectric characteristics of n-type SiGe alloy were investigated. It is shown that using reduced electrical conductivity it is possible to calculate the figure of merit of a material. The values of the ratio of the effective mass to the rest

REFERENCES

1. F.D. Rosi, "Thermoelectricity and thermoelectric power generation," Solid-State Electronics, 11(9), 849-868 (1968).

2. F. de Winter, "Xenon-filled silicon germanium thermoelectric generators," JPL Technical Review, 2(3), 22-31 (1972)

3. B. Cook, "Silicon–Germanium: The legacy lives on," Energies, 15(8), 2957 (2022)

4. K. Barbakadze, G. Bokuchava and Z. Isakadze, "High temperature thermoelectric generator based on SiGe alloy," Sci. JLEPL – Agmashenebeli Nat. Defence Acad. of Georgia, 47-52 (2022).

---

[1] Sometimes $\sigma/\sigma(0)$ and $\sigma - \sigma(300^o K)$ are also called reduced electrical conductivity.

[2] N-Si$_x$Ge$_{1-x}$ has a number of advantages over the P-type: At the same temperatures is characterized with a larger figure of merit [24], is more resistant to radiation [25], etc.

[3] $\sigma' = (q_e/k_B)^2 \sigma/B_E \cong 1.347 \cdot 10^8 \sigma/B_E$ [28] ($B_E = \sigma S^2/B_S$ is the electronic quality factor,

$$B_S = \left[\frac{S_r^2 e^{2-S_r}}{1 + e^{-5(S_r-1)}} + \frac{\frac{\pi^2}{3} S_r}{1 + e^{5(S_r-1)}} \right] \cong \left[\frac{S_r^2 e^{2-S_r}}{1 + e^{-5(S_r-1)}} + \frac{3.29 S_r}{1 + e^{5(S_r-1)}} \right]$$

is the scaled power factor and $S_r = (q_e/k_B)|S| \cong 1.16 \cdot 10^4 |S|$ is reduced Seebeck coefficient.

5. C. Schwinge, K. Kühnel, J. Emara, L. Roy, K. Biedermann, W. Weinreich, S. Kolodinski, M. Wiatr, G. Gerlach, and M. Wagner-Reetz, "Optimization of LPCVD phosphorous-doped Si Ge thin films for CMOS-compatible thermoelectric applications," Appl. Phys. Lett., 120, 031903 (2022)

6. A. Big-Alabo, "Finite element modelling and optimization of Ge/Si Ge super lattice based thermoelectric generators," Appl. Sci., 3, 189 (2021)

7. K. Jang, Y. Kim, J Park and J. Yi, "Electrical and structural characteristics of excimer laser-crystallized polycrystalline $Si_{1-x}Ge_x$ thin-film transistors," Materials, 12(11), 1739 (2019)

8. H. Murata, K. Nozawa, T. Suzuki, Y. Kado, T. Suemasu and K. Toko, "$Si_{1-x}Ge_x$ anode synthesis on plastic films for flexible rechargeable batteries," Sci. Reports, 12, 13779 (2022)

9. A. Idda, L. Ayat and N. Dahbi, "Improving the performance of hydrogenated amorphous silicon solar cell using a-SiGe:H alloy," Ovonic Res., 15(5), 271-278 (2019)

10. A.K. Singh, M. Kumar, D. Kumar and S.N. Singh, "Heterostructure silicon and germanium alloy based thin film solar cell efficiency analysis," Engin. and Manufacturing, 2, 29 (2020)

11. B. Kalas, Z. Zolnai, G. Sáfrán, M. Serényi, E. Agocs, T. Lohner, A. Nemeth, N.Q. Khánh, M. Fried and P. Petrik, "Micro-combinatorial sampling of the optical properties of hydrogenated amorphous $Si_{1-x}Ge_x$ for the entire range of compositions towards a database for opto-electronics," Sci. Reports, 10, 19266 (2020)

12. J. Aberl, M. Brehm, T. Fromherz, J. Schuster, J. Frigerio and P. Rauter, "SiGe quantum well infrared photo detectors on strained-silicon-on-insulator," Opt. Express, 27(22), 32009 (2019)

13. A. Ruzin, S. Marunko and Y. Gusakov, "Study of bulk grown silicon–germanium radiation detectors," Appl. Phys., 95, 5081-5087 (2004)

14. I. Yaroslavski and A. Rusin, "Characterization of radiation-related damage in bulk-grown silicon–germanium detectors," Nucl. Instruments and Methods in Phys., 562(1), 311-319 (2006)

15. A. Erko, N.V. Abrosimov and S.V. Alex, S.V. "Laterally-graded SiGe crystals for high resolution synchrotron optics," Crystal Res. and Techn. 37(7), 685-704 (2002)

16. C.A. Londos, E.N. Sgourou and D. Hall, D. "Vacancy-oxygen defects in silicon: the impact of isovalent doping," Mater. Sci.: Mater in Electronics, 25, 2395-2410 (2014)

17. L. Tayebi, Z. Zamanipour, M. Mozafari, P. Norouzzadeh, J.S. Krasinski and K.F. Ede, Thermal and thermoelectric properties of nanostructured versus crystalline SiGe. IEEE Green Technology Conference, 19-20 April 2012, Tulsa, OK, USA (2012)

18. Y. Li, G. Wang, M. Akbari-Saatlu, M. Procek and H.H. Radamson, "Si and SiGe nanowire for micro-thermoelectric generator: A review of the current state of the art," Frontiers in Materials, 8, 611078 (2021)

19. R.C. Teixeira, I. Doi, M.B.P. Zakia, J.A. Diniz and J.W. Swart, "Low electrical resistivity polycrystalline SiGe films obtained by vertical

LPCVD for MOS devices," Materials Sci. and Engin. B, 124/125, 138-142 (2005)

20. F. Fan, J. Liang, J.-L. Chen, Y. Peng, H. Lai, J. Nong, Ch. Liu, W. Ding and L. Miao, "Realizing high thermoelectric performance for p-type SiGe in medium temperature region *via* TaC compositing," Materiomics, 9(5), 984-991 (2023)

21. Y. Li, J. Han, Q. Xiang, Ch. Zhang and J. Li, "Enhancing thermoelectric properties of p-type SiGe by SiMo addition," Materials Sci.: Mater. in Electronics, 30, 9163-9170 (2019)

22. Sh. Sakane, T. Ishibe, T. Fugita and Y. Nakamura, "Temperature dependences of thermoelectric properties of bulk SiGeAu composites," JJAP Conference Proceedings, 10, 011001 (2023)

23. M.N. Tripathi and C.M. Bhandari, "Material parameters for thermoelectric performance," Phamana – J. Physics, 65(3), 469–479 (2005)

24. Ahmad, S. & Singh, A. (2024) Dopant dependent microstructure of hot-pressed SiGe alloys and its implications on thermoelectric properties. Phys. B: Condensed Matter, 674, 415534 (2024)

25. G. Bokuchava, G. Physical-mechanical and electrophysical properties of polycrystalline silicon-germaniumalloys. Thesis, Tbilisi, 2008, 135.

26. G. Bokuchava, I. Nakhutsrishvili and K. Barbakadze, "Si_xGe_{1-x} thermoelectric: determination of electronic quality factor, universal electrical conductivity, effective mass, mobility of charge carriers and preparation of monolithic module based on $Si_{0.7}Ge_{0.3}$ alloy," Fundamental Res. and Appl. of Physical Sci., 3, 113-126 (2023)

27. I. Nakhutsrishvi and R. Kokhreidze, "Reduced electrical conductivity of p-Si_xGe_{1-x} thermoelectric," Bull. Georg. Acad. Sci. (in press).

28. X. Zhang, Z. Bu, X. Shi, Z. Chen, S. Lin, B. Shan, M. Wood, A.H. Snyder, L. Chen, G.J. Snyder and Y. Pei, "Electronic quality factor for thermoelectric," Sci. Adv., 6(46), eabc0726 (2020)

29. G. Bokuchava, K. Barbakadze and I. NakhutsriShvili, "On the thermoelectric alloy n-Si_xGe_{1-x}," Material Sci. & Eng., 7(2), 54–57 (2023)

30. G.J. Snyder, A. Pereyra and R. Gurunathan, "Effective mass from Seebeck coefficient," Adv. Funct. Materials, 33(20), 2112772 (2022)

31. G.J. Snyder, A.H. Snyder, M. Wood, R. Gurunathan, B.H. Snyder and Ch. Niu, "Weighted mobility," Adv. Materials, 32(25), 2001537 (2020)

32. F. Schäffler, "Silicon-germanium ($Si_{1-x}Ge_x$). in: Properties of advanced semiconductor materials: GaN, AIN, InN, BN, SiC, SiGe," Eds.: Levinstein, M.E., Rumyantsev, S.L. & Shur, M.S., 148-187 (2001)

33. D. Lu, P. Morin, B. Sahu, T.B. Hook, P. Hashemi, A. Scholze, B. Kim, P. Kerber, A. Khakifirooz and P. Oldiges, "(Invited) silicon germanium FinFET device physics, process integration and modeling considerations," ECS Transactions, 64(6), 337-345 (2014)

34. M. Markwitz, P.P. Murmu, S.Y. Back, T. Mori, B.J. Ruck and J. Kennedy, "Effect of grain boundary scattering on carrier mobility and

thermoelectric properties of tellurium incorporated copper iodide thin films," Surf. and Interfaces, 41, 103190 (2023)

35. E. Karvannan, V. Vijay, T.S. Nivin, M. Navaneethan, J. Archana and A. Karthigeyan, "Tailoring charge carrier dynamics for improved thermoelectric properties in nickel-incorporated Bi_2S_3," Materials Chem. and Phys., 335, 130490 (2025),

36. A. Salem, K. Alshehri, J.A. Mohammed Abdulwahed and S.A. Hussein, S.A. "Examination of thermoelectric power of the $CuInGaSe_2$ crystals," Acta Phys. Pol. A, 142(2), 211-215 (2022).

N-SixGe1-x შენადნობის დაყვანილი ელექტრული გამტარობა და სხვა თერმოელექტრული მახასიათებლები ოთახის ტემპერატურაზე

გ. კახნიაშვილი[1], ზ. ადამია[2], ი. ნახუცრიშვილი[1]

[1] საქართველოს ტექნიკური უნივერსიტეტის კიბერნეტიკის ინსტიტუტი, ანჯაფარიძის ქ. 6, 0186 თბილისი

[2] სოხუმის სახელმწიფო უნივერსიტეტი, პოლიტკოვსკაიას ქ. 61, 0186, თბილისი

E-MAIL: iraklinakhutsrishvili52@gmail.com

რეზიუმე: *მიზანი.* ნაშრომში წარმოდგენილია მონაცემები დაყვანილი ელექტროგამტარობის, ასევე მუხტის მატარებელთა კონცენტრაციისა და ძვრადობის დამოკიდებულების შესახებ N-ტიპის Si_xGe_{1-x} შენადნობის შემადგენლობაზე. ელექტრონის ეფექტური მასისა და უძრაობის მასათა თანაფარდობის მნიშვნელობები მერყეობს (0.67–1.47) დიაპაზონში, ხოლო შეწონილი მობილურობა - (29.6 – 112.3) სმ²/Vვ·წმ დიაპაზონში. შესაბამისი გამოთვლები ჩატარდა ოთახის ტემპერატურისთვის. ნაშრომში განხილულია მუხტის მატარებელთა გაფანტვის პარამეტრი.

მეთოდი. SiGe ნიმუშები მიღებული იქნა ზონური დნობის ზოდებიდან მიღებული ფხვნილების ვაკუუმური ცხელი დაპრესვით. Si და Ge-ს ნარჩენების მასა დაქუცმაცდა ფოლადის ღეროთი და გაცრილი იქნა 0.2 მმ უჯრედების მქონე საცერში. შემდეგ ის ჩაიტვირთა REK PM-100 SM საფქვავის კამერაში და ისევ დაქუცმაცდა 20-25 საათის განმავლობაში. ფხვნილის გრანულომეტრიული შემადგენლობა შეფასდა Nikon-ის ოპტიკური მიკროსკოპისა და DRON-3M რენტგენული დიფრაქტომეტრის გამოყენებით.

შედეგი ZT-ის გამოთვლა შესაძლებელია σ"-ის გამოყენებით უნივერსალურ ელექტროგამტარობასთან (σ') კომბინაციით: უნივერსალური და დაყვანილი ელექტროგამტარობის

განმარტებებიდან ირკვევა, რომ $\sigma''/\sigma'=(k_B/q_e)^4 B_E T/\lambda_L \cong 5.512 \cdot 10^{-17}(ZT/B_S)[(\lambda_E/\lambda_L)+1]$. ამრიგად, σ''/σ'-ს საშუალებით შესაძლებელია ვარგისიანობის მაჩვენებლის პროგნოზირება. ოთახის ტემპერატურაზე შესწავლილი ყველა შემადგენლობის $N-Si_x Ge_{1-x}$-ისთვის ZT მეასედების ტოლია. თუმცა, 1073^oK-ზე $ZT\cong0.8$.

დასკვნა. გამოკვლეული იქნა N-ტიპის SiGe შენადნობის ზოგიერთი თერმოელექტრული მახასიათებელი. ნაჩვენებია, რომ დაყვანილი ელექტროგამტარობის გამოყენებით შესაძლებელია მასალის ვარგისიანობის მაჩვენებლის გამოთვლა. ელექტრონის ეფექტური და უძრაობის მასათა თანაფარდობის მნიშვნელობები მერყეობს (0.67–1.47) დიაპაზონში, ხოლო შეფონილი ძვრადობა - (29.6 – 112.3) $სმ2/\dot{V}\cdot s$ დიაპაზონში. გაფანტვის პარამეტრის გამოთვლა აჩვენებს, რომ A ≈ 3, რაც ნიშნავს იმას, რომ ხდება ოპტიკური ფონონების პოლარული გაფანტვა.

საკვანძო სიტყვები: SiGe შენადნობი, თერმოელექტრული მახასიათებლები, ოთახის ტემპერატურა.

UDC 666. 762.93

HETEROMODULAR COMPOSITE IN THE B₄C-SiC-TiC SYSTEM

Z. Kovziridze, N. Nijaradze, M. Mshvildadze, T. Loladze, N. Loladze, G. Tabatadze,

T. Cheishvili, M. Kapanadze, M. Balakhashvili, V. Qinqladze, N. Darakhvelidze, M. Tabatadze,

M. Cerodze

Georgian Technical University. Faculty of Chemical Technology and metallurgy, Institute of Bionano-ceramics and Nanocomposite Technology, Bionanoceramic and Nanocomposite Materials Science Center. Georgia, 0175, Tbilisi, Kostava Str. 69

E-mail: kowsiri@gtu.ge

Resume: Objective: To develop a composite material with enhanced technical and operational properties based on the B_4C–SiC–TiC system.

Method: The composite was fabricated via hot-pressing. Phase composition and microstructural characterization were performed using X-ray diffraction (DRON-3) and scanning electron microscopy (SEM). Mechanical properties were evaluated using a German R-100 tensile testing machine and a Rockwell hardness tester for hardness assessment.

Result: The hot-pressing process induced a solid-state reaction between titanium carbide (TiC) and boron carbide (B_4C), leading to the in-situ formation of titanium diboride (TiB_2) grains, which contributed significantly to the composite's mechanical reinforcement. The addition of perlite facilitated the development of a glassy intergranular phase, forming continuous "bridges" between carbide grains, thereby enhancing grain boundary cohesion and mechanical stability.

Conclusion: The synthesized composite demonstrates outstanding mechanical performance:
- **Flexural strength**: 389 MPa
- **Compressive strength**: 1923 MPa
- **Impact toughness**: 11.2 kJ/m²

These properties make the material well-suited for wear-resistant applications operating under high-impact, thermomechanical loading and other conditions.

Key words: Composite, correlation, porous phase, mechanical strength, structure.

MAIN PART

The development and implementation of new technologies are currently considered fundamental prerequisites for creating competitive, multifunctional materials, advancing integrated materials science, and promoting national economic development.

High-temperature, heteromodular, advanced ceramic composite materials are exemplary in this regard. These materials are characterized by superior physical and mechanical properties (such as hardness, strength limits, fracture toughness, and modulus of elasticity), excellent technological properties (such as good machinability with cutting tools), and outstanding operational performance

(including wear resistance, resistance to static and dynamic loading, radiation resistance, and more).

The foundation for producing such materials lies in the use of refractory compounds, including: boron carbide, boron nitride, tantalum carbide, zirconium, aluminum, and yttrium oxides, silicon nitride, silicon carbide, titanium and zirconium borides, and carbides of titanium, tungsten, and tantalum. These compounds exhibit high thermodynamic stability, exceptional hardness, and wear resistance - properties they retain even under elevated temperature conditions. This thermal resilience is one of the key factors enabling their effective application in demanding technological environments.

This study focuses on the synthesis and investigation of composite ceramic materials based on boron carbide (B_4C) and silicon carbide (SiC). For the fabrication of the composite, the following initial composition (in wt.%) was selected: B_4C – 60%, SiC – 20%, TiC – 13%, Perlite – 3% (appendage).

The selection of these compounds was driven by their unique combination of properties, including high hardness, high melting point, excellent corrosion resistance, wear resistance, and low density. However, unlike other advanced ceramics, they exhibit low fracture toughness and impact resistance, which limits their broader application despite their advantageous properties. Numerous studies have been devoted to the development of composites based on these compounds for various purposes, particularly in armor applications, due to their low density [1–13].

In addition to boron carbide and silicon carbide, titanium carbide (TiC) was introduced into the composition. This inclusion was based on the known reaction that occurs between titanium carbide and boron carbide during high-temperature processing, resulting in the in-situ formation of titanium diboride (TiB_2), as confirmed by X-ray diffraction analysis (Fig. 1). Titanium diboride is also known for its excellent mechanical properties.

The aim of this study was to achieve a highly dispersed and uniform distribution of the newly formed TiB_2 grains within the composite matrix. This uniform distribution is facilitated by an amorphous glassy phase formed by volcanic perlite, which acts as a bonding medium between the grains (Fig. 2).

The chemical composition of perlite is as follows (wt.%):

- SiO_2 – 72.11
- Al_2O_3 – 15.56
- Fe_2O_3 – 0.53
- CaO – 0.71
- MgO – 0.35
- K_2O – 4.87
- Na_2O – 3.27
- Loss on ignition – 3.03

The melting point of perlite is approximately 1240°C. It contains 76 wt.% glassy phase, with the remainder consisting of crystalline phases and gases trapped during the rapid cooling of erupted lava. Its density ranges from 2.3 to 2.4 g/cm³.

Structural–morphological and elemental composition of the samples was examined using a JEOL JSM-6510LV scanning electron microscope, manufactured in Japan, equipped with an Oxford Instruments X-MaxN energy-dispersive X-ray spectroscopy (EDS) system. Surface imaging was performed using both secondary electrons (SEI)

and backscattered electrons (BES) under an accelerating voltage of 20 kV. In certain cases, to reduce surface charging, samples were coated with a ~10 nm Pt layer using a JEOL JEC-3000FC vacuum sputter coater.

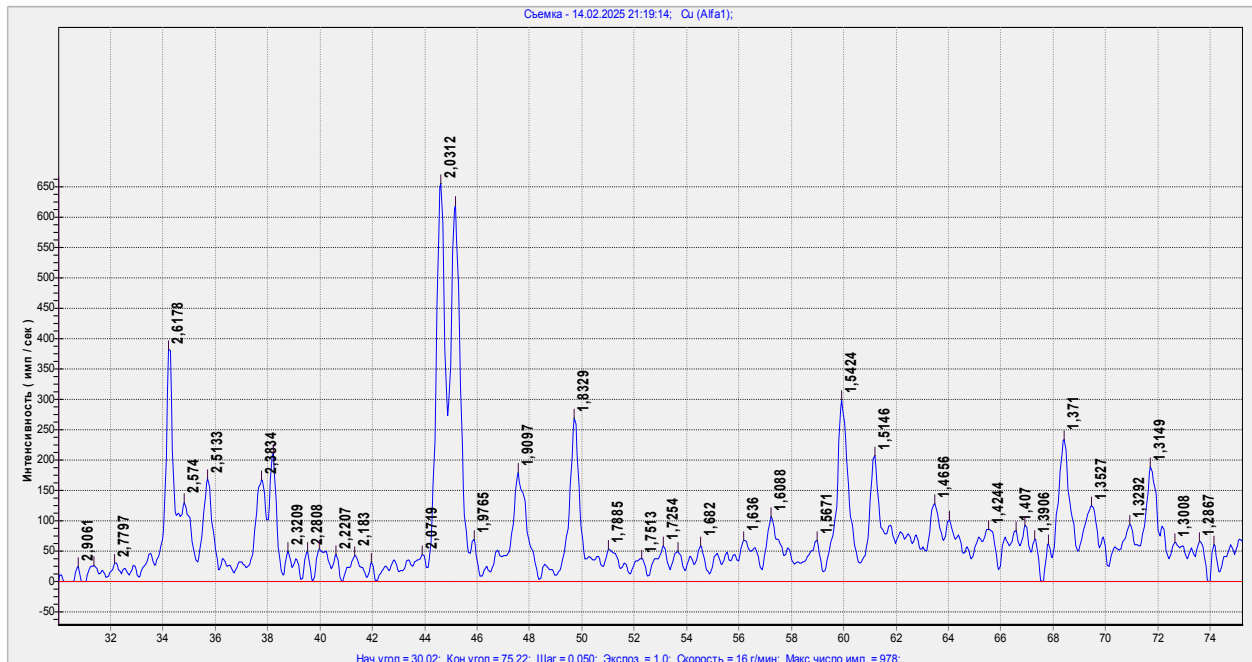Fig. 1. X-ray diffraction pattern of the obtained composite.

TiB_2 - dhkl - 1.3149; 1.371; 1.5146; 1.6088; 2.0312; 2.6178 Å .

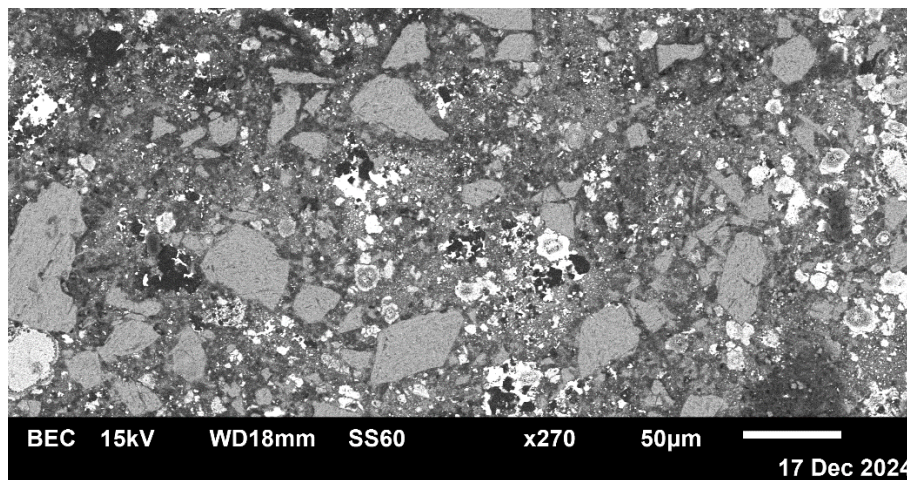SiC - dhkl - 1.5424; 1.9097; 2.3834; 2.5133; 2.574 Å

B_4C - dhkl - 238 Å

Fig. 2. Microstructure of the composite

The results of the morphological analysis of the polished sample surface are presented in Fig. 2. Gray silicon carbide and white boron carbide grains are clearly distinguishable. Newly formed titanium diboride is also observed between them, the presence of which is confirmed by microspectral and electron imaging data (Fig. 4, 5).

To examine the fracture mechanism of the composite at the microscopic level, a freshly fractured sample was prepared, and its fracture surface was analyzed using a scanning electron microscope (SEM). SEM image of the fracture surface is presented in Fig. 3.
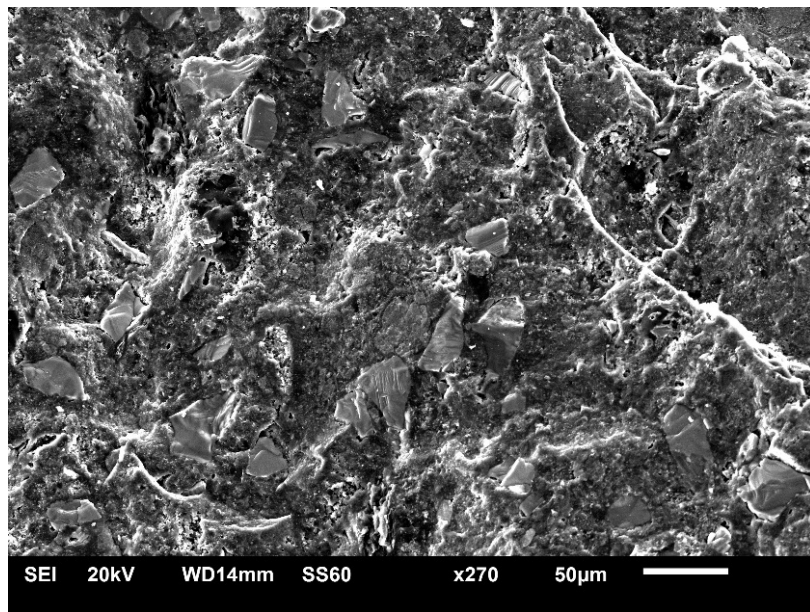
Fig. 3. Fracture surface SEM micrograph
of the studied composite

Figure 3 illustrates that the morphological features are consistent and uniform throughout both the surface and the volume of the sample. The fracture mechanism is characterized by a combination of transcrystalline and ductile modes.

Furthermore, the crystals exhibit stepwise fracture, which effectively impedes crack propagation. This behavior is corroborated by the mechanical strength data presented in Table 1.
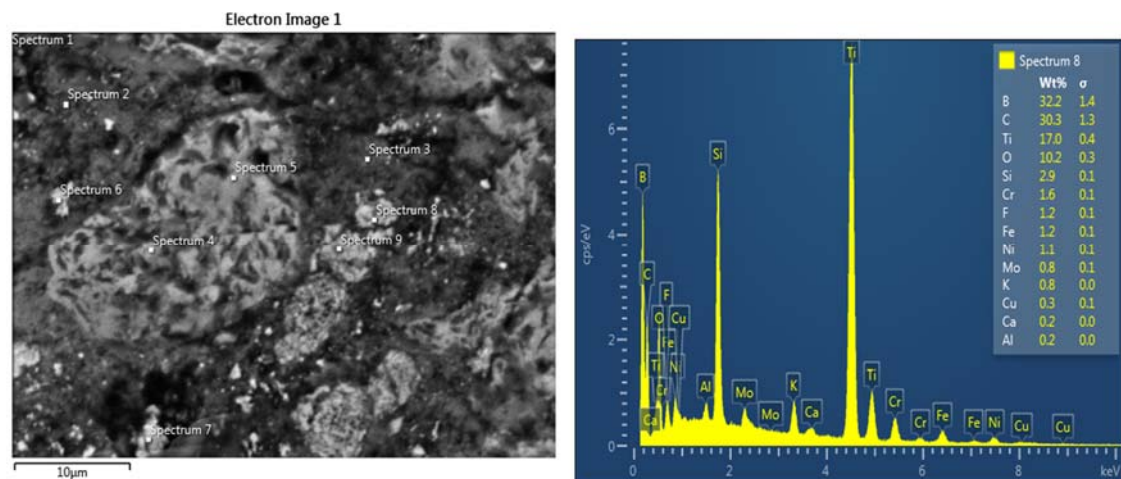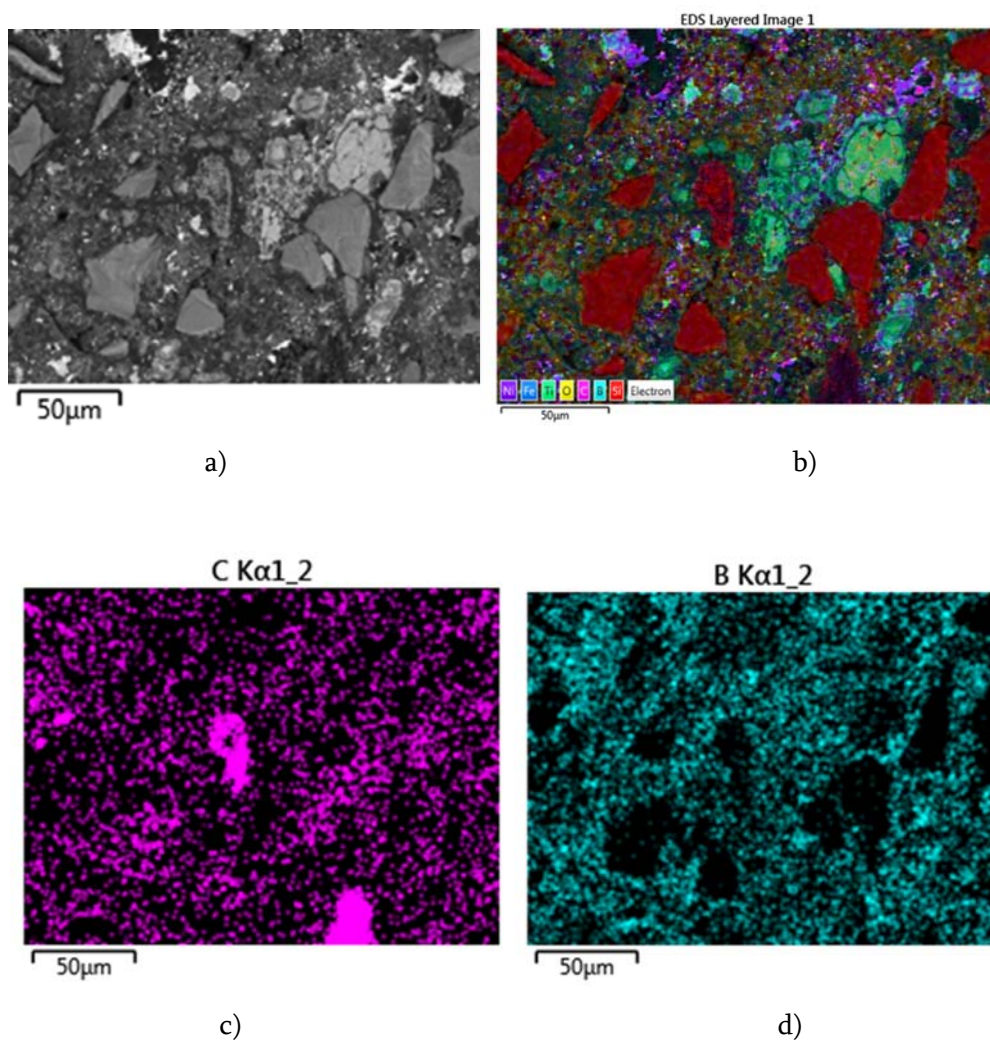
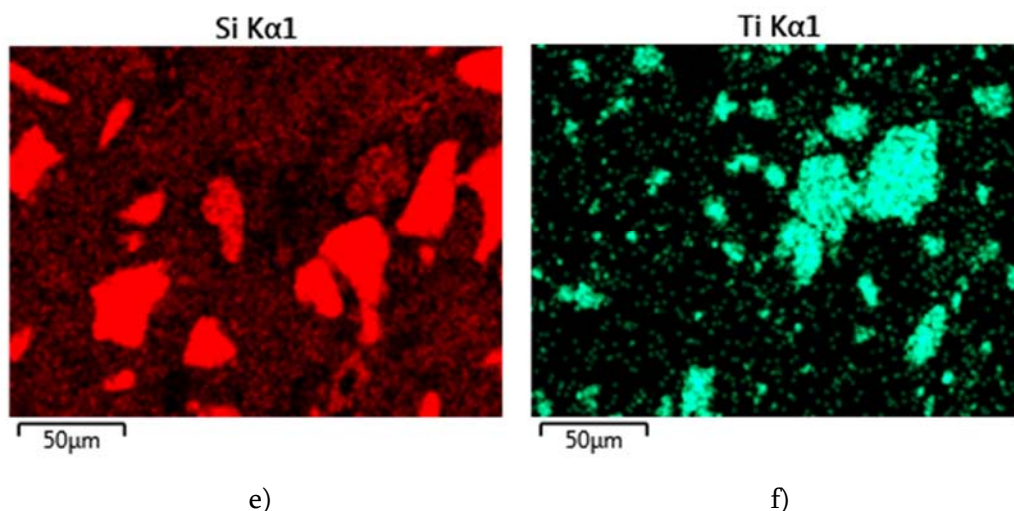Fig. 4. Micro X-ray spectral images of the investigated composite

a)

b)

c)

d)

Fig. 5. SEM images illustrating the spatial phase distribution within the composite

As observed in Fig. 5, titanium diboride forms a shell around the silicon carbide grains. In the event of crack initiation within a carbide grain, it localises the crack and reduces its propagation rate [1]. Additionally, unreacted boron carbide and titanium diboride grains are interconnected by thin amorphous glassy bridges [2]. The composite was fabricated using the hot-pressing method at 1620 °C. The physical and technical properties of the composite are presented in Table 1.

Table 1

Physical and technical characteristics of the composite

Composite B$_4$C-SiC-TiB$_2$-Perlite	Theoretical density, Υ_{th}, g/cm^3	Relative density, Υ_r	Open porosity п, %	Hardness, HRA	Compressive strength, σ_c. MPa	Flexural strength, $\sigma_в$. MPa	Impact toughness, A kJ/m²
	3,1	0,96	<1,0	91	1923	389	11.2

As shown in the table 1, the obtained composite is characterized by high physical and mechanical properties and low volume porosity, which enhances its application potential. To further characterize the composite, Z. Kovziridze's formulas describing the dependence of mechanical properties on the porous phase and the correlation between the morphology of the crystalline phase and macromechanical characteristics were applied [14]. For this purpose, the morphology of pores and crystals was examined using microstructural images. The data presented in Tables 2 and 3 were utilized as input for the corresponding formulas.

19

Table 2

Porous phase morphology

Visual field area, S, mkm^2	Total pore area, S, µM^2	Maximum pore size, D$_{max}$, µM	Minimum pore size, Dmin, µM	Pore shape factor, Fp=D$_{max}$/ D$_{min}$	Pore distribution factor in the matrix, P$_d$	Volume fraction of the porous phase, P$_{vol}$, %	Average pore size, P$_m$, µM	Load under bending, P, MPA
36500	303	10	5	2	0,9	0,83	7	389

Table 3

Crystalline phase morphology

Visual field area, S, µM^2	Total crystal area, S$_{cryst}$, µM^2	Maximum crystal size, D$_{max}$, µM	Minimum crystal size, D$_{min}$, µM	Crystal shape factor, F$_{kf}$= D$_{max}$/ D$_{min}$	Crystal distribution factor in the matrix, F$_{kd}$	Volume fraction of the crystalline phase, K$_v$, %	Average crystal size, K$_m$, µM	Load under bending, P$_{MPa}$
36500	36197	18	4	4.5	0,9	89,17	6	389

$$\sigma_{m/p} = P/F_p \cdot P_d \cdot P_{vol} \cdot P_m$$

Where:

P – applied load in bending mechanics (MPa);

F_p – pore shape factor;

P$_d$ – pore distribution factor in the matrix;

P$_{vol}$ – volume fraction of the porous phase in the matrix;

P$_m$ – average pore size.

$$\sigma m/p = P/Fp.Pd.Pvol.Pm = 389/\ 2 \cdot 0,9 \cdot 0,83 \cdot 7 = 389/10,46 = 37.2 \text{ MPa.}$$

$$\sigma_d = PF_{kd}/K_m K_v F_{kf}$$

Where:

P – applied load in bending or compression mechanics (MPa);

F$_{kd}$ – crystal distribution factor in the matrix;

K$_m$ – average crystal size (µm);

K$_v$ – volume fraction of crystals in the matrix (wt.%);

F$_{kf}$ – crystal shape factor.

$$\sigma_d = PxF_{kd}/K_mK_vF_{kf} = 389 \times 0{,}9/\ 6 \cdot 89{,}17 \cdot 4.5 = 389.0{,}9/\ 2407.6 = O.17$$

$$\sigma_d = PxF_{kd}/K_mK_vF_{kf} = 1923 \times 0{,}9/\ 6 \cdot 89{,}17 \cdot 4.5 = 1730.7/2407.6 = O.\ 72$$

The formula accounts for both volumetric and surface defects of crystals, as well as the micro- and macrostructural volumetric and surface morphology of the crystalline phase, its distribution within the matrix, and the transformations occurring due to chemical and physicochemical processes during material consolidation. These properties are determined experimentally.

Notably, the proposed formula is applicable to a wide range of ceramic materials and ceramic composites, including metal-ceramics, bioceramics, glass-ceramics, and glass-metal-ceramics. It captures the relationship between the macromechanical properties of these materials, specifically, their ultimate failure characteristics, and key morphological parameters of the crystalline phase, such as crystal size, shape, distribution, and volume fraction within the matrix, as well as the crystal shape factor. In addition, the formula accounts for the contribution of the most mechanically robust phase in the consolidated material, reflecting its critical role in determining the overall performance characteristics essential for industrial application and long-term service reliability.

During thermal treatment, key factors influencing the final properties of ceramic materials include the dynamics of crystal formation, their spatial distribution within the matrix, and the evolution of crystal morphology. These aspects, thoroughly examined in this study, are closely linked to the physicochemical processes that occur

under thermal stress. The proposed formula offers a comprehensive framework for modeling the correlation between the morphology of the crystalline phase and the macromechanical properties of ceramic components. Its applicability extends to all types of ceramics and ceramic composites employed in advanced technologies, diverse engineering sectors, and everyday applications.

The B_4C-TiC-SiC-TiB_2-perlite composite, which demonstrates high mechanical and operational properties, was fabricated via hot pressing at a temperature of 1620℃. However, as the results indicate, the correlation is not strong. This may be attributed to the high crystal shape factor. Notably, attrition milling and planetary ball milling of the mixture were deliberately avoided, maintaining the materials' original dispersion. The disparity between the smallest and largest particles was substantial, which significantly contributed to the reduction in correlation. Consequently, the correlation coefficient was found to be 0.17 for bending and 0.72 for compression.

Ideally, the crystal shape factor should not exceed 3, and the crystal size should preferably remain within the range of 7–8 microns, while also being uniformly distributed throughout the matrix. Experimental evidence shows that fine-grained samples exhibit higher strength compared to coarse-grained ones [15–19], since the length of Griffith microcracks is determined by grain size. This phenomenon is presumably related to stress

accumulation at grain boundaries caused by anisotropic thermal expansion [20–26].

The volume and surface electrical resistivity (ρ_v and ρ_s) of the obtained material was experimentally determined as a function of temperature in the range of 25–300°C. Measurements were conducted using a specially designed thermally controlled cell, simultaneously on two samples, with an electronic ohmmeter employed for resistance measurements. The test samples were disk-shaped, with a diameter-to-height ratio of approximately D/H ≈ 5. Air-dried samples (25°C, relative humidity 47.5%) were placed in the measurement cell, and their volume (R_v) and surface (R_s) resistance values (Ω) were recorded. Subsequent measurements in the temperature range of 100–300°C were performed at 50°C intervals. Using the corresponding calculations, specific resistivity values ρ_v ($\Omega{\cdot}m$) and ρ_s (Ω) were obtained. The resulting "$\rho_{v,s}$ - t" relationships are presented in Figure 6.
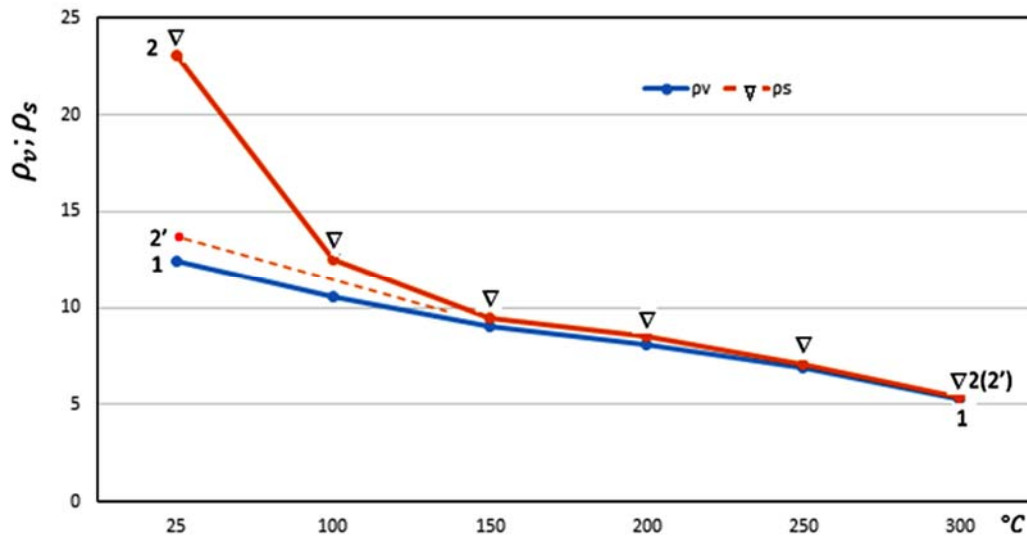

Fig. 6. Temporal dependencies of the material's
volumetric density (ρ_v) (curve 1) and
surface density (ρ_s) (curves 2 and 2[1])

It was established that the variation of volume resistivity (ρ_v) with temperature is linear, and within the 25–300°C interval, a nearly twofold decrease in specific resistivity is observed. A noteworthy behavior is exhibited by the surface resistivity (ρ_s), whose values were determined under conditions of reversible temperature cycling in the range of 25–300°C. For the initial sample (Curve 2), the ρ_s values were relatively high at room temperature, showed a sharp decline in the range of 25–150°C, and subsequently aligned with the ρ_v values. During the cooling phase (Curve 2'), ρ_s values closely matched those of ρ_v, with only a minor deviation (≈1 Ω).

The distinct behavior of the "ρ_s–t" curve under temperature reversal is likely attributable to

condensed moisture on the surface of the initial sample, which evaporated during heating, leading to the convergence of ρ_s and ρ_v values at higher temperatures.

The key electrical properties of the investigated material, calculated across the temperature range of 25–300°C, are presented in Table 4.

Principal electrical characteristics of the studied material

N	Electrical Properties			
	Title	Conventional Symbol	Unit of Measurement	Values
1	Temperature Coefficient of Electrosensitivity	B	$\Omega \cdot m \cdot K$	529.1
2	Temperature Coefficient of Electrical Resistivity	$\Delta\alpha_T$	$\Omega \cdot m \cdot K^{-1}$	-2,7$\cdot 10^{-3}$
3	Activation Energy of Electrical Conductivity	ΔE	eV	0,334

The resulting material, primarily composed of titanium, silicon, and boron carbides, well-known for their electrical properties, exhibits electrical behavior characteristic of semiconductor materials.

CONCLUSION

During the hot pressing at 1620°C, a reaction occurred between titanium carbide and boron carbide, resulting in the formation of titanium diboride. This reaction contributed to a significant enhancement of the composite's mechanical properties. Additionally, the presence of perlite in the composite led to the formation of a glassy phase that creates so-called "bridges" with the carbide grains, further improving the mechanical performance of the material. A clear correlation was established between the matrix composition and the mechanical properties of the material, specifically showing the dependence of mechanical characteristics on the content of the porous phase.

The resulting composite in the B_4C-SiC-TiC-TiB_2 system, doped with 3 wt.% glassy perlite, primarily composed of titanium, silicon, and boron carbides known for their electrical properties, exhibits electrical behavior characteristic of semiconductor materials.

REFERENCES

1. V.V. Lensky, A.A. Chikina, et al., "Development of Armor Shells for Personal Protective Equipment from Reaction-Bonded Silicon Carbide," Scientific and Technical Collection.

Issues of Defense Technology, Series 15, Issue 1 (148)-2 (149), 2008.

2. Method for producing a ceramic armor material based on silicon carbide and boron carbide, US Patent 3,796,564, class C22C 1/04, published May 12, 1974.

3. Composite ceramic material, US Patent 6,805,034, class F41H 5/00, published October 19, 2004.

4. Bo Wang, Delong Cai, Haoyi Wang, Wenhua Zou, Zhihua Yang, Xiaoming Duan, Peigang He, Daxin Li, Wenjiu Duan, Dechang Jia, Hua-Tay Lin, Chao Zhao, Yu Zhou, Microstructures and mechanical properties of B_4C–SiC and B_4C–SiC–TiB_2 ceramic composites fabricated by hot pressing·Journal of the American Ceramic Society·06, Apr 2023 DOI:10.1111/jace. 19136 ISBN: 1551-2916

5. Kovziridze, Z., Mestvirishvili, Z., Tabatadze, G. Influence of TiB_2 and ZrB_2 additives on the properties of boron carbide. *Ceramics*, 2012, Vol. 27, No. 1, pp. 33–39.

6. Srivatsan T.S., Guruprasad G., Black D., Radhakrishnan R., Sudarshan T.S. Influence of TiB_2 content on microstructure and hardness of TiB_2–B_4C composite. Powder Technol., 2005, 159, 3, 161–167.

7. Huang S.G., Vanmeensel K., Malek O.J.A., Van der Biest O., Vleugels J. Microstructure and mechanical properties of pulsed electric current sintered B_4C–TiB_2 composites. Materials science and Engineering A, 2011, 528, 1302–1309.

8. Kriener M., Muranaka T., Kato J., Ren Z.A., Akimitsu J., Maeno Y. Superconductivity in heavily boron-doped silicon carbide. Sci. Technol. Adv. Mater., 2008, 9, 044205-044213

9. Z. Kovziridze, N. Nizharadze, G. Tabatadze, E. Nikoleishvili, Z. Mestvirishvili, V. Kinkladze. Multifunctional hetero-modulus composites in the B_4C-BN-TiC-SiC-C system. Journal of the European Ceramic Society, Elsevier, vol.31, issue 10, September 2011, pp. 1921-1926.

10. Z. Kovziridze, N. Nijaradze, G. Tabatadze, M. Mshvildadze, E. Nikoleishvili, Z. Mestvirishvili. Improvement of Boron Carbide Mechanical Properties in B_4C-TiB_2 and B_4C-ZrB_2 Systems. Journal of Electronics Cooling and Thermal Control, Vol. 3 No. 2, pp. 43-48 2013. Delaware, USA

11. Z. Kovziridze, N. Nijharadze, G. Tabatadze, Z. Mestvirishvili, Ceramic composite in the Al_2O_3–B_4C–TiC system. Journal of the Georgian Ceramicists Association "Ceramics", No. 2 (30), 2013, pp. 19–22.

12. Z. Kovziridze, N. Nijaradze, G. Tabatadze, N. Darakhvelidze, Z. Mestvirishvili. Smart Materials in the SiAlON-SiC-Al_2O_3 System. Journal of Material Science and Engineering, International Conference and Expo on Ceramics. August 17-18, 2015 Chicago, USA.

13. Z. Kovziridze, N. Nijharadze, G. Tabatadze, N. Darakhvelidze, M. Balakhashvili. Synthesis of self-healing composites by reactive sintering in the SiC–B_4C–Si–Al–Al_2O_3 system via metallothermal and nitriding processes. Journal of the Georgian Ceramicists Association "Ceramics and Advanced Technologies", Vol. 20, No. 2 (40), 2018, pp. 13–17.

14. Z. Kovziridze, N. Nijharadze, G. Tabatadze, Z. Mestvirishvili, N. Darakhvelidze. Investigation of the phase composition of composites in the SiC–B_4C–Si–Al–Al_2O_3 system. Journal of the

Georgian Ceramicists Association "Ceramics and Advanced Technologies", Vol. 21, No. 1 (41), 2019, pp. 44–51.

15. Z. Kovziridze, Sintering Physics and Kinetics, monograph. Publishing House "Technical University," Tbilisi, 2022, p. 702.

16. Griffith A.A. Phil. Trans.Roy. Soc. London. A221. 163.1920. First International Congress for Applied Mechanics (Delft). 1924. ed.J. Waltman Delft 1925.

17. Griffith A.A. Phil.Trans. Roy. Soc. London. A221. 163. 1920.

18. Inglis C.E. Trans. Inst. Nav. Archit. 55. 1. 219. 1913.

19. Orowan E. Z. Krist. A89. 327. 1934.

20. Charles R.J. Journ. Appl. Phys. 29. 1549. 1958.

21. Baker T.C. Preston F. W. Journ. Appl. Phys. 17. 170. 1946.

22. Z. Kovziridze. Formula for the dependence of macromechanical properties on the porous phase. Sakpatent (Georgian Patent), Certificate No. 7276, March 7, 2018.

23. Zviad Kovziridze, Jimsher Aneli, Natela Nijaradze, Gulnazi Tabatadze. Ceramic and Polymer Composites. Monograph. Lambert Academic Publishing. ISSN:978-620-2-06984-7 International Book Market Service LTD,

Member of Omni Scriptum Publishing Group. 2017. Germany.

24. Z. Kovziridze, N. Nijharadze, G. Tabatadze, J. Aneli. Ceramic and Polymer Composites. Monograph. Georgian Technical University, Tbilisi, Georgia, 2016. ISBN 978-9941-20-685-6. http://www.gtu.ge

25. Z. Kovziridze, N. Nijharadze, G. Tabatadze, N. Darakhvelidze. Self-healing and Low-Tungsten Composite Materials. Monograph. Georgian Technical University, Tbilisi, Georgia, 2017.
ISBN 978-9941-20-808-9. http://www.gtu.ge

26. Z. Kovziridze, N. Nijharadze, G. Tabatadze. High-Strength Heteromodular Composites. Monograph. Georgian Technical University, Tbilisi, Georgia, 2014. ISBN 978-9941-20-479-1. http://www.gtu.ge

27. W. Kollenberg. Technische Keramik. Vulkan14. W. Kollenberg. Technische Keramik. Vulkan Verlag ESSEN. 2004. S. 52. Germany.

28. Zviad Kovziridze et All. Obtaining of SiAlON Composite via Metal-Thermal and Nitrogen Processes in the SiC-Si-Al-Geopolymer System. Journal of Electronics Cooling and Thermal Control. 2017. 7. 103-122.
http://www.scirp.org/journal/jectc
USA. Delaware.

ჰეტერომოდულური კომპოზიტები B₄C-SiC-TiC სისტემაში

ზ. კოვზირიძე, ნ. ნიჟარაძე, მ. მშვილდაძე, თ. ლოლაძე, ნ. ლოლაძე, გ. ტაბატაძე, თ. ჭეიშვილი, მ. კაპანაძე, მ. ბალახაშვილი, ვ. ქინქლაძე, ნ. დარახველიძე, მ. ტაბატაძე, მ. წეროძე

საქართველოს ტექნიკური უნივერსიტეტი. ქიმიური ტექნოლოგიისა და მეტალურგიის ფაკულტეტი. ბიონანოკერამიკისა და ნანოკომპოზიტების ტექნოლოგიის ინსტიტუტი. ბიონა-ნოკერამიკისა და ნანოკომპოზიტების მასალათმცოდნეობის საუნივერსიტეტო ცენტრი. საქართველო 0175. თბილისი. კოსტავას 69

E-MAIL: kowsiri@gtu.ge

რეზიუმე: მიზანი: B₄C–SiC–TiC სისტემის საფუძველზე გაუმჯობესებული ტექნიკური და ექსპლუატაციური თვისებების მქონე კომპოზიტური მასალის შემუშავება.

მეთოდი: კომპოზიტი დამზადდა ცხელი დაწნეხვის მეთოდით. ფაზური შემადგენლობა და მიკროსტრუქტურული დახასიათება ჩატარდა რენტგენის დიფრაქციის (DRON-3) და სკანირების ელექტრონული მიკროსკოპიის (SEM) გამოყენებით. მექანიკური თვისებები შეფასდა გერმანული R-100 დაჭიმვის ტესტირების აპარატისა და Rockwell-ის სიმტკიცის ტესტერის გამოყენებით სიმტკიცის შესაფასებლად.

შედეგი: ცხელი დაწნეხვის პროცესმა გამოიწვია მყარი მდგომარეობის რეაქცია ტიტანის კარბიდსა (TiC) და ბორის კარბიდს (B₄C) შორის, რამაც გამოიწვია ტიტანის დიბორიდის (TiB₂) მარცვლების ადგილზე წარმოქმნა, რამაც მნიშვნელოვნად შეუწყო ხელი კომპოზიტის მექანიკურ გამაგრებას. პერლიტის დამატებამ ხელი შეუწყო მინისებრი მარცვლოვანთაშორისი ფაზის განვითარებას, რაც ქმნიდა უწყვეტ „ხიდებს" კარბიდის მარცვლებს შორის, რითაც აძლიერებდა მარცვლების სასაზღვრო თანმიმდევრულობას და მექანიკურ სტაბილურობას.

დასკვნა: სინთეზირებული კომპოზიტი ავლენს გამორჩეულ მექანიკურ მახასიათებლებს:

• მოხრის სიმტკიცე: 389 მპა

• შეკუმშვის სიმტკიცე: 1923 მპა

• დარტყმის სიმტკიცე: 11.2 კჯ/მ²

ეს თვისებები მასალას შესაფერისს ხდის ცვეთამედეგი აპლიკაციებისთვის, რომლებიც მუშაობენ მაღალი დარტყმის, თერმომექანიკური დატვირთვის და სხვა პირობების ქვეშ.

საკვანძო სიტყვები: კომპოზიტი, კორელაცია, ფოროვანი ფაზა, მექანიკური სიმტკიცე, სტრუქტურა.

UDC 666.762.93

SMART HETEROMODULAR NANOCOMPOSITE IN THE TiC-TiB$_2$-BN-SiC-B$_4$C-SiAlON-Al$_2$O$_3$ -C SYSTEM

Z. Kovziridze, N.Nijaradze, G. Tabatadze, T. Cheishvili, N. Darakhvelidze, M. Balakhashvili

Georgian Technical University, Institute of Bionanoceramics and Nanocomposite Technology, Bionanoceramics and Nanocomposite Materials Science Center, Georgia, 0175, Tbilisi, Kostava Str. 69

E-mail: kowsiri@gtu.ge

Resume: *Goal* - to obtain on first stage β - SIALON containing nanocomposites by reactive sintering method at 1400^{0}C, with nitrogen process from origin composition in TiC-BN-**SiC-B$_4$C-Si-Al-Al$_2$O$_3$** system. By using this method of synthesis, it became possible to receive nanocomposites with different percentages of β - SIALON. Our task was to study the phase composition of received consolidated materials in the TiC-TiB$_2$-BN-SiC-B$_4$C-β-SiAlON-Al$_2$O$_3$ (nanopowder-400nm.) system.

Method. The obtained mass was grounded in an attritor and the consolidated composite was obtained by hot pressing at 1620^{0}C during 40 minutes, with glass perlite (Armenia) dope 2 mass%, delaying at final temperature for 8 min, under 30 MPa pressure and vacuum – 10^{-3} Pa. Perlite from Aragatc contained 96 mas. % glass.

To study the phase composition of the composites, we conducted an X-ray structural analysis on the DRON-3 device. And to study the microstructure, we conducted research on an optical microscope -AC100 and a raster electron microscope "Nanolab 7" of the company "OPTON". The values of the electrical parameters of the studied composites were calculated on the basis of the obtained "lgp- t" dependence. We have studied mechanical properties.

Result. In TiC-TiB$_2$-BN-**SiC-B$_4$C-** β-**SiAlON-Al$_2$O$_3$** system we obtained nanocomposites with high mechanical properties. The advantage of this method is that compounds, which are newly formed thanks to interaction going on at thermal treatment: Si$_3$N$_4$, Si, AlN are active, which contributes to **β**-SiALON formation at relatively low temperature, at 1300-1350^{0}C. It is evident that inculcation of ALN in crystal skeleton of ß-Si$_3$N$_4$ is easier since at this temperature interval crystal skeleton of Si$_3$N$_4$ is still in the process of formation. ß-SiAlON was formed at 1450^{0}C. Part of boron carbide was transformed into boron nitride in nitrogen environment and in titanium diboride, which in the case of both composites is in small quantities.

Conclusion. The phase composition of the obtained composite provides high physical-technical and performance properties of these nanocomposites. Compression strength-2198 MPa, Bending strength-271 MPa, Thermal expansion coefficient a$_{20-700}$-3.8 10^{-6} ^{0}C.

Key words: nanocomposite; hot press; electron microscope; phase composition; B$_4$C-BN-TiC-TiB$_2$-SiC-β-SIALON-Al$_2$O$_3$ nano-powder system.

1. INTRODUCTION

SIALON is a general name for a large family of silicon nitride-based ceramic alloys, it was first adopted in the beginning of 1970.β-SIALON is the most well-known phase. Its chemical formula $Si_{6-z}Al_zO_zN_{8-z}$ (z = 0–4.2) and its hexagonal crystal structure are similar to the structure of β-Si_3N_4.

SIALON is distinguished by: high hardness, strength, wear resistance. It retains these properties under high temperature conditions.

Composites working at high temperatures should be characterized by high density, hardness, thermal resistance and should retain these properties when working at high temperatures. Composites obtained from highly refractory oxide ceramics retain their hardness at high temperatures but are characterized by a high coefficient of thermal expansion and therefore low thermal resistance. Carbide-based ceramics have a relatively high coefficient of thermal expansion, but they are oxidized easily when working at high temperatures. Because of this, science has turned its attention to obtain super high-strength composites - SIALONs [1-7]. The results of our work [8-10] show that the composites obtained with the SIALON matrix are highly refractory materials with high performance properties and retain these properties when working at high temperatures. For the study we used electron microscopic, optical and X-ray phase analysis methods.

The paper describes the preparation of a super-ceramic composite with high macro and micro-mechanical properties of SIALON carbide at relatively low temperatures using an innovative, simple technology. As is known, SIALONS are obtained at temperatures of 1800-2000 °C. With the help of vitrified (96 mas. % glass phase) perlite-2-3 mas. %

dopant, we obtained similar material at 1450 °C and in the composition with titanium carbide, boron nitride, boron carbide, silicon carbide and aluminum oxide (nanopowder), we were able to obtain eutectic precipitation at relatively low temperature - 1620 °C by hot pressing. The material is so hard, that it damaged the diamond beads when trying to treat it, and a 3000 atmosphere water jet failed to cut the specimen.

X-ray is performed on DRON-3. Electron microscopic research was performed on a raster electron microscope "Nanolab 7" of the company "OPTON". No special form of samples is required for this study, only a sample fracture is required. It should be noted that the fracture is better to be new, because after some time the surface of the fracture might be covered with dust particles or oxides, which reduces the contrast and makes it difficult to distinguish phases In addition, the ions continue to move on the surface of the new fracture for some time, which makes the study very interesting.

2. MAIN PART

To obtain the composites, we prepared mixtures, the composition of which is given in Table 1. To C-18 composite we have added carbon fiber, which is characterized by high elasticity modulus (200-935GPa), high- tensile strength (1-3 GPa), with these properties it is the desired component, since it strengthens the composite material [11].

The samples were made in a cylindrical shape by the semi-dry method, the molding pressure was 20 MPa. After drying the samples were burned out in a silite oven at a temperature of 1450°C. Mode 5°C /min. At the final temperature the samples were kept for 40 minutes.

The physical-technical characteristics and electrical properties of the finished samples, compression strength and bending strength, impact viscosity, density, thermal resistance and thermal expansion coefficients were studied.

MATERIAL COMPOSITION OF COMPOSITES. TABLE 1

Composition of the initial component, mass%												
Composite index	kaolin (Ukraine)	TiC	Al	Al_2O_3	SiC	Si	Perlite Aragats (Armenia)	BN	Y_2O_3	MgO	B_4C	Carbon fiber
C-19	5	-	17	22	21	20	2	-	1.5	1	10.5	_
C-18	_	-	18	20	23	19	_	-	1.5	1	14.5	3
C-16	-	5	16	18	20	17	2	9	1.5	1	10.5	-
C-17	-	6	16	18	22	17	2	11	1.5	1	5.5	-

The bending strength was measured on a German-made disrupting machine R-100, which has a device determining the strength limit of the specimens on a three-point bend. The loading speed was 5 mm/hr.

When determining the bending strength limit, the maximum stress is calculated by the following formula:

$\sigma_{bend.} = 3/2. Pl_0/bh^2$,

where :P- is the force at which the sample was disrupted, kg; l_0- distance between supports at 3-point load = 25 mm; b- sample cross-section width, mm; h- the height on which the stress is applied to the specimen, mm. The test results of C-19 and C-18 composites are given in Table 2.

Table 2

THE PHYSICAL-TECHNICAL CHARACTERISTICS OF COMPOSITES

Composite name	Density g/cm^3	compression strength $\sigma_{press.}$ MPa	Bending strength $\sigma_{bend.}$ MPa	Impact viscosity a, kj/m^2	Thermal expansion coefficient α, $10^{-6}(20-700^0C)$
C-19	3,11	1844,4	262	17,62	3,81
C-18	2,99	2189,8	264	18,14	3,83
C-16	3.12	2194.4	268	18.90	3.78
C-17	3.16	2198.5	271	18.80	3.82

Impact viscosity was determined by the pendulum impact testing machine. When the sample is crushed, the scale marks the swing angle of the pendulum β. Impact-bending strength is calculated by the following formula:

$$A_{imp.} = A/S$$

where: A - work spent to crush sample, kilo joules (kJ); S - the cross-sectional area of the samples, m^2. For the C-19 composite samples: the cross-sectional dimensions were 1 cm x 0.35 cm; a $= \frac{6,17}{1 \times 0,35} = 17,62$ kJ/m^2 ; for the C-18 composite samples: the cross-sectional dimensions were 1 cm x 0.2 cm; a $= \frac{6,17}{1 \times 0,34} = 18.14$ kJ / m^2.

As can be seen from Table 2, the bending strength and the impact viscosity of both composites (C-19, C-18) are almost the same and amount to 262; 264 MPa and 17.62; 18.14 kj/m^2 respectively. Ceramic composites experience thermal load sand gas-thermal impacts when working at high temperatures. In all ceramic materials there are invisible micro-cracks [12] and when the strength of the product is less than the loads, these loads are converted into the decomposition stress energy. At critical loads, high energies develop, causing decomposition of the product.

To determine these energies, Z. Kovziridze proposed a formula for calculating the failure stress energy [13-14], which establishes a universal interdependence between the failure stress energy of a product, the mass of the product, and the rate of crack development under critical stress conditions. The Z. Kovziridzes formula for calculating the failure stress energy is as follows:

$$E_{td} = ma_{c.p.,}$$

Where E_{td} is the failure stress energy, kilo joules; m- sample mass, g; $a_{c.p.}$- the crack development rate -2000 m/sc.

In our case the sample dimensions were 5,2x5,2x45mm, the sample mass was 3.86g. According to Z. Kovziridze's formula the failure stress energy is:

$$E_{td} = ma_{c.p.} = 3,86 \times 2000 = 7,72 \text{ kJ.}$$

The thermal expansion coefficient of the composites (C-19, C-18) was determined with the help of a quartz vertical dilatometer -DKV for measuring the temperature coefficient of linear thermal expansion in the temperature range (20-700^{0}C). Table 2 and Figure 1 show that this indicator is the same for both composites and is a = 3.88 and $3.80 \cdot 10^{-6}$, respectively.

It is known from the literature [13] that the coefficient of thermal expansion of corundum ceramics is high and is $\alpha_{20-300C} = 6,2 \cdot 10^{-6}$. While the low-oxygen content of refractory compounds, namely silicon carbide, is $a=5,18 \cdot 10^{-6}$ and is characterized by high thermal resistance [15] It should be noted that the composites we obtained (C-19, C-18) are characterized even by a lower coefficient of thermal expansion, respectively $a=3,88$ and $3.80 \cdot 10^{-6}$ and a correspondingly higher thermal resistance, which is very important for composites that have to work for a long time at high temperatures and in an aggressive medium (Fig. 1).
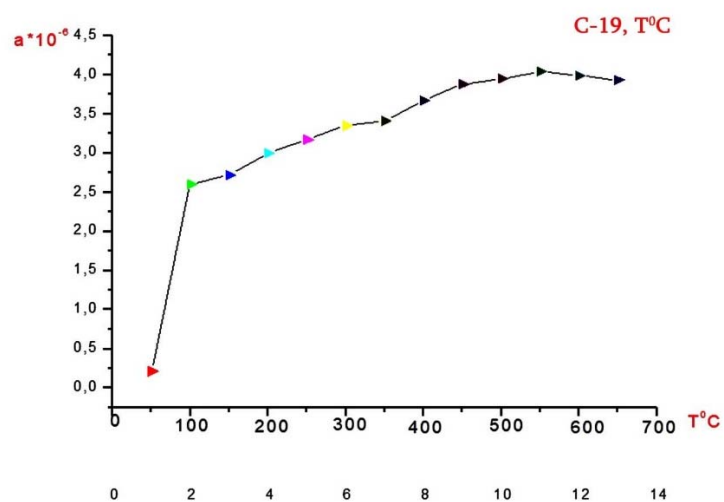
a
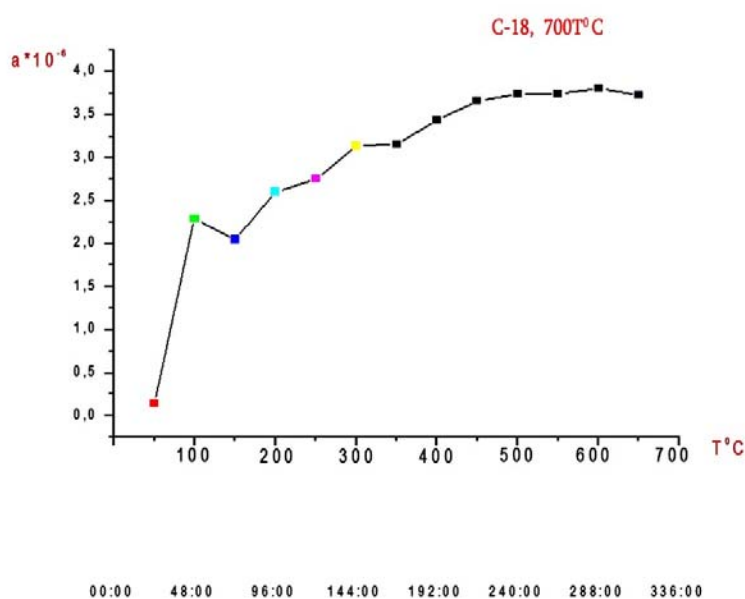
b

Fig. 1. Thermal expansion coefficient and temperature interdependence

Electrical characteristics have been established for the composite of compositions (on the device created by Prof. T. Cheishvili - CH-24) which were obtained as a result of the "resistance-temperature" dependence experiment. The volumetric electrical resistance of the composites was determined in the section allowing measurements at high-temperatures in the range of 20-300⁰C, by using an electron ohm meter as the measuring instrument. Graphite electrodes were placed on the surface of

the prismatic samples (the upper measuring electrode had a diameter of 14 mm and the lower measuring electrode had a diameter of 16 mm).The dependence of the test specimens on the "specific resistance-temperature" is linear, revealing the peculiarities that an increase in temperature causes a decrease in electrical resistance. Besides the C-19 specimen is characterized by lower values of electric resistance than the specimen C-18, C-16, C17. The difference between the electrical resistances is particularly noticeable at room temperature (the difference is approximately by three degree), but it is less evident at high temperatures (the difference decreases to one degree), which is clear from the material reflecting the results of the experiment (Fig. 2). The values of the electrical parameters of the study composites were calculated on the basis of the obtained "lgp- t" dependence. Three electrical characteristics were determined for composites: the temperature coefficients of electrical sensitivity (B) and electrical resistivity (α_T) the activation energy of electrical conductivity (Ea), the value of which are presented in Table 3. The difference between the electrical characteristics was found to be significant (C-18 composite data are approximately 5 times higher than those obtained for C-19 composite).

It should be noted that composites have a negative α_T (resistance decreases with increasing temperature) and low value of Ea- (realization of electronic type of electrical conductivity is expected for both materials).

The results obtained should be related to the basic phases represented in C-19 and C-18 composites obtained by the synthesis at 1450^0C, under the same conditions. Regarding the compositions C-16 and C-17, the "log $_{P-T}$" dependences, which occupy an intermediate position between C-19 and C-18, it can be noted that the compositions contain two "new" ingredients - TiC and BN. In some high-temperature synthesis of composites, one cannot exclude the participation of these in the formation of a new semiconductor phase - TiB_2. Based on the composition of the composition C-16 and C-17 (Table 1), the expected amount of TiB_2 should be greater in the composition of C-17. This is also confirmed by the electrical properties in comparison with composition C-16; composition C-17 has lower values of resistivity and activation energy.

According to the results of X-ray phase analysis, the leading phase in the composite of both compositions is SIALON. They also contain five other crystalline compounds of different nature. Due to their electrical properties they can be divided into two groups: Dielectrics (a- Al_2O_3, BN, AlN) and semiconductors (SiC, Si). Considering the identical conditions for obtaining the C-19 and C-18 composites, the factor determining their low resistance and activation energy values could have been the number of SiC and Si solid phases with semiconductor properties existed in the study materials.
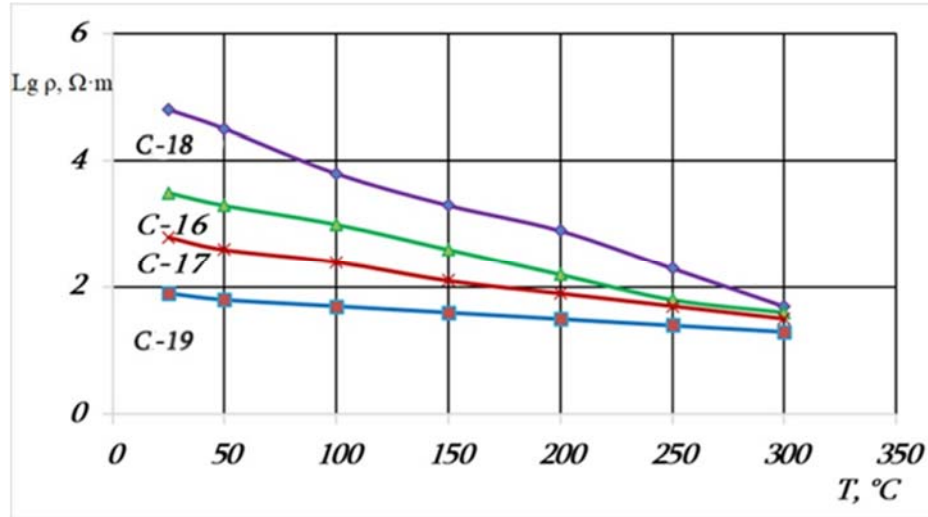
Fig. 2. Specific electrical resistance and temperature dependence

Based on the comparison of the electrical characteristics of composites, it can be assumed that the concentrations of SiC and Si in the C-19 composite must be higher than in the C-18 composite. This could be detected by two approaches: by determining the amount of SiC and Si or by the density of the materials. Both approaches proved to be unusable for C-19 and C-18 composites, since quantitative calculations based on the available X-ray were impossible (due to the abundance of crystal phases and the coincidence of their characteristic intensity peaks) and also the negligible differences between mass densities. (d = 3.11 for C-19; d = 2.99 g /cm^3 for C-18). In any case, the number of SiC in C-19 could not have been higher than in C-18, judging by the material composition of the test composites.

At the same time, X-ray phase analysis revealed the presence of Si in both composites, which could affect the electrical conductivity of the composite. But the Si content in the initial mixture (according to the material compositions) is identical and amounts to wt. 20%. At the same time, the C-19 composite body contains two natural rocks (kaolin and perlite) that contain silicon dioxide. Kaolin (5 wt.%) and perlite (2.0 wt.%) provide approximately 5.2 wt.% and 3.0 wt.% Si in the C-19 composition, respectively. The reason for this is the structural breakdown of the mineral kaolinite in the geopolymer (kaolin) caused by the temperature and the possibility of conducting the parallel alumothermic process:

$$4\,Al + 3\,SiO_2 = 2\,Al_2O_3 + 3Si.$$
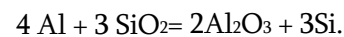
This process will result in an additional 2.4% by weight of Si in the C-19 composite, and it is practically expected that the amount of Si in C-19 will be 24.4% by weight. A contributing factor to the uptake of Si from SiO$_2$ may be the formation of a liquid phase caused by the low-temperature melting of perlite-1240^{0}C. Aluminum nitride is formed by the reaction of a portion of the aluminum powder in the initial mixture with nitrogen by the following reaction:

$$2\,Al + N_2 = 2\,AlN.$$

Table 3

Electrical characteristics values of the composites

Sample №	Coefficient of electrical sensitivity, $B(\Omega mK)$	Activation energy of electrical conductivity, $\Delta E(ev)$	Temperature coefficient of electrical resistance, $a\Delta_t$ (ΩmK^{-1})
C-18	-7170	1,24	$-2{,}6 \cdot 10^{-2}$
C-19	-1560	0,27	$-5{,}7 \cdot 10^{-3}$
C-16	-1625	0.65	$-1.4.10^{-2}$
C-17	-815	0.32	$-6.8.10^{-3}$

As a result of decomposition of kaolinite at high temperatures part of the aluminum powder restores silicon from SIO_2 according to the reaction above. This process could lead to a change in the ratio between an increase of the amount of semiconductor Si and AlN carrying the insulating properties in favor of Si, this would lead to the increase in electrical conductivity in the C-19 composite.

Structural study

The test specimens were prepared using the same technology as described in previous papers [16-21], i.e. the SIALON was synthesized in the nitrogen medium at 1400–1450⁰ C, and then the obtained mass was grounded in an attritor and the consolidated composite was obtained by hot pressing at 1620⁰C. , 40 minutes, delaying at final temperature for 8 min. under 30 MPa pressure.

70 μM of study samples of the composite obtained in this mode were cut from 70 mm diameter and 8 mm thick discs. The cut was made on a 395-M profile grinding machine with a 100 mm-diameter metal binding diamond cutting disc, diamond grain size 50/40 μm, cutter rotation speed 4000 rpm, cutting speed 0.7 mm / min.

The surface of the cut specimens was ground on a 3 G71 flat-bottomed grinding machine with a 200 mm- diameter diamond abrasive disc on a Bakelite binder, diamond grainsize-50/40μm.

Phase analysis of hot-pressed samples was performed on an X-ray machine DRON-3 using CuKα rays.
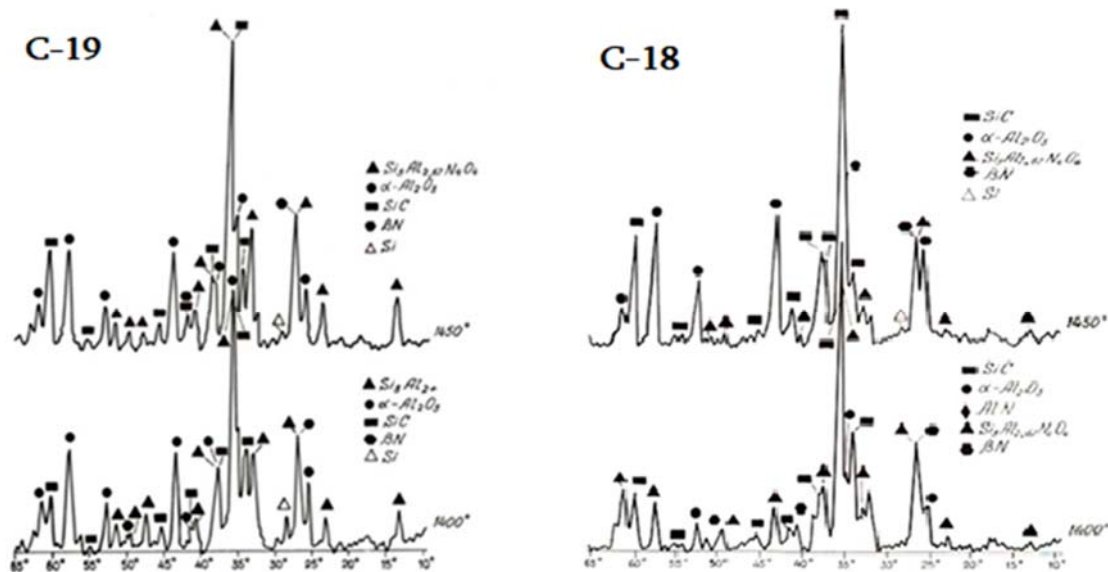
FIg. 3. C-19 and C-18 composites X-ray (1400-1450⁰C)

Examination of the X-Ray patterns of the samples burned out at 1400-1450⁰C (Fig. 3) shows that at 1400⁰C the characteristic reflexes of the SIALON are already observed in both composites, and at 1450⁰C their intensity is relatively increased. Judging by the intensity of the characteristic peaks of the SIALON, the number of SIALONs formed in the C-19 composite is relatively larger than in the C-18 composite, which can be explained by the presence of kaolin in the C-19 composition. In our opinion, this is due to the nitrogenation of the thermodynamically active kaolinite core $Al_2O_3.2SiO_2$, which was formed as a result of the decomposition of the mineral kaolinite. The following phases have been observed in both composites: Si-AL-O-N, SiC, α-Al_2O_3, BN, and Si (small amount unreacted.).

Part of boron carbide and titanium carbide in the composites was converted to boron nitride and titanium diboride upon burning out in nitrogen medium at 1400⁰C by the following reaction: $B_4C+2N_2=4BN+C$, and $B_4C+2TiC=2TiB_2+3C$, which

in the case of both composites is in small quantities. Newly formed, fine-grained boron nitride improves the microstructure, which is a prerequisite for high mechanical properties, such as: high thermal conductivity, low thermal expansion, good resistance to thermal shocks, easy workability, chemical inertness and low wettability with molten metals. It is used in radiators, boron-alloyed silicon semiconductors, welding trays, crucibles, microwave tubes, sputtering targets, high-precision welding, foundry production, etc.

Analysis performed using an optical microscope showed that the composites in both cases were silicon car bide and corundum grains located in the matrix (Fig. 2). At the same time the microstructure of C-18 composite is more fine-grained. It can be assumed that during the sintering process of C-19 composite, due to the composition of these composites, more liquid phase is generated than during the sintering process of C-18, contributing to the sintering intensity, which is evidenced by the relatively low porosity of C-19 composite. At the

35

same time, the liquid phase promotes the appearance of small grains and their subsequent recrystallization into large grains.

Electron microscopy shows the surface of a well-sintered specimen, on which crystals of the basic phases contained in C-19 composites are clearly seen, namely silicon carbide and corundum grains distributed in the SIALON matrix, even the finest grains of boron nitride are also observed, which are better seen when magnified at close-up (Fig. 4).

When identifying grains of silicon carbide and corundum, along with SEM images, we relied on the results of X-ray diffraction analysis and X-ray spectral microanalysis.

Figure 5 and 6 shows the micro-X-ray spectral analysis image s of the C-19 and C-18 composites, the spectrum of the 3 sections and the scheme of the constituent elements, their percentage content, which shows that the main constituent (matrix) of the composite is SiAlON-BN.

a)

b)

c)

d)
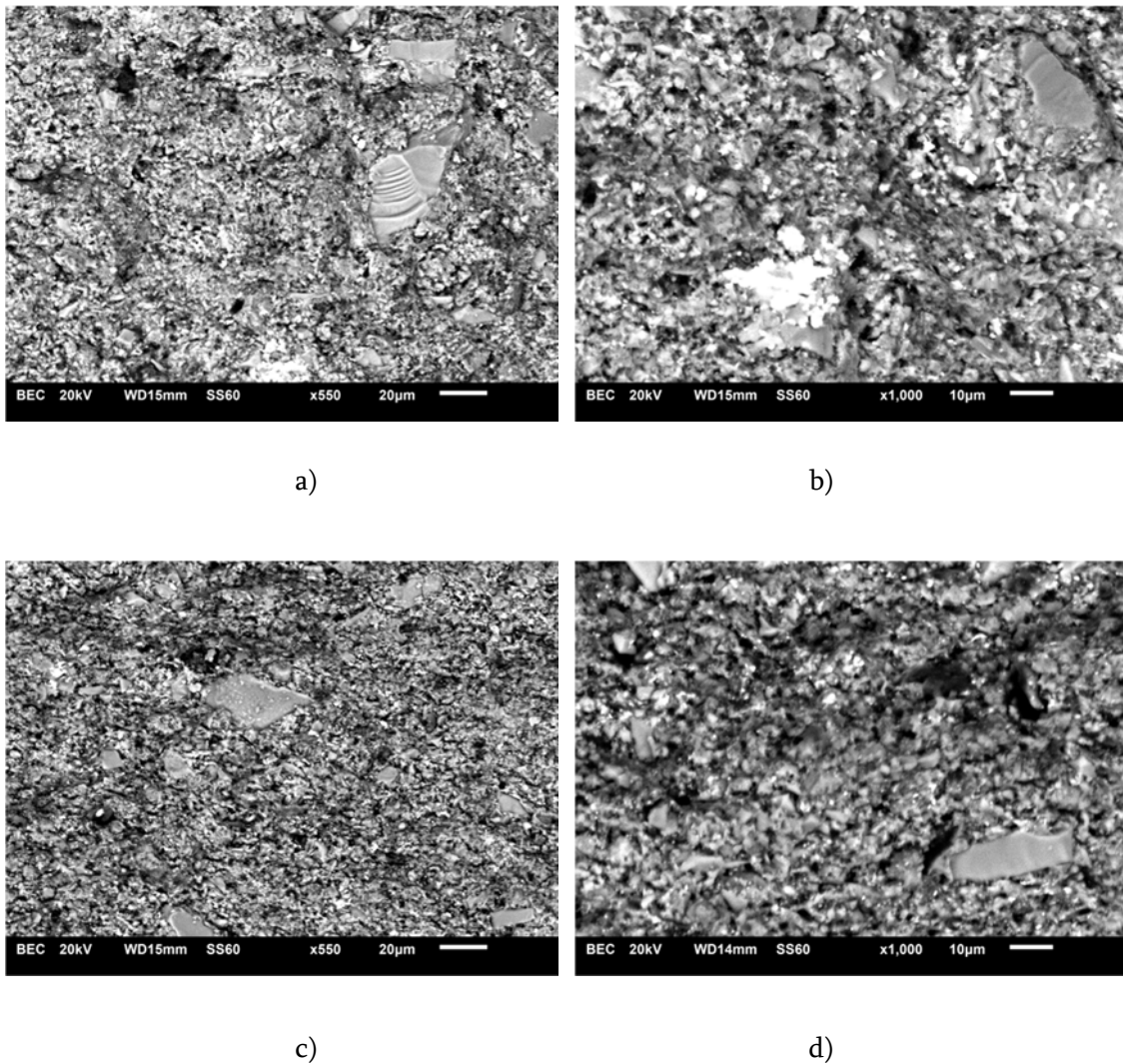
Fig.4. C -19 (a, b) and C -18 (c, d) composites Electronic-microscopic images at different magnifications X - 550; X-1000
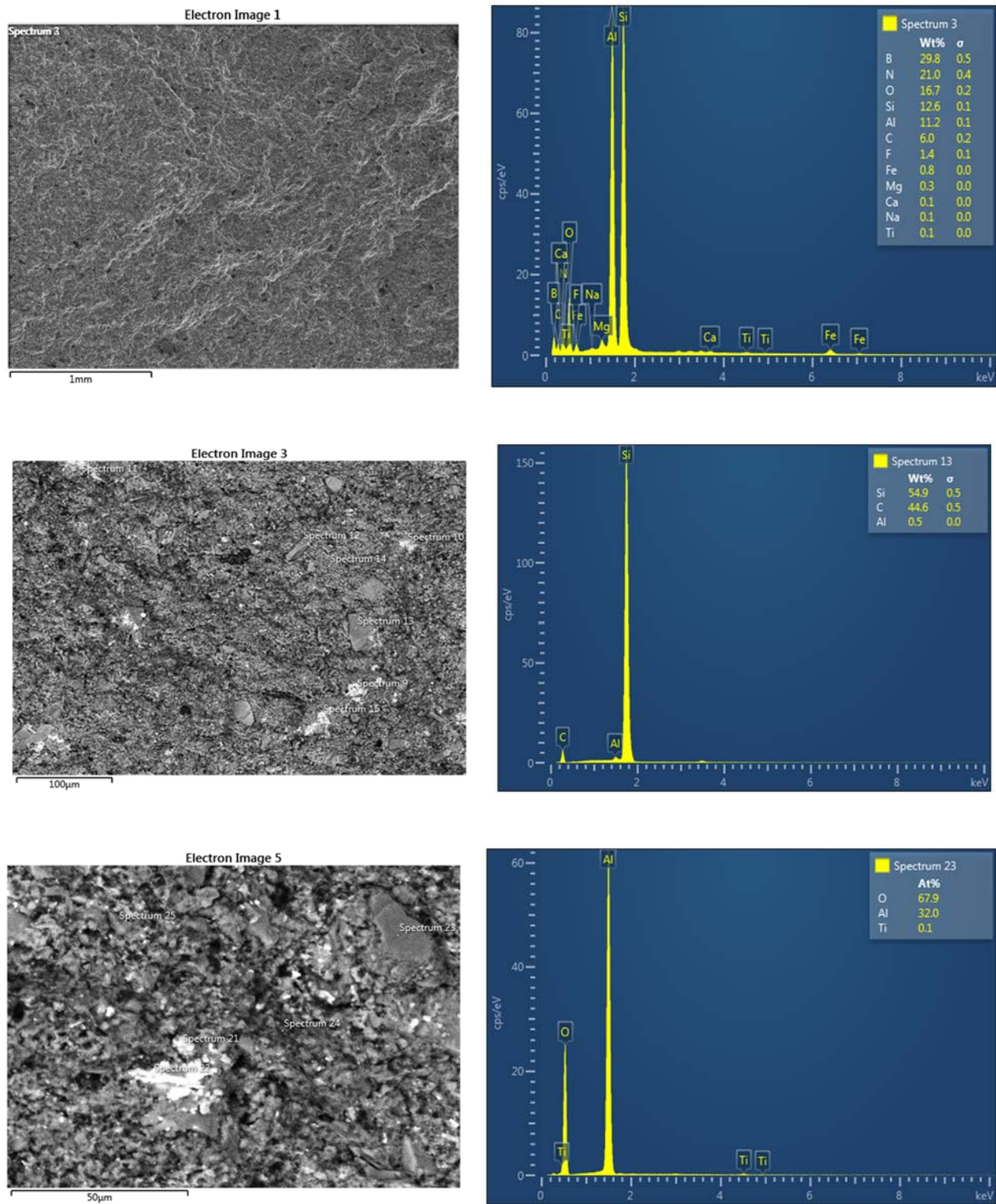
Fig. 5. Electronic-microscopic and
micro -X-ray spectral images of C -19 composite
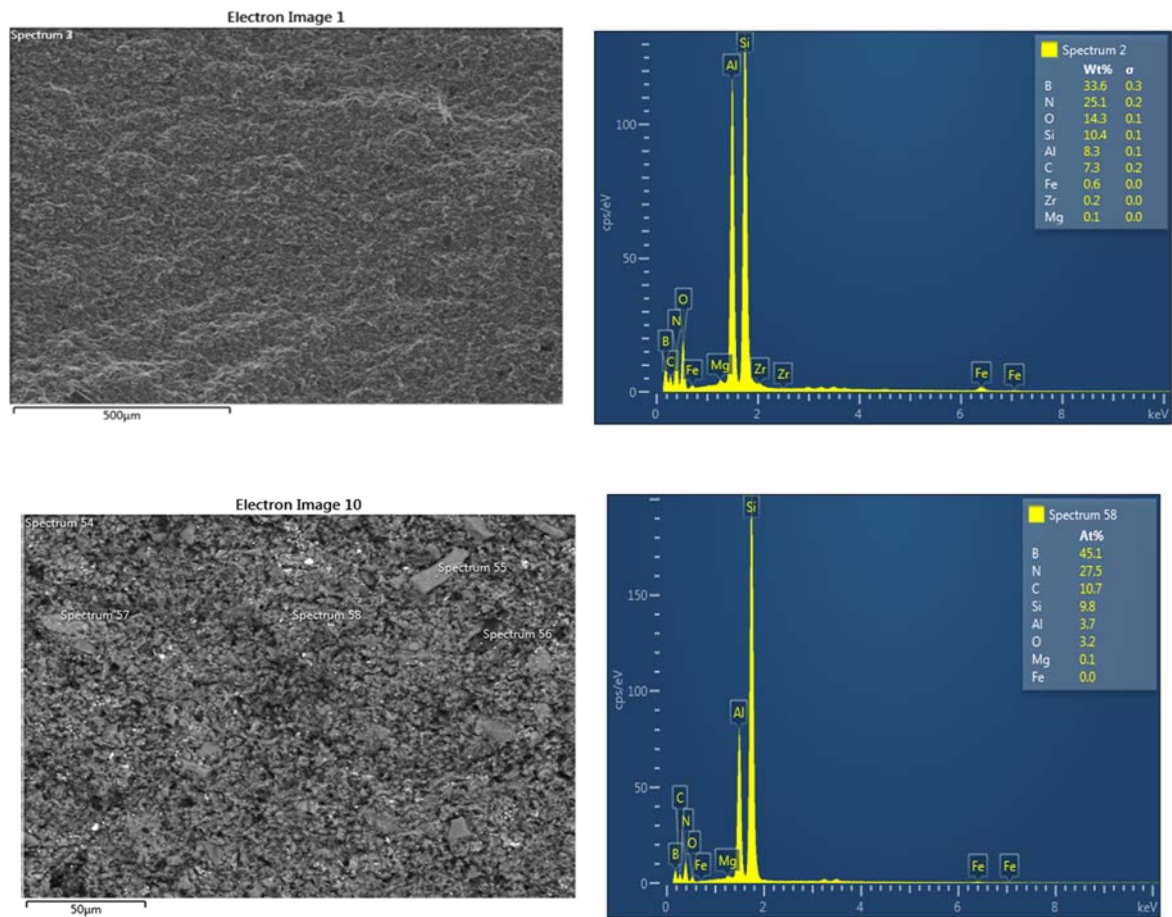
Fig. 6. Electronic-microscopic and microrentgeno -X-ray spectral images of C -18 composite
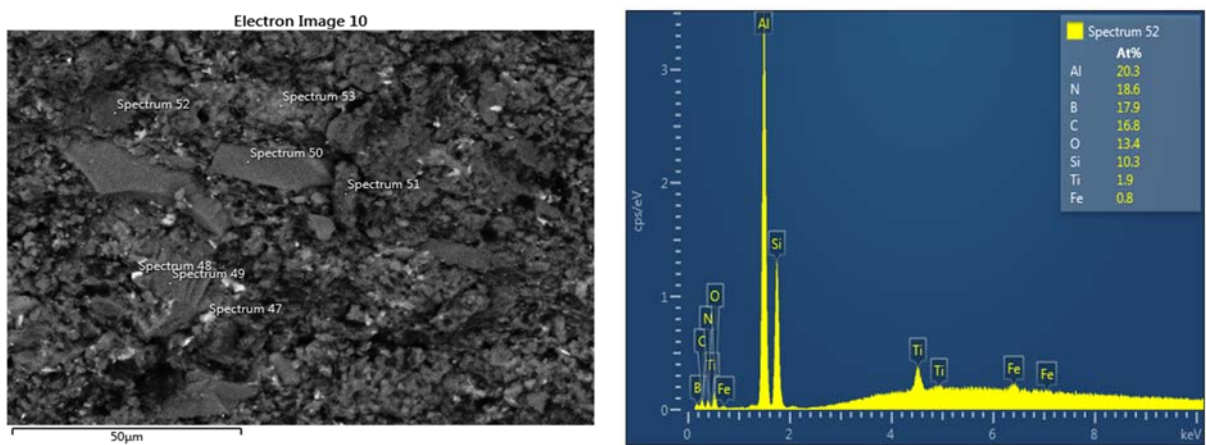
Fig.7 Electronic-microscopic and microrentgeno -X-ray spectral images of C -16 composite

Fig.7 and Fig 8 shows the micro-X-ray spectral analysis image s of the C-16 and C-17 composites, the spectrum of the sections and the scheme of the constituent elements, their percentage content, which shows that the main constituent (matrix) of the composite is TiC, B_4C, TiB_2, SiC, Al_2O_3, SiAlON-BN.
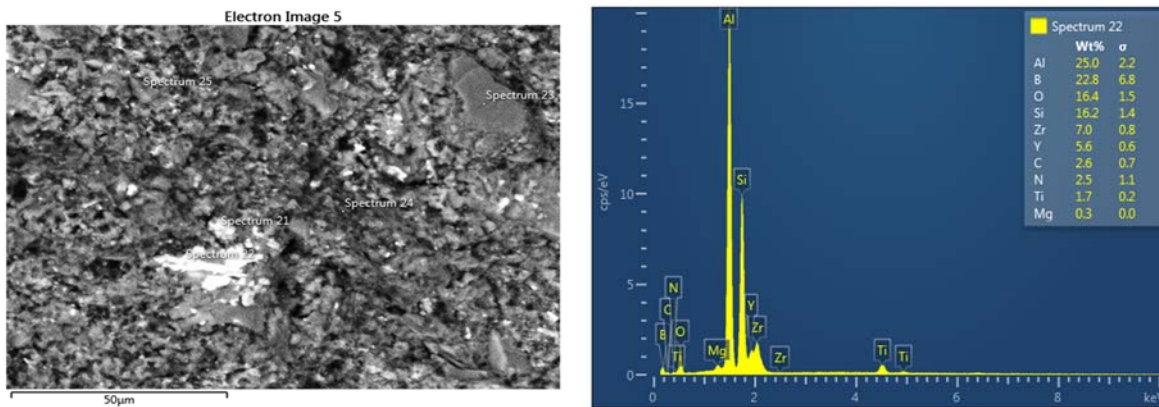
Fig.8 Electronic-microscopic and microrentgeno –
X-ray spectral images of C -17 composite

Table 4

shows the test condition of SIALON.

<<* Test condition-SiAlON-100 ***>>**

Test mode	Load-unload		
Sample name	SiAlon-zv	Sample No.	#1
Test force	100.000[gf]	Minimum force	0.200[gf]
Loading speed	1.0(7.1448[gf/sec])	Hold time at load	5[sec]
Hold time at unload	3[sec]	Test count	23
Parameter name	Temp	Parameter	20
Comment	20.06.17-SiAlon-zv-100;DHV5-3		
Poisson's ratio	0.190		
Cf-Ap,As Correction	ON	Indenter type	Vickers
Read times	2	Objective lens	50
Indenter elastic	1.140e+006[N/mm2]	Indenter poisson's ratio	0.070

<<*** Test result ***>>

SEQ	Fmax	hmax	hp	hr	DHV-1	DHV-2	Eit	Length	HV	Data name
	[gf]	[um]	[um]	[um]			[N/mm2]	[um]		
1	100.753	2.0927	1.0353	1.3623	1124.606	4595.143	2.023e+005	12.133	1269.108	SiAlon-100(1)
2	100.862	2.1408	1.1973	1.4454	1075.849	3439.729	2.028e+005	10.673	1641.878	SiAlon-100(2)
3	100.954	2.1185	1.0085	1.3472	1099.608	4852.203	1.911e+005	11.989	1302.427	SiAlon-100(3)
4	100.844	2.1300	0.9980	1.3526	1086.598	4949.256	1.881e+005	11.623	1384.295	SiAlon-100(4)
5	100.935	2.1822	1.1183	1.4290	1036.181	3945.265	1.855e+005	12.721	1156.721	SiAlon-100(5)
6	100.624	2.0945	1.0240	1.3135	1121.301	4691.482	1.921e+005	11.843	1330.428	SiAlon-100(6)
7	100.551	2.1229	1.0193	1.3350	1090.715	4731.042	1.868e+005	11.551	1397.624	SiAlon-100(7)
8	100.826	2.1357	1.0016	1.3362	1080.626	4912.610	1.834e+005	11.550	1401.679	SiAlon-100(8)
9	100.826	2.1173	0.9846	1.2881	1099.473	5084.458	1.815e+005	11.404	1437.730	SiAlon-100(9)
10	100.825	2.1761	1.0974	1.4160	1040.858	4092.733	1.848e+005	11.697	1366.620	SiAlon-100(10)
11	100.807	2.1566	1.0491	1.3859	1059.580	4477.130	1.857e+005	----	----	SiAlon-100(11)
Average	100.801	2.1334	1.0485	1.3646	1083.218	4524.641	1.895e+005	11.718	1368.851	
Std. Dev.	0.120	0.029	0.064	0.049	28.966	502.835	7155.469	0.529	125.730	
CV	0.119	1.372	6.141	3.617	2.674	11.113	3.777	4.518	9.185	

<<*** Force-Depth graph ***>>

Force-Depth graph

Depth[um]
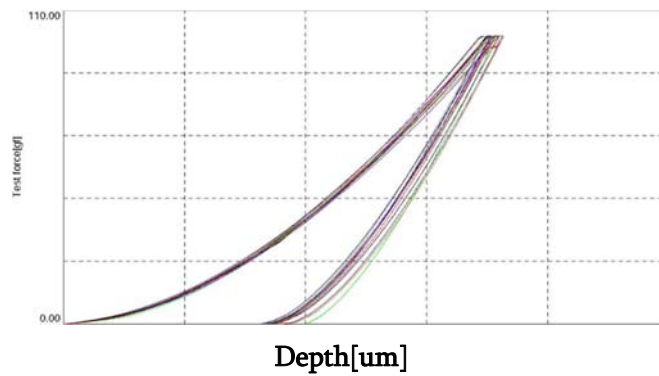
<<*** Depth-Time graph ***>>
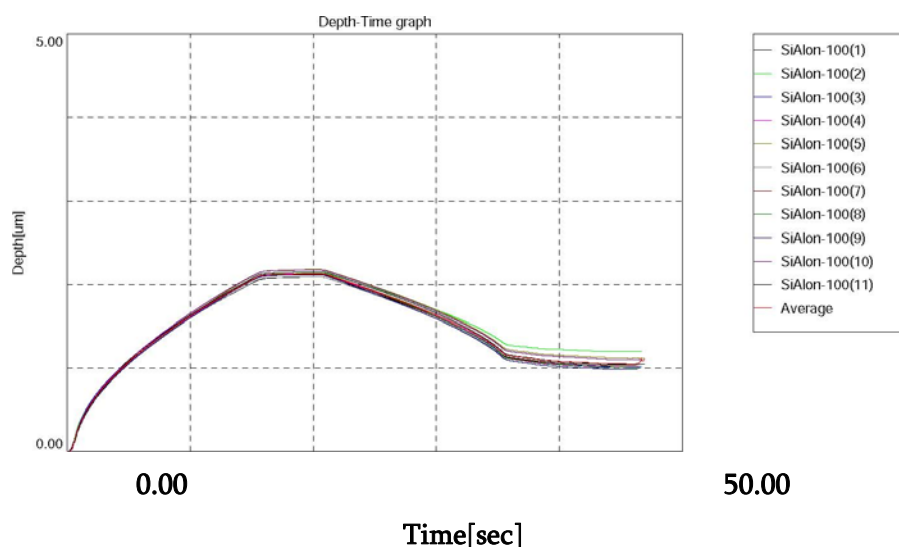
Fig. 9 Mikromechanical charaqteristics of SIALON

The results of micro-X-ray spectroscopy and electron microscopy of the given composites are consistent with X-ray structural analysis. In the matrix of composites C-19 and C-18 there are represented: β-SiALON-Al$_2$O$_3$-SiC, BN crystals are distributed in the matrix and In the Composites CH-16 and CH-17 there are represented TiC-TiB$_2$-BN-SiC-B$_4$C-β-SiAlON-Al$_2$O$_3$ phases. Table 5 shows d the data on phase components in C-19 and C-18 composites.

To determine the porosity, we selected the field of vision and determined its area. In the field of vision, we calculated the number of pores according to the size of their diameter; determined the volumetric content and the middle diameter of pores for each composite. The total pore content in C-19 composite is approximately Pvol = 3,7%, for C-18 -Pvol = 4,8%, the middle size of the pores makes up Pm ≈ 3,75 and 4.5 μM accordingly.

The maximum and minimum size of SiC grains in C-19 composite is 9-3 μM, middle size = 6 μM; in C -18 composite - 8-4 μM, middle size = 6 μM.

The maximum and minimum size of aluminum oxide grains is 1 / 1μM for C-19 composite and 1/ 0,8 μM for C-18 composite. The average size of aluminum oxide grains in each composite is 1 and 0.8μM, respectively. As for boron nitride, its dimensions are minimal and approximately equal to an average of 200 nM.

The average grain size in total Km = 6.5 and 6.6 μM, respectively. Glassy phase volume fraction Gvol = 3 and 1% respectively;

Crystal shape factor

F_{kf}C-9=Dmax/Dmin=10.56/5.54=1.91;

F_{kf}C-10=Dmax/Dmin=10.56/6.25=1.69.

Crystal distribution factor in the matrix by our visual estimation, F_{kd} = 0.9.

The unreacted residue of silicon is about 2 wt.%. In other cases, the Si mass in the than initial composition should be taken to be no more 18-19 percent. The carbon fiber dopant increased the mechanical properties by

Table 5

Data on phase components in C-19 and C-18 composites

Composite	Phase name	Field of vision S, μM²	Number of counted grains (pores), n	Grains (pores) Dmid. μM	Max. size of grain (pore) Dmax. μM (average)	Min. size of grain (pore) Dmin. μM (average)	Fкf-shape factor Dmax/Dmin
C-19	SiC	2070	12	11	9	3	
	Al2O3		250	1	1	1	
	SiALON		55	14	32	18	
	BN		45	0.2	0.25	0.16	
	Average		90.5	6.5	10.56	5.54	1.91
	Pores		10	3.75	4	3,5	1,15
C-18	SiC	2070	15	10	8	4	
	Al2O3		280	0.8	1	0.8	
	SiALON		50	9	33	20	
	BN		45	0.22	0.27	0.18	
	Average		97.5	6,6	10.56	6.25	1.69
	Pores		12	4.5	5	4	1.25

3 wt.% in C-18 (Table 2). The crystalline phase is: in C-19, 100-(V porous +V glassy)=100-(3.7+3) =93.3, while in C-18: 100-(V porous++V glassy) = 100-(4.8 + 1) = 94.2.

The dependence of the micro- and macro-mechanical characteristics of the materials on the crystalline phase content in the composite was calculated according to Z.Kovziridze's [22] formula:

$$\sigma_d = \frac{P.Fkd}{Km\ Kv\ Fkf},$$

Where: P-load; Km- middle size of crystals; K v- volume fraction of crystals in the matrix; F kd- crystals distribution factor in the matrix, which is determined by the researcher; in case of equal distribution it equals to 1, in case of unequal

distribution = 0.9; Fkf-crystal shape factor, is taken as the ratio of the largest characteristic size of a crystal to the smallest, which allows us to characterize the shape of a given set of crystals, according to which we are able to define correlation of mechanical characteristic in the matrix from the crystal phase characteristics in our proposed formula. By inserting the data of Table 4 into the formula we get:

$$\sigma_d = \frac{2187.5 \times 0.9}{6.5 \times 94.2 \times 1.69} = \frac{1968.75}{1035} = 1.9.$$

The dependence of the macro-mechanical characteristics of the materials on the porous phase

content in the composite was also determined according to Kovziridze [23] formula.

$$\sigma_{m/p} = \frac{P}{F_p \cdot P_d \cdot P_{vol} \cdot P_m} =$$

$$= \frac{2187.5}{0.9 \times 1.25 \times 4.5 \times 4.8} = \frac{2187.5}{24.3} = 90 \text{ MPa/}\mu M^2$$

Where: P-is load, MPa; F_p- shape factor of the pore; P_d- pores distribution factor in the matrix. Determination of this value and the evaluation of its significance depends on the researcher, based on the morphological picture depending on how the pores are distributed in the material and what size they are. The value of the factor can vary from 1 to 0.8. If the pores are evenly distributed in the matrix and are about the same size, the factor is determined to be equal to 1; if the pores are unevenly distributed, the factor equals to 0.9 and if the coalescence process of pores is initiated, factor is 0.8; P_{vol}.-volumetric fraction of the porous phase in the matrix; P_m- the average size of the pores.

3. CONCLUSION

The obtained composites have been studied and determined the phase composition of the composites; in the case of both composites the main phase, i.e. the matrix is $TiC-TiB_2-B4C-$ $SiAlON-SiC-BN-Al2O3$, in which the BN grains are distributed, originated in the nitrogenation process as a result of the decomposition of boron carbide by nitrogen and the replacement of carbon with nitrogen. The composites are well sintered and the crystals are bonded together with a layer of SiAlON. Material of high physical-technical characteristics is obtained. The advantage of this method is that compounds, which are newly formed thanks to interaction going on at thermal treatment: Si_3N_4, Si, AlN are active, which contributes to **β-SiALON** formation at relatively low temperature, at $1300-1350^0$C. It is evident that inculcation of ALN in crystal skeleton of ß-Si_3N_4 is easier since at this temperature interval crystal skeleton of Si_3N_4 is still in the process of formation. ß-SiAlON was formed at 1450^0C. Part of boron carbide was transformed into boron nitride in nitrogen environment and in titanium diboride, which in the case of both composites is in small quantities. Composite with low resistance (specific resistance approximately about 10^2 Ohm.M), activation energy (E = 0.27 eV) and the temperature coefficient of electrical resistance ($\Delta\alpha$ T = 0.057 k^{-1}) with main part of β-SiAlON. Compression strength-2198 MPa, Bending strength-271 MPa, HV=1368. Thermal expansion coefficient a_{20-700}-3.8 10^{-6} ^{0}C.

REFERENCES

1. Osman Sahin, Orhan Uzun, Malgorzata Sopicka-Lizer, Hasan Gocmez, Ugur Kolemen. Dynamic hardness and elastic modulus calculation of porous SiAlON ceramics using depth-sensing indentation technique. Journal of the European Ceramic Society 28 (2008) p.1235–1242.

2. Z. Hou, F. Ye, L. Liu, - Effects of pore shape and porosity on the dielectric constant of porous β-

SiAlON ceramics, J. Eur. Ceram. Soc. 35 (2015) 4115–4120.

3. G.J. Zhang, J.F. Yang, T. Ohji, - Fabrication of porous ceramics with unidirectionally aligned continuous pores, J. Am. Ceram. Soc. 84 (6) (2001) 1395–1397.

4. B. Li, K. Liu, C.R. Zhang, S.Q. Wang, - Fabrication and properties of borazine derived boron nitride bonded porous silicon aluminum oxynitride wave-transparent composite, J. Eur. Ceram. Soc. 34 (15) (2014) 3591–3595.

5. J.F. Yang, Y. Beppu, G.J. Zhang, T. Ohji, S. Kanzaki, - Synthesis and properties of porous single-phase β-SiAlON ceramics, J. Am. Ceram. Soc. 85 (7) (2002), 1879–1881.

6. C. Zhang, R. Janssen, N. Claussen, - Pressureless sintering of β-SiAlON with improved green strength by using metallic Al powder, Mater. Lett. 57 (2003)3352–3356.

7. S.-L. Hwang, I.-W. Chen, - Reaction hot pressing of α- and β-SiAlON ceramics, J. Am. Ceram. Soc. 77 (1994) 165–171.

8. F. Çalıskan, Improvement in sinterability of β-SiAlON produced from kaolin, J. Alloy. Compd. 602 (2014) 14–149.

9. Z. Kovziridze, N. Nijharadze, G. Tabatadze, T. Cheishvili, Z. Mestvirishvili, E. Nikoeleishvili, M. Mshvildadze, N. Darakhvelidze. Obtaining of Nanocomposites in SiC-SiAlON and Al2O3-SiAlON System by Alumothermal Processes. //Journal of Electronics Cooling and Thermal Control, 2014, 4, 105-115. http://dx.doi.org/10.4236/jectc.2014.44012

10. Bradley A. Newcomb, Han G.Chae, - Handbook of Properties of Textile and Technical Fibres (Second Edition) 2018, Pages 841-871.

11. Z. Kovziridze, N. Nijharadze, G. Tabatadze, N. Darakhvelidze, Z. Mestvirishvili, -Smart Materials in the System SiAlON-SiC-Al2O3-TiB2-ZrB2, Bit's 2nd Annual World Congress of Smart materials 2016. p. 558. Singapore

12. Griffith A.A-phil, Trans. Roy. Soc. London A. 221.1920.1963.

13. Kovzirize Z. The Decomposition Stress Energy Formula. Georgian Ceramics Association, Journal "Ceramics and Advanced Technologies"#1 (39), 2018. pg. 11-23.

14. Z.Kovziridze. Failure Stress Energy Formula. Journal of Electronics Cooling and Thermal Conrtol. 2018.8.pp.31-47.
Http: // www.scirp.org/journal/jectc.

15. SamsonovG.V., Physico-chemical Properties of Oxides, M., Metallurgy, 1978.

16. SamsonovG.V., Properties of High-melting-point Compounds, Short Reference Book. M., Metallurgy. 1978.

17. Kovziridze Z., NiJaradze N., Tabatadze G., Cheisvili T., Daraxvelidze N., Mestvirisvili Z., Msvildadze M., Nikoleisvili E. – Obtaining SiAlON,s by Nitroalumthermal Processes, Georgian Ceramics Association, Journal "Ceramics and Advanced Technologies", № 2 (32), 2014, pg. 23-31.

18. Z. Kovziridze, N. Nijharadze, G. Tabatadze, T. Cheishvili, Z. Mestvirishvili, E. NikoeleiShvili, M. Mshvildadze, N. Darakhvelidze. – Obtaining of Nanocomposites in SiC-SiAlON and Al2O3-SiAlON System by Alumothermal Processes. Journal of Electronics Cooling and Thermal Control, 2014, 4, pg. 105-115.
http://dx.doi.org/10.4236/jectc.2014.44012

19. Enquan He, Jianshe Yue, Lei Fan, Chao Wang and Hongjie Wang, - Synthesis of single phaseb-SiAlON ceramics by reaction-bonded sintering using Si and Al$_2$O$_3$ as raw materials. doi:10.1016/j. scriptamat. 2011.03.040.

20. Peng Jiang, Xiao fang Wu,Wendong Xue, JunhongChen,Wei Wang,Yong Li; - In-situ synthesis and reaction mechanism of β-SiAlON in the Al-Si$_3$N$_4$-Al$_2$O$_3$ compositematerial /http://dx.doi.org/10.1016/ j.ceramint. 2016.10.088.

21. Xing Deng, Xiangcheng Li, Boquan Zhu, Pingan Chen; - In-situ synthesis mechanism ofplate-shaped β-Sialon an ditseffect on Al$_2$O$_3$–Crefractory properties http://dx.doi.org/10.1016/j.ceramint. 2015.07.071

22. Z. Kovziridze. - The Formula of Dependence of Mechanical Characteristics of Materials on Crystalline Phase Composition in the Matrix. Advances in Materials Physics and Chemistry Vol.10 No.8, August 2020. ISSN: 2331-1959. DOI: 10.4236/ampc.2020.108013.

23. Z. Kovziridze. Macro-Mechanical Properties Porous Phase Dependence Formula. Journal of the Georgian Ceramists Associstion. Ceramics and Advanced Technologies.Vol. 20 1(39). 2018. Pp.28-34.

ჩქვიანი ჰეტერომოდულური ნანოკომპოზიტი TiC-TiB$_2$-BN-SiC-B$_4$C-SiAlON-Al$_2$O$_3$-C სისტემაში

ზ. კოვზირიძე, ნ. ნიჟარაძე, გ. ტაბატაძე, თ. ჭეიშვილი, ნ. დარახველიძე, მ. ბალახაშვილი

საქართველოს ტექნიკური უნივერსიტეტი. ბიონანოკერამიკისა და ნანოკომპოზიტების ტექნო-ლოგიის ინსტიტუტი. ბიონანოკერამიკისა და ნანოკომპოზიტების საუნივერსიტეტო მასალათ-მცოდნეობის ინსტიტუტი. 0175 თბილისი. სქართველო. კოსტავას 69

E-MAIL: kowsiri@gtu.ge

რეზიუმე: მიზანი. მიზანი - პირველ ეტაპზე β - SIALON შემცველი ნანოკომპოზიტების მიღება 1400⁰C ტემპერატურაზე რეაქციული სინთეზის მეთოდით, აზოტირების პროცესით საწყისი შედგენილობიდან TiC-BN-SiC-B$_4$C-Si-Al-Al$_2$O$_3$ სისტემაში. სინთეზის ამ მეთოდის გამოყენებით შესაძლებელი გახდა β - SIALON-ის სხვადასხვა პროცენტული შემცველობის მქონე ნანო-კომპოზიტების მიღება.

ჩვენი ამოცანა იყო მიღებული კონსოლიდირებული მასალების ფაზური შედგენილობის შესწავლა TiC-TiB$_2$-BN-SiC-B$_4$C-β-SiAlON-Al$_2$O$_3$ (ნანოფხვნილი - 400 ნმ.) სისტემაში..

მეთოდი. მიღებული მასა დაფქვილი იქნა ატრიტორში და კონსოლიდირებული კომპოზიტი მიღებულ იქნა ცხელი დაწნეხვით 1620⁰C ტემპერატურაზე 40 წუთის განმავლობაში, მინისებური პერლიტის (სასომხეთი) დოპირებით 2 მას.%, საბოლოო ტემპერატურაზე 8 წუთის დაყოვნებით, 30 მპა წნევისა და ვაკუუმის - 10^{-3} Pa wnevis ქვეშ. არაგაცის პერლიტი შეიცავდა 96 მას. % მინას.

კომპოზიტების ფაზური შედგენლობის შესასწავლად, ჩვენ ჩავატარეთ რენტგენოსტრუქტურული ანალიზი DRON-3 დანადგარზე. მიკროსტრუქტურის შესასწავლად კვლევა ჩატარდა კომპანია „OPTON"-ის ოპტიკურ მიკროსკოპზე -AC100 და რასტრულ ელექტრონულ მიკროსკოპზე „Nanolab 7". შესწავლილი კომპოზიტების ელექტრული პარამეტრების მნიშვნელობები გამოითვალა მიღებული „lgp-t" დამოკიდებულების საფუძველზე. შევისწავლეთ მექანიკური თვისებები.

შედეგები. TiC-TiB₂-BN-SiC-B₄C-β-SiAlON-Al₂O₃ სისტემაში მივიღეთ მაღალი მექანიკური თვისებების მქონე ნანოკომპოზიტები. ამ მეთოდის უპირატესობა ის არის, რომ თერმული დამუშავების დროს მიმდინარე ურთიერთქმედების შედეგად ახლად წარმოქმნილი ნაერთები: Si₃N₄, Si, AlN აქტიურია, რაც ხელს უწყობს β-SiALON-ის წარმოქმნას შედარებით დაბალ ტემპერატურაზე, 1300-1350⁰C-ზე. აშკარაა, რომ ALN-ის შეყვანა ß-Si₃N₄-ის კრისტალურ ჩონჩხში უფრო ადვილია, რადგან ამ ტემპერატურულ ინტერვალში Si₃N₄-ის კრისტალური ჩონჩხი ჯერ კიდევ ფორმირების პროცესშია.

ß-SiAlON წარმოიქმნა 1450⁰C ტემპერატურაზე. ბორის კარბიდის ნაწილი გარდაიქმნა ბორის ნიტრიდად აზოტის გარემოში და ტიტანის დიბორიდში, რომელიც ორივე კომპოზიტის შემთხვევაში მცირე რაოდენობითაა.

დასკვნა. მიღებული კომპოზიტის ფაზური შედგენლობა უზრუნველყოფს ამ ნანოკომპოზიტების მაღალ ფიზიკურ-ტექნიკურ და საექსპლუატაციო თვისებებს. სიმტკიცე კუმშვაზე - 2198 მპა, სიმტკიცე ღუნვაზე- 271 მპა, თერმული გაფართოების კოეფიციენტი a₂₀₋₇₀₀-3.8 10^{-6} ⁰C

საკვანძო სიტყვები: ნანოკომპოზიტი; ცხლად დაწნეხილი მასალა; ელექტრონული მიკროსკოპი; ფაზური შედგენილობა; B₄C-BN-TiC-TiB₂-SiC-β-SIALON-Al₂O₃ ნანოფხვნილის სისტემა.

UDC 666.621.9.02

ASSESSMENT OF MATRIX PROPERTIES IN COMPOSITE MATERIALS VIA LINEAR ANALYSIS METHOD

Z. Kovziridze, G. Tabatadze, N. Nizharadze, T. Loladze

Georgian Technical University, Institute of Bionanoceramics and Nanocomposite Technologies, GTU Center for Materials Science of Bionanoceramics and Nanocomposites, 69 Kostava Street, 0175 Tbilisi, Georgia

E-mail: kowsiri@gtu.ge

Resume: Objective. This study aims to develop a method for determining the sizes of microstructural components, specifically grains and pores, in composite materials.

Method. Electron microscopy was used to analyze microstructural images, and a linear measurement technique was applied to determine the dimensions of crystalline grains and pores based on the obtained micrographs.

Results. The developed method enables the determination of the maximum and minimum sizes of particles or pores, their shape factor and average dimensions.

Conclusion. Using the measured parameters of particles and pores in conjunction with the formulas developed by Prof. Kovziridze, a correlation is established between the mechanical properties and the crystalline and porous phases of the composite material.

Key words: composite, correlation, porous phase, mechanical strength, structure, grain/pore size.

1. INTRODUCTION

The properties of metal-ceramic and ceramic composites are primarily determined by their microstructure [1–5]. To achieve optimal properties in any system, microstructural control is essential. Therefore, the microstructure differs according to the specific application of the material.

For optimal mechanical performance, the most favorable microstructure is typically characterized by a uniform distribution of fine particles of the solid phase within the metallic binder phase.

A thin metallic film separating the solid phase grains is advantageous in two ways:

1. It lacks the plasticity typical of bulk metal, thus increasing the composite's strength;

2. A continuous metallic phase helps prevent crack formation in the brittle high-hardness phase.

For example, in various WC-Co compositions with different binder systems, the maximum strength is achieved when the binder phase thickness averages around 0.5 μm. This can be explained by changes in the distribution and properties of the binder phase. When the binder thickness is below 0.3 μm, it is insufficient to fully encapsulate carbide grains, leading to carbide-carbide contacts that reduce composite strength [2, 4, 5].

Experimental findings show that during sintering, a continuous ceramic skeleton is not

formed. The strength of WC-Co composites depends on the properties of the binder phase, while the fracture behavior of metal-ceramic composites is governed by the grain size of the solid phase [2, 4, 5]. Studies of the Ni-Mo-TiC system indicate that as carbide grain size increases, fracture initiates from the grains rather than the binder. Moreover, average binder layer thickness varies with carbide grain size [2, 4, 5].

It is also noteworthy that cermets, in which the fracture path passed through the carbide grains, exhibited lower strength. The microstructures examined in this study primarily belong to systems sintered through liquid-phase processes; however, there are composite systems for which solid-state sintering is essential

2. MAIN PART

Accurate quantification of all relevant microstructural parameters is essential for the analysis and comparison of composites with varying compositions and for establishing correlations with their mechanical properties. To this end, a methodological approach was developed as follows: a metallographic section is prepared from the composite specimen under investigation [2,6]. The microstructure is observed using an electron microscope, and 2-3 regions with distinct microstructural features are selected. Images are captured at magnifications sufficient to clearly resolve the shapes and sizes of grains belonging to different phases (Fig. 1a, b).

The actual area of the field of view is determined based on the image magnification. For example, Fig. 1a and 1b display the microstructures of different ceramic composites. In Fig. 1a, the magnification is 2000×, while in Fig. 1b, a scale bar is provided. To determine the actual magnification for Fig. 1b, the length of the scale bar is measured. If it equals 12 mm (i.e., 12,000 μm) and represents 50 μm in reality, the magnification is calculated as 12,000 μm ÷ 50 μm = 240×.

a.   b.
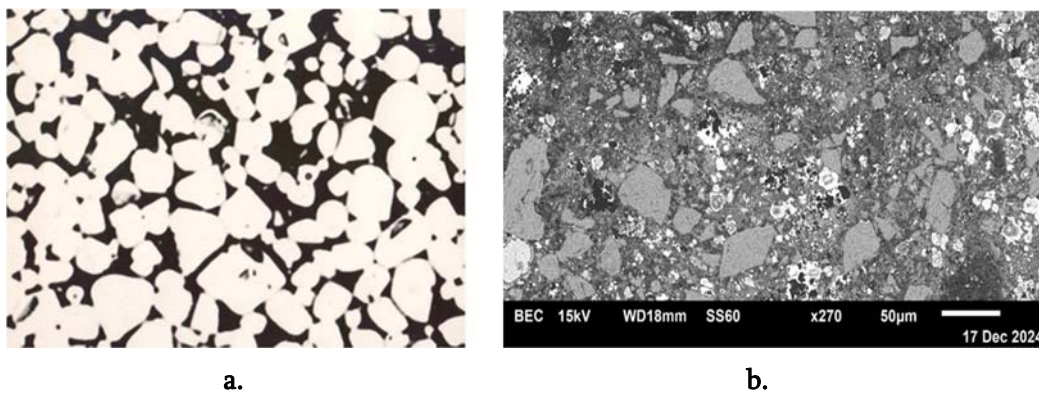
Figure 1

a) Microstructure of a metal-ceramic composite (×2000 magnification)

b) Microstructure of a ceramic composite

To determine the real field of view area, the image's length and width are measured and converted to actual dimensions based on the magnification. For instance, if the image length is 100 mm (100,000 μm), the actual length is 100,000 μm ÷ 240 = 416 μm. Similarly, if the width is 55 mm (55,000 μm), the actual width is 55,000 μm ÷ 270 = 200 μm. Therefore, the total observed area is:

$$S = 416\ \mu m \times 200\ \mu m = 83{,}200\ \mu m^2.$$

Prof. Z. Kovziridze investigated the correlation between mechanical properties and both porous (a) and crystalline (b) phases of composite materials, proposing the following formulas [7–11]:

(a) Porous phase correlation:

$$\sigma_{m/p} = P/F_p.P_d.P_{vol}.P_m$$

Where:

- P = applied load (MPa),
- F_p = pore shape factor (ratio of maximum to minimum pore diameter),
- P_d = pore distribution factor in the matrix (ranges from 1 to 0.8 depending on uniformity. If the pores are uniformly distributed and of similar size, the factor is taken as 1. A value of 0.9 is assigned when the pore distribution is non-uniform, and 0.8 if pore coalescence has begun),
- P_{vol} = volume fraction of the porous phase,
- P_m = average pore size.

(b) Crystalline phase correlation:

$$\sigma_d = PF_{kd}/K_m K_v F_{kf}$$

Where:

- P = applied load (MPa),
- F_{kd} = crystal distribution factor (1 for uniform, 0.9 for non-uniform),
- K_m = average crystal size (μm),
- K_v = volume fraction of the crystalline phase,
- F_{kf} = grain shape factor (ratio of max to min grain diameter).

Based on Fig. 1a, it can be concluded that the grains of the crystalline phase are uniformly distributed; therefore, the crystal distribution factor (F_{kd}) can be considered equal to 1. As for the crystal shape factor (F_{kf}), in the first case, the largest grain is approximated as spherical, and its diameter is measured. For example, if D_{max} = 15 mm (15,000 μm) and the image magnification is 2000×, then Dmax = 15,000 μm ÷ 2000 = 7.5 μm. Likewise, if Dmin = 1 mm (1,000 μm), then Dmin = 1,000 μm ÷ 2000 = 0.5 μm. Thus, the shape factor is F_{kf} = Dmax / Dmin = 7.5 / 0.5 = 15.

The average crystal size (K_m) is determined by measuring the diameters of all grains within the selected field of view, calculating the average diameter, and dividing by the magnification. For instance, if the average measured grain diameter is 12 mm (12,000 μm), then

$$K_m = 12{,}000\ \mu m \div 2000 = 6\ \mu m.$$

The volume fraction of the crystalline phase in the matrix (K_v, in wt.%) is estimated using relative density. If the relative density is 0.97, the volume fraction of the crystalline phase is considered to be the same.

Based on the microstructure shown in Fig. 1b, the crystal distribution factor (F_{kd}) may be taken as 0.9, and the shape factor (F_{kf}) as Dmax / Dmin = 9 mm / 1 mm = 9.

The same method is applied in the case of pores. The measured data are entered into tables and substituted into the corresponding formulas. The table format is as follows:

Morphology of the Porous Phase

View Area S, μm²	Maximum pore size D_{max}, μm	Minimum pore size D_{min}, μm	Pore shape factor $F_p=D_{max}/D_{min}$	Pore distri-bution factor in the matrix, P_d	Volume fraction of the porous phase P_{vol}, %	Average pore size P_m, μm	Bending load P, MPA
1	2	3	4	5	6	7	8

Morphology of the Crystalline Phase

View Area S, μm²	Maximum crystal size D_{max}, μm	Minimum crystal size D_{min}, μm	Crystal shape factor $F_p=D_{max}/D_{min}$	Crystal distribution factor in the matrix, P_d	Volume fraction of the crystalline phase P_{vol}, %	Average crystal size P_m, μm	Bending load P, MPA
1	2	3	4	5	6	7	8

To measure irregularly shaped grains or pores, we can use the model shown in Figure **2**, which allows the irregular object to be approximated by an equivalent sphere and measured accordingly. In the diagram, line 3 represents its measured dimension.
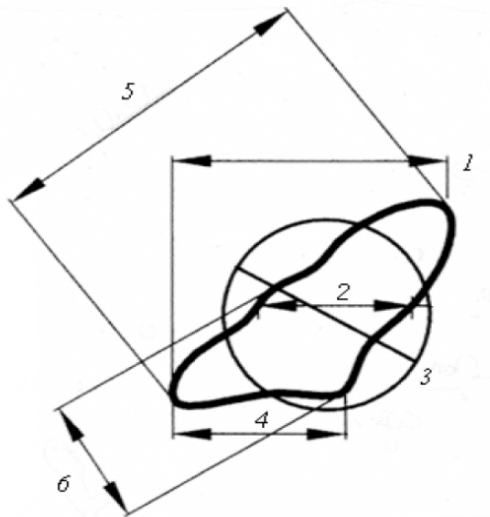
Figure 2. Method for determining the size of irregularly shaped grains [12]

3. CONCLUSION

A linear analysis method has been developed for determining the size of structural particles in composite materials, enabling the prediction of mechanical properties based on the composite's microstructural characteristics.

REFERENCES

1. Mikdam, A., Makradi, A., Koutsawa, Y., & Belouettar, S. (2013). Microstructure effect on the mechanical properties of heterogeneous composite materials. Composites Part B: Engineering, 44(1), 714–721.

2. Kovziridze, Z., Nizharadze, N., & Tabatadze, G. (2007). Cutting Tool Materials. Monograph. Tbilisi: Technical University.

3. Gnesin, G.G. (Ed.). (1991). Ceramic Tool Materials. Kiev: Tekhnika.

4. Tinklepo, J. (Ed.). (1962). Cermets. Moscow: Foreign Literature Publishing.

5. Tretyakov, V.I. (1976). Fundamentals of Metallurgy and Sintered Hard Alloys Production Technology. Kiev: Metallurgy.

6. Kovziridze, Z., Tabatadze, G., Nizharadze, N., & Donadze, G. (2007). Composite Tool Materials – Laboratory Guidelines. Tbilisi: Technical University.

7. Kovziridze, Z. (2018). Formula for the dependence of macromechanical characteristics on the porous phase. Patent No. 7276.

8. Kovziridze, Z. (2023). The formula for correlation between porous phase and macromechanical characteristics. Ceramics and Advanced Technologies, 25(1), 38–48.

9. Kovziridze, Z. (2022). The formula of dependence of mechanical characteristics on crystalline phase composition. Ceramics and Advanced Technologies, 24(2), 23–34.

10. Kovziridze, Z. (2022). Failure Stress Energy Formula. Ceramics and Advanced Technologies, 24(2), 34–51.

11. Kovziridze, Z. (2022). Physics and Kinetics of Sintering. Monograph. Tbilisi: Technical University.

12. Russian Ministry of Health (2023). Optical Microscopy. Pharmacopoeial Article OFS.1.2.1.0009.15, Order No. 377.

კომპოზიციური მასალების მატრიცული მახასიათებლების განსაზღვრა ხაზობრივი ანალიზის მეთოდით

ზ. კოვზირიძე, გ. ტაბატაძე, ნ. ნიჟარაძე, თ. ლოლაძე

საქართველოს ტექნიკური უნივერსიტეტი. ქიმიური ტექნოლოგიისა და მეტალურგიის ფა-კულტეტი. ბიონანიკერამიკისა და ნანოკომპოზიტების ტექნოლოგიის ინსტიტუტი. სტუ ბიო-ნანიკერამიკისა და ნანოკომპოზიტების მასალათმცოდნეობის ცენტრი. 0175 თბილისი. სა-ქართველო. კოსტავას 69

E-mail: kowsiri@gtu.ge

რეზიუმე: მიზანი. კომპოზიციური მასალების მიკროსტრუქტურული შემადგენლების (მარც-ვლები, ფორები) ზომების განსაზღვრის მეთოდის შემუშავება.

მეთოდი. მიზნის განსახორციელებლად გამოვიყენეთ მიკროსტრუქტურული სურათის ელექ-ტრონულ-მიკროსკოპიული კვლევის მეთოდი და მიკროსკოპიული სურათის მიხედვით კრისტალური ნაწილაკების (მარცვლების) და ფორების გაზომვის ხაზობრივი მეთოდი.

შედეგი. შემუშავებული მეთოდი საშუალებას გვაძლევს დავადგინოთ მაქსიმალური და მონიმალური ნაწილაკების ან ფორების ზომები და მათი ფორმის ფაქტორის სიდიდე, აგრეთვე ნაწილაკებისა და ფორების საშუალი სიდიდე,

დასკვნა. ნაწილაკებისა და ფორების დადგენილი პარამეტრებისა და პროფ. კოვზირიძის მიერ შემუშავებული ფორმულების გამოყენებით ვახდენთ მექანიკური თვისებების კორელაციას კომპოზიტის კრისტალური და ფორიანი ფაზისაგან დამოკიდებულებით..

საკვანძო სიტყვები: კომპოზიტი, კორელაცია, ფორიანი ფაზა, მექანიკური სიმტკიცე, სტრუქ-ტურა, მარცვლი (ფორა) ზომა.

UDC 666.1

OBTAINING AN EFFECTIVE POZZOLANIC ADDITIVE BASED ON SUBSTANDARD NATURAL RAW MATERIALS AND INDUSTRIAL WASTE

<u>T. Petriashvili</u>, <u>E. Shapakidze</u>, I. Kamushadze, I. Gejadze, M. Makadze

Ivane Javakhishvili Tbilisi State University, Alexander Tvalchrelidze Caucasian Institute of Mineral Resources. 11 Mindeli str., 0186, Tbilisi, Georgia

E-mail: t.petriashvili25@gmail.com, elena.shapakidze@tsu.ge

Resume: Goal. The aim of this work is to study Georgian kaolinized clays, which are considered as substandard kaolin raw material, and fly ash, waste from thermal power plants, in order to obtain metakaolin, a highly effective pozzolanic additive for cement/concrete.

Method. The mineral composition of clays was determined using an Optika B-383POL polarization microscope (Italy).

For thermogravimetric analysis, a NETZSCH derivatograph with STA-2500 REGULUS thermogravimetric and differential thermal analyzer (TG/DTA) was used. Samples were heated to 1000 ° C, in a ceramic crucible, heating rate 10 °C / min. Reference substance a-Al2O3.

The X-ray phase analysis was carried out using a Dron-4.0 diffractometer ("Burevestnik", St. Petersburg, Russia) with a Cu-anode and a Ni-filter. U=35kv. I=20mA. Intensity - 2 degrees/min. λ = 1.54178 Å.

The pozzolanic activity of heat-treated clays was determined by absorbing lime from a lime mortar according to GOST R 56592-2015 (Mineral admixtures for concretes and mortars. General specifications).

Results. Parameters for the synthesis of highly active metakaolin have been determined, such as the ratio of raw components, processing temperature, pozzolanic activity, mechanical strength, etc. Under laboratory conditions, cements with high physical and mechanical properties were obtained based on the developed pozzolanic additive.

Conclusion. By heat treatment of kaolinized clays of Georgia at 600 -700°C it is possible to obtain an effective pozzolanic additive – metakaolin.

Joint heat treatment of kaolinized clays with FA allows reducing the temperature of metakaolin synthesis to 550-590°C, improving the pozzolanic properties of metakaolin and increasing the mechanical strength of cements.

Key words: pozzolanic additive, kaolinite clay, metakaolin, fly ash

1. INTRODUCTION

Cement/concrete is the main building material used globally in all modern construction projects. At the same time, cement production consumes a huge number of natural materials, the widespread use of which has led to the depletion of natural resources as well as CO_2 emissions into the environment during clinker firing. These processes

have a great impact on global warming and the ecological condition of our planet [1].

In 2020 alone, the global annual cement production was around 5.9 billion tons, which corresponds to 4.8 billion tons of CO_2 emitted [2]. In addition, sulfur oxide (SO_3) and nitrogen oxides (NO_x) are some of the other harmful greenhouse gases that are released during the cement production process and can also have adverse effects on the environment. In addition to the emission of toxic greenhouse gases into the atmosphere, the Portland cement production process is also responsible for the consumption of large amounts of raw materials and energy [3].

To solve this problem, different approaches are used, one of which is to reduce the amount of clinker in cement/concrete using effective pozzolanic additives.

Pozzolanic materials contain reactive silica or alumina and when mixed with Portland cement, react with $Ca(OH)_2$, which is formed during cement hydration, resulting in the additional formation of calcium hydrosilicates and hydrogarnets, initially in a gel-like state, which subsequently crystallizes and gives additional strength to the cement stone. Pozzolanic additives are introduced into cement to improve such construction and technical properties as water resistance and sulfate resistance. A high-quality pozzolanic additive should have a partially amorphous or glassy structure.

In recent years, metakaolin has become increasingly popular worldwide as a high-performance pozzolanic additive. It is an artificial environmentally friendly material that is obtained by treating kaolin clay at temperatures between 600 and 800°C, which leads to dehydroxylation of the kaolinite crystal structure to form metakaolin [4-8].

The main mineral of kaolin clays is kaolinite – $Al_2Si_2O_5(OH)_4$, i.e., $2SiO_2 \cdot Al_2O_3 \cdot 2H_2O$, the rest are quartz, mica, and feldspar. Under normal natural conditions, it is quite stable, but in the temperature range of 600–850°C it loses 14% of its mass, which was present in the form of hydroxyl ions. As a result of heat treatment, the structure of kaolin is destroyed and amorphous, i.e. reactive metakaolin - $2SiO_2 \cdot Al_2O_3$ is formed.

In the process of cement hydration, new phases are formed by the interaction of clinker minerals and metakaolin: calcium hydrosilicates (C-S-H), calcium hydroaluminates (C_2AH_8, C_4AH_{13}, C_3AH_6), calcium hydrogranates (C_3ASH_4) and the highly active mineral stratlingite C_2ASH_8, which give cement additional strength [9-14].

The high reactivity of metakaolin causes a high degree of cement hydration, low porosity of cement stone, high mechanical strength at all ages of curing, and hence durability. In addition, the introduction of metakaolin increases the density of cement/concrete, which reduces their water permeability, which in turn increases frost and sulfate resistance. Thus, the introduction of metakaolin into the cement-concrete mixture leads both to a decrease in the clinker fraction and to an increase in the mechanical strength of the final product and other construction-technical indicators.

The use of metakaolin for the production of geopolymer materials of alkaline activation is widely known. Geopolymer materials obtained based on metakaolin are characterized by high physical and mechanical parameters [15-20].

Kaolin clays usually contain 35-45% Al_2O_3. The reserves of such clays in the world are very limited. Large deposits are in Ukraine (Prosyanovskoye, Glukhovetskoye, Chasov Yar), in Russia (Ural, Far East), etc.

Georgia has no kaolin clays. There are only substandard kaolinized clays, in which the content of Al_2O_3 varies within 20-30%.

For over 30 years, Georgia has been experiencing a deficit of effective pozzolanic additives due to the lack of local high-quality natural raw materials. Therefore, it is of great practical interest to identify resources of such raw materials in the country and develop methods to increase their activity.

The clay rocks of Georgia (shales, argillites, fusible clays) were studied to obtain artificial pozzolanic additives based on metakaolin. A mode of thermal activation of clay rocks was developed and cements and concretes were obtained using them [21-23]. However, kaolinized clays were not studied in this direction.

The aim of this work is to study Georgian kaolinized clays, which are considered as substandard kaolin raw material, and fly ash, waste from thermal power plants, in order to obtain metakaolin, a highly effective pozzolanic additive for cement/concrete.

2. MAIN PART

Kaolinized clays from different deposits of Georgia were used for the research (Table 1).

Table 1

Chemical composition of kaolinized clays of Georgia, wt.%

*No.	LOI	SiO₂	Al₂O₃	Fe₂O₃	FeO	CaO	MgO	SO₃	Na₂O	K₂O
1	9.40	45.51	21.50	4.74	1.13	7.92	3.72	1.53	2.30	1.50
2	9.68	50.79	22.03	7.42	0.62	2.80	2.03	0.21	1.59	1.44
3	5.59	57.18	21.27	1.44	1.69	2.43	2.86	0.32	3.41	2.08
4	4.14	57.70	27.80	1.14	1.15	0.99	1.97	0.54	2.01	2.05
5	1.8	60.62	29.51	2.15	-	0.51	0.58	1.03	1.58	1.04

*No.1- Qobuleti, No.2 – Makhinjauri, No.3 – Brili, No.4 – Makvaneti, No.5 – Kandara.

1. Results and discussion

According to microscopic descriptions, the mineralogy of clays is almost identical: the main mass is represented by weakly carbonized clay mass, pelitic substance. Silty clastic material is represented by feldspars and quartz fragments.

Microphotographs of clays are shown in Fig. 1-5.
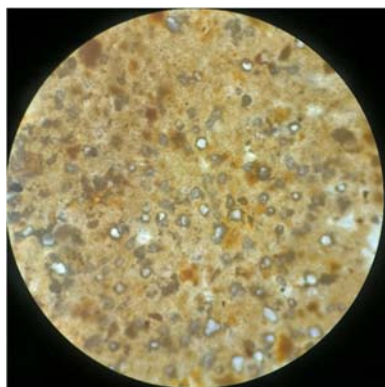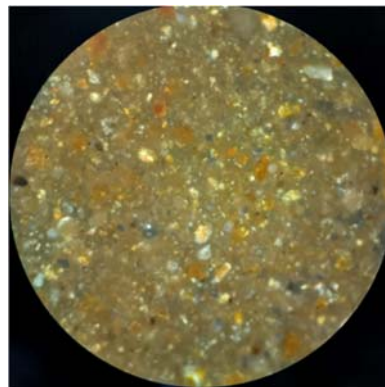
a- b+

Fig. 1. Qobuleti. Fragments of quartz-feldspar material interspersed
in kaolinite-a hydrosluidic clay fraction. 135x
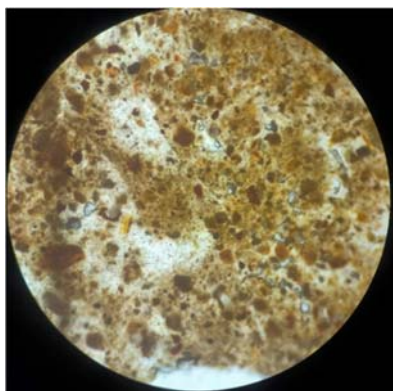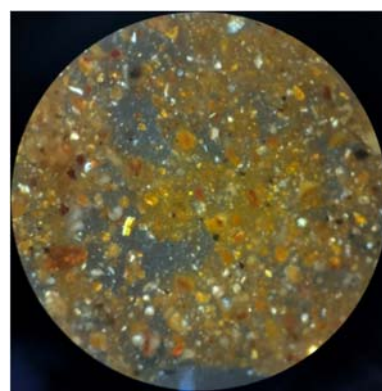
a- b+

Fig. 2. Makhinjauri. Fragments of quartz-feldspar material interspersed
in kaolinite-a hydrosluidic clay fraction. 135x
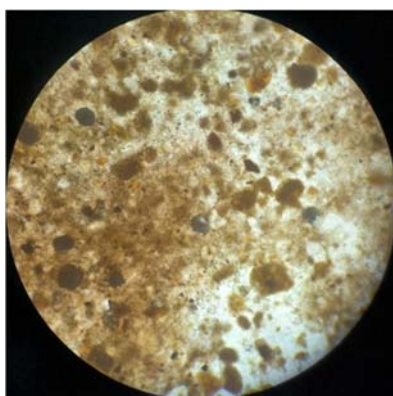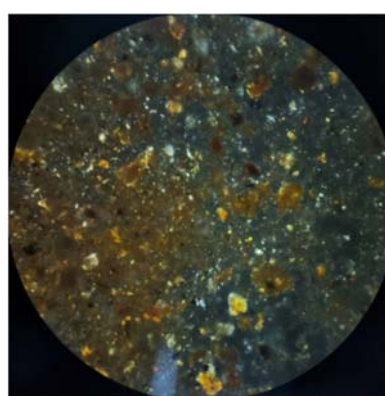
a- b+

Fig. 3. Brili. Fragments of quartz-feldspar material interspersed
in kaolinite-a hydrosluidic clay fraction. 135x

<div align="center">a-   b+</div>
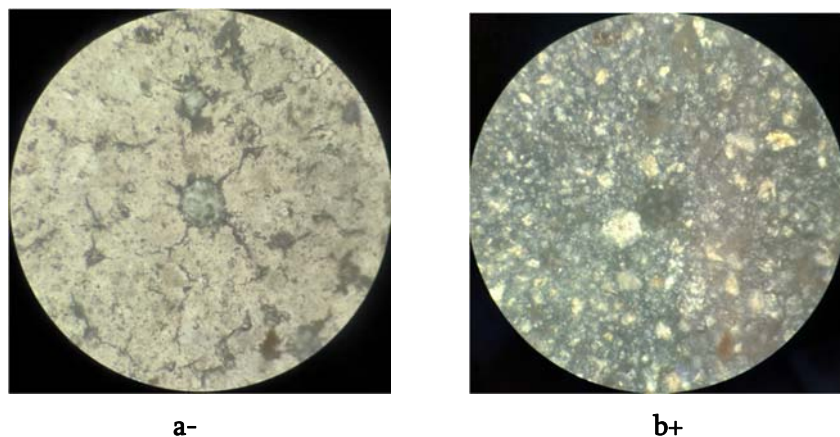
Fig. 4. Makvaneti. Fragments of quartz-feldspar material interspersed in kaolinite-a hydrosluidic clay fraction. 135x

<div align="center">a-   b+</div>
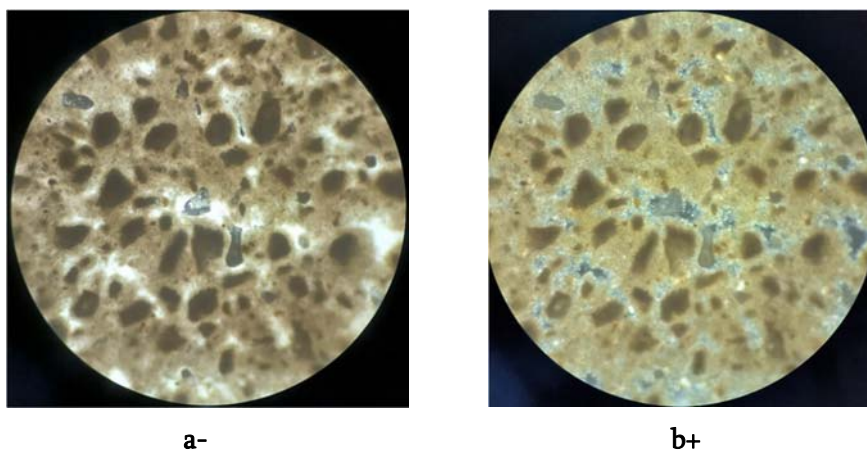
Fig. 5. Kandara. Fragments of quartz-feldspar material interspersed in kaolinite-a hydrosluidic clay fraction. 135x

XRD patterns and DTA curves are shown on Fig. 6 and Fig. 7.
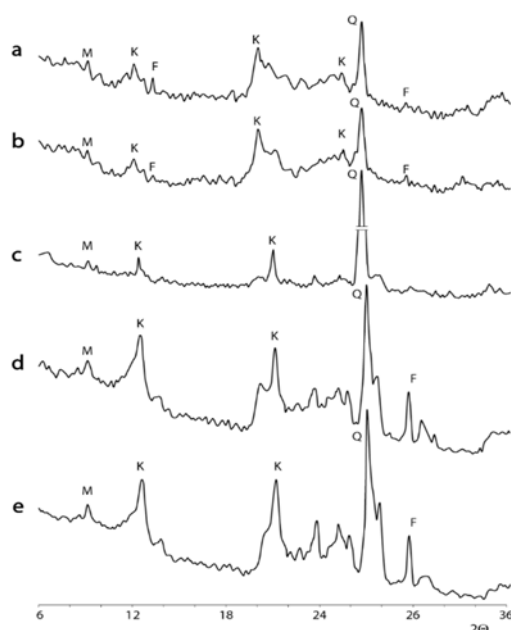
Fig. 6. XRD patterns of clays: a) Qobuleti, b) Makhinjauri, c) Brili, d) Makvaneti and e) Kandara
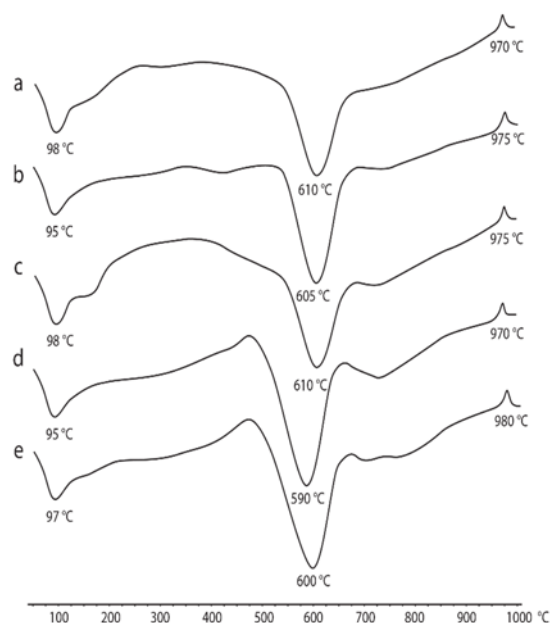
Fig. 7. DTA curves of clays: a) Qobuleti, b) Makhinjauri, c) Brili, d) Makvaneti and e) Kandara

In order to obtain metakaolin, clays were treated at temperatures of 550, 600, 700, 800°C with a holding time of 1 hour at the maximum temperature.

Kinetics of lime absorption by kaolinized clays from a saturated solution are shown in Fig. 8.
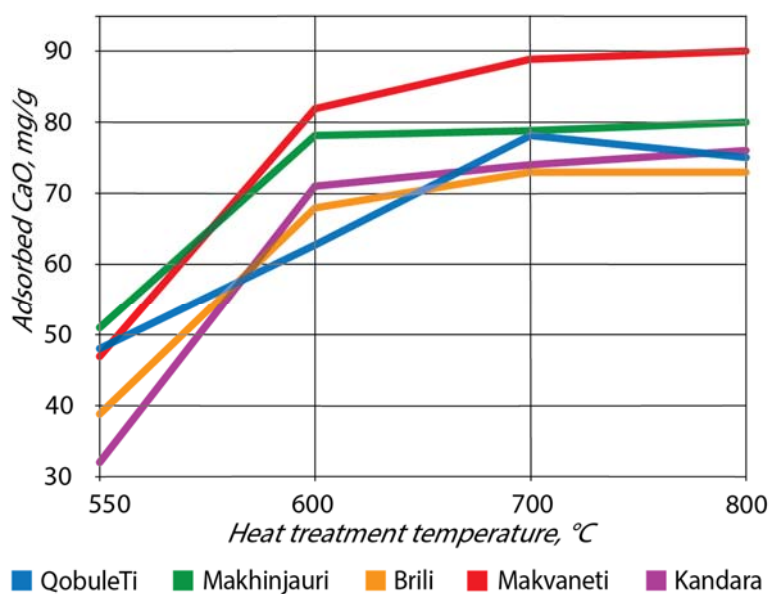
Fig. 8. Kinetics of lime absorption by heat-treated kaolinized clays from saturated solution

58

According to the requirements of the standard, the additive has high pozzolanic properties, if the amount of absorbed CaO from a saturated solution is more than 70 mg/g, medium - from 30 to 70 mg/g and low - up to 30 mg/g.

The test results showed that all the studied clays have different pozzolanic activity depending on the heat treatment temperature. Heat treatment from 550°C to 800°C increases their ability to absorb CaO. All clays after heat treatment at 700°C and above are classified as highly active pozzolanic additives. Although at 800°C the absorption of CaO does not increase much compared to 700°C.

The cements were prepared with the addition of 20% heat-treated kaolinized clays with different heat treatment temperatures. For comparison, a control composition was prepared without the additive (Fig. 9).
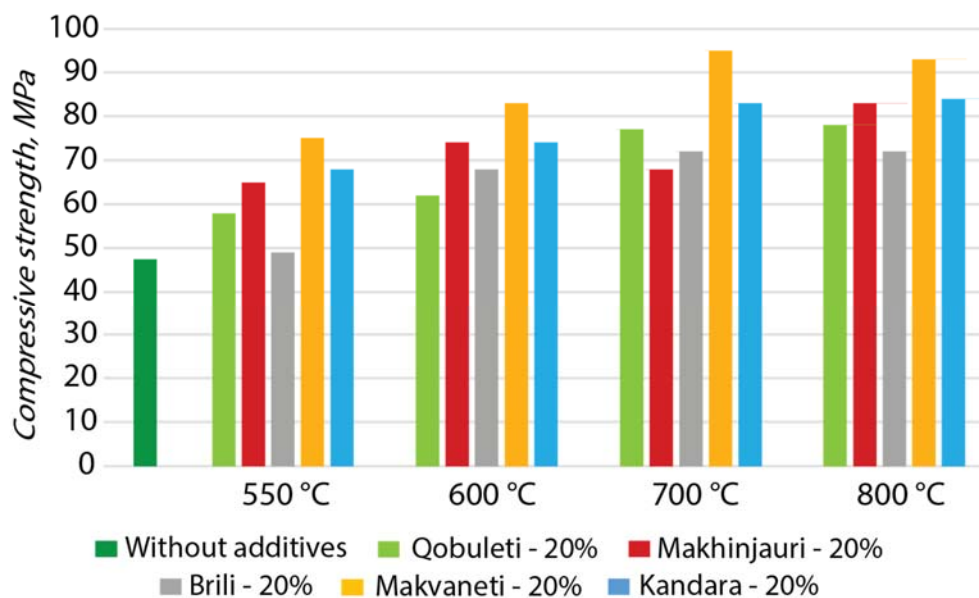
Fig. 9. Compressive strength of cement samples
after 28 days hardening with different temperatures
of heat treatment of kaolinized clays

According to the test results (Fig.9), kaolinized clays heat-treated at 600–800°C showed high mechanical strength, exceeding the indicators of cement without additives. However, heat treatment of clays at 800°C led to an insignificant increase in strength, and the optimum temperature can be considered to be 600–700°C.

In order to optimize the metakaolin synthesis process, it was proposed to add fly ash to kaolinized clays and subject them to joint thermal treatment.

Fly ash from the Kutaisi Thermal Power Plant was used, the composition of which is as follows (wt. %): LOI – 6.13, SiO_2 – 52.14, Al_2O_3 – 31.59, Fe_2O_3 – 5.17, CaO – 0.69, MgO – 0.74, SO_3 – 0.53, Na_2O – 0.99, K_2O – 0.29, P_2O_5 – 0.05, TiO_2 -1.32.

During the heat treatment of fly ash together with kaolinized clay, the coal particles contained in the fly ash are burned, which creates additional heat and the formation temperature of metakaolin decreases. In addition, fly ash has a high Al_2O_3 content, which serves as an additional source for the synthesis of metakaolin.

This technology for obtaining an effective pozzolanic additive based on metakaolin, synthesized from kaolinized clay and fly ash, was patented ("Raw material mixture for producing pozzolanic additive to cement", U 2024 2197 Y).

Using Makvaneti clay as an example, it was shown that the addition of 10-20% fly ash made it possible to reduce the metakaolin synthesis temperature to 550 - 590℃ (Fig. 10).
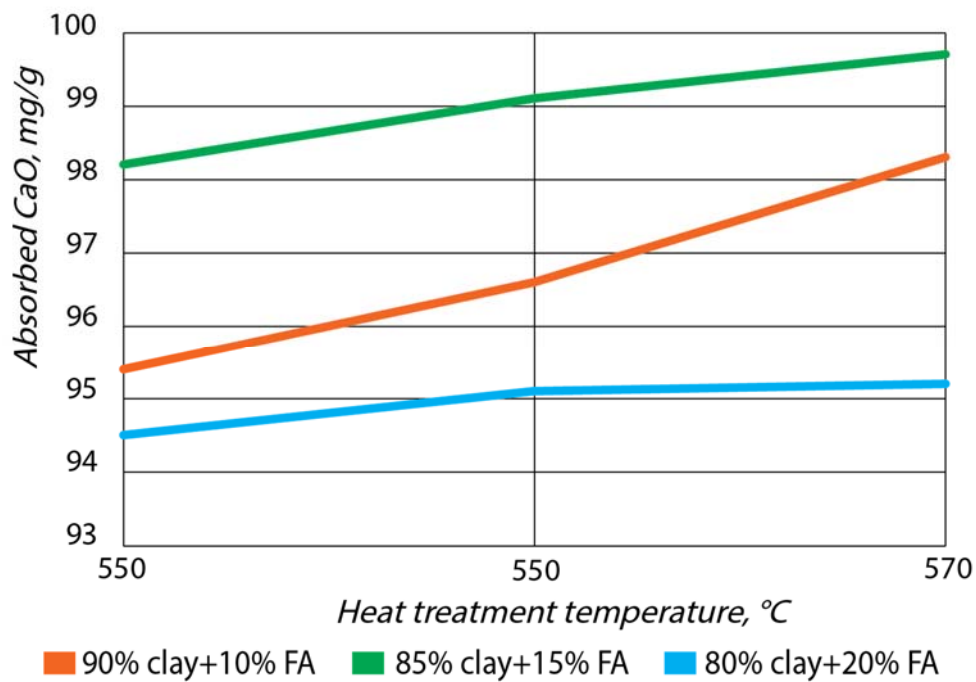
Fig. 10. Kinetics of lime absorption by heat-treated Makvaneti clay together with FC from a saturated solution

To determine the mechanical strength of cements, compositions were prepared using kaolinized clays: Makhinjauri, Brili, and Makvaneti. Thermal treatment of clays was carried out together with FA at a temperature of 570℃.
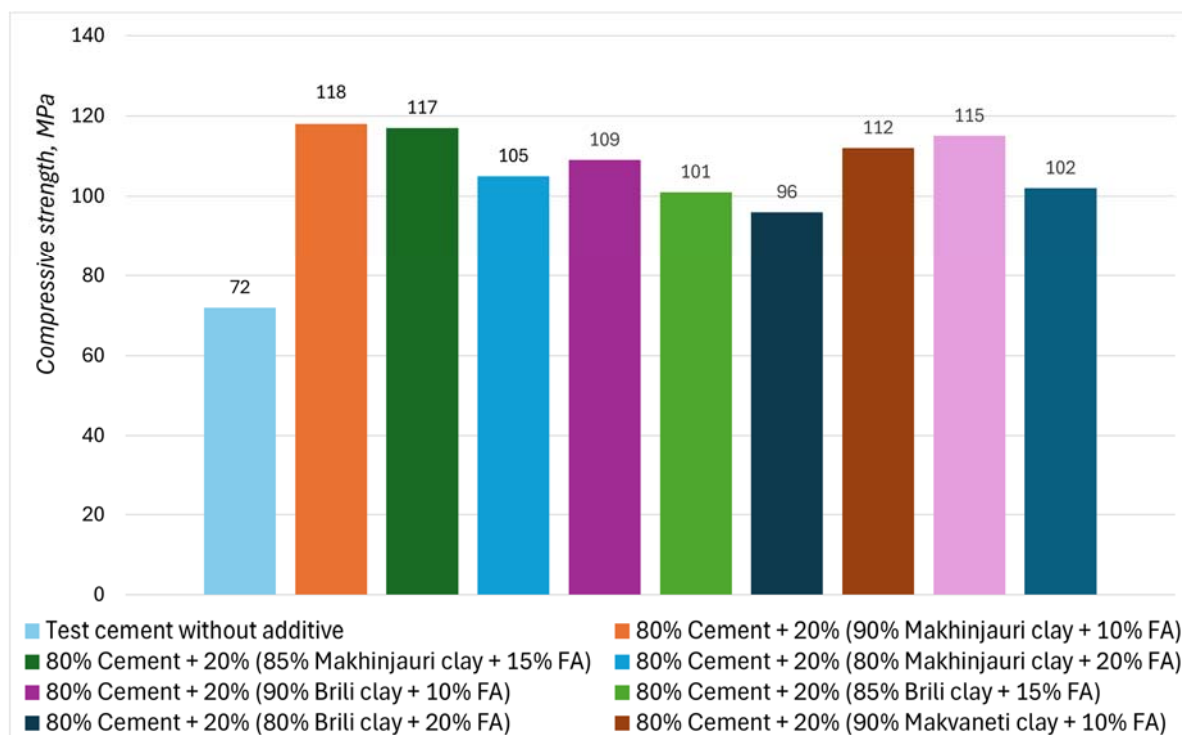
**Fig. 11. Compressive strength after 28 days of hardening
of cement samples with the addition of kaolinized clays and FA,
jointly processed at 570℃**

As the test results showed, all cements have higher mechanical strength compared to cement without additives (Fig. 11).

3. CONCLUSION

Based on the conducted studies, it can be concluded that by heat treatment of kaolinized clays of Georgia at 600 -700℃ it is possible to obtain an effective pozzolanic additive – metakaolin.

Joint heat treatment of kaolinized clays with FA allows reducing the temperature of metakaolin synthesis to 550 - 590℃, improving the pozzolanic properties of metakaolin and increasing the mechanical strength of cements (Patent of Georgia U 2024 2197 Y).

FA during thermal treatment creates additional heat (due to the combustion of coal particles) and the temperature of metakaolin synthesis decreases. At the same time, FA with a high content of Al_2O_3 creates an additional amount of metakaolin.

REFERENCES

1. M. Schneider. The cement industry on the way to a low-carbon future. Cement and Concrete Research, vol. 124, p. 105792, 2019.
2. N. B. Singh and B. Middendorf. Geopolymers as an alternative to Portland cement: an overview.

Construction and Building Materials, vol. 237, p. 117455, 2020.

3. D.L. Pillay, O.B. Olalusi, P.O. Awoyera, C. Rondon, A.M. Echeverrıa, J.T. Kolawole. A Review of the Engineering Properties of Metakaolin Based Concrete: Towards Combatting Chloride Attack in Coastal/Marine Structures. Advances in Civil Engineering. 2020 (8), ID 8880974, 13 pages. https://doi.org/10.1155/2020/8880974.

4. R. Siddique, J. Klaus, Influence of metakaolin on the properties of mortar and concrete: A review, Applied Clay Science. 43 (2009) 392–400.

5. Dr. K. Srinivasu, M. L. N. Krishna Sai, Venkata Sairam Kumar N., A. Review on Use of Metakaolin in Cement Mortar and Concrete. IJIRSET. 3 (2014). 14697- 14701.

6. A. Kostuch, V. Walters, T.R Jones, High performance concretes incorporating metakaolin: a review. Concrete 2000. 2 (1993) 1799-1811.

7. Deveshan L. Pillay, Oladimeji B. Olalusi, Paul O. Awoyera, Carlos Rondon, Ana Marrıa Echeverrıa and John Temitope Kolawole. A Review of the Engineering Properties of Metakaolin Based Concrete: Towards Combatting Chloride Attack in Coastal/Marine Structures

8. M. A. Akinpelu, A.S. M. Salman, Y. A.a Jimoh, I. T. Yahaya, H. M. Salami, Impact of treatment temperature of metakaolin on strength and sulfate resistance of concrete. Res. Eng. Struct. Mater. 10(3) (2024) 1261-1279.

9. S. Boonphan, S. Prachakiew, A. Klinbumrung, Crystallization and exfoliation of metakaolin under molten salt treatment, Ceramics – Silikáty 68 (1) (2024) 7-13.

10. A. Palomo, M.T. Blanco-Varela, M.L. Granizo, F. Puertas, T. Vazquez, M.W. Grutzeck, Chemical stability of cementitious materials based on metakaolin, Cement and Concrete Research. 29 (1999) 997–1004.

11. M. Rashad. Metakaolin as cementitious material: History, scours, production and composition – A comprehensive overview. Construction and Building Materials. 41 (2013) 303–318.

12. G. L. Thankam, N. T. Renganathan. Ideal supplementary cementing material – Metakaolin: A review, International Review of Applied Sciences and Engineering. 11 (2020) 58-65.

13. M. A. H. Kamal, N. Salleh, N. A. A. Hamid, Z Jamellodin, N. Ali1, S. R. Abdullah, S. H. Adnan, Review on metakaolin impact on the workability and compressive strength of concrete, IOP Conf. Ser.: Earth Environ. Sci. 1347 (2024) 012085.

14. E. Shapakidze, T. Petriashvili, I. Kamushadze, L. Gabunia, I. Gejadze, E. Khuchua. Study of the possibility of regulating the parameters of metakaolin synthesis using clay rocks of Georgia. Proceedings of the 7th International Conference "Nanotechnology". GTUnano 2024.

15. J. Davidovits, Review. Geopolymers: Ceramic-Like Inorganic Polymers, J. Ceram. Sci. Technol., 08(3) (2017) 335-350.

16. A. Palomo, M.W. Grutzeck, M. T. Blanco, Alkali-activated fly ash cement for future, Cement and Concrete Research. 29 (1999) 1323–1329.

17. P. Duxon, A. Fernandes-Jimenes, J. Provis et al., Geopolymer technology: the current state

of the art. Journal of Materials Science. 42(9) (2007) 2917-2933.

18. A. Palomo, P. Krivenko, I. Garcia-Lodeiro, E. Kavalerova, O. Maltseva, A. Fernández-Jiménez, A review on alkaline activation: new analytical perspectives. Materiales de Construcción. 64(315) (2014) e022. ISSN-L: 0465-2746.

19. E. Shapakidze, M. Avaliani, M. Nadirashvili, V. Maisuradze, I. Gejadze, T. Petriashvili, Geopolymers based on local rocks as a future alternative to Portland cement, in Composite materials engineering: modeling and technology, Materials science. Apple Academic Press, USA, 2020, pp. 351-358.

20. E. Shapakidze, M. Avaliani, M. Nadirashvili, V. Maisuradze, I. Gejadze, T. Petriashvili, Obtaining and studying the properties of new geopolymer binders based on calcined clay rocks and local industrial waste, Eur. Chem. Bull. 11(6) (2022) 67 – 73.

21. E. Shapakidze, M. Avaliani, M. Nadirashvili, V. Maisuradze, I. Gejadze, T. Petriashvili, Synthesis and study of properties of geopolymer materials developed using local natural raw materials and industrial waste. Chem. Chem. Technol. 17(4) (2023) 711–718.

22. E. Shapakidze, M. Nadirashvili, V. Maisuradze, I. Gejadze, M. Avaliani and G. Todradze, Elaboration of optimal mode for heat treatment of shales for obtaining metakaolin, Eur. Chem. Bull. 8(1) (2019) 31-33.

23. E. Shapakidze, I. Gejadze, M. Nadirashvili, V. Maisuradze, T. Petriashvili, A. Skhvitaridze, Using Clay Rocks of Georgia to Obtain High-Active Pozzolanic Additives to Portland Cement, IJAER. 14(18) (2019) 3689-3695.,

---

არასტანდარტული ბუნებრივი ნედლეულისა და სამრეწველო ნარჩენების საფუძველზე ეფექტური პუცოლანური დანამატის მიღება

თ. პეტრიაშვილი, ე. შაფაქიძე, ი. ქამუშაძე, ი. გეჯაძე, მ. მაქაძე

ივანე ჯავახიშვილის სახელობის თბილისის სახელმწიფო უნივერსიტეტი, ალექსანდრე თვალ-ჭრელიძის სახელობის მინერალური ნედლეულის კავკასიის ინსტიტუტი. საქართველო, 0186, თბილისი, მინდელის 11

E-MAIL: t.petriashvili25@gmail.com   elena.shapakidze@tsu.ge

რეზიუმე: *მიზანი.* სამუშაოს მიზანია საქართველოს კაოლინიზირებული თიხების, რომლებიც კაოლინის არასტანდარტულ ნედლეულად განიხილება, და თბოელექტროსადგურების განატაცი ნაცრის შესწავლა მეტაკაოლინის მისაღებად, რომელიც წარმოადგენს მაღალეფექტურ პუცოლანურ დანამატს ცემენტ/ბეტონისთვის.

მეთოდი. თიხების მინერალური შედგენილობა განისაზღვრა Optika B-383POL პოლარი-ზაციული მიკროსკოპის (იტალია) გამოყენებით.

თერმოგრავიმეტრული ანალიზები ჩატარდა NETZSCH დერივატოგრაფზე, STA-2500 REGULUS ანალიზატორის (TG/DTA) გამოყენებით.

რენტგენოფაზური ანალიზისთვის გამოყენებულ იქნა დიფრაქტომეტრი Дрон-4.0, НПП "Буревестник", სპილენძის ანოდით და ნიკელის ფილტრით. U (ძაბვა)-35kv. I (დენის ძალა) - 20mA. გადაღების სიჩქარე - 2 გრად/წთ. λ = 1.54778 Å.

პუცოლანური აქტიურობა განისაზღვრა თერმულად დამუშავებულ ნიმუშებზე გაჯერებული ხსნარიდან კირის შთანთქმის მეთოდით გოსტი რ 56592-ის (მინერალური დანამატები ბეტონების და ხსნარებისთვის. ტექნიკური პირობები) მიხედვით.

ცემენტების ფიზიკური და მექანიკური გამოცდები ჩატარდა მცირე ნიმუშებზე (ზომით 2x2x2 სმ), რომლებიც დამზადებული იყო ნორმალური სიმკვრივის ცემენტის ცომისგან.

შედეგი. განისაზღვრა მაღალაქტიური მეტაკაოლინის სინთეზის პარამეტრები, როგორიცაა ნედლი კომპონენტების თანაფარდობა, დამუშავების ტემპერატურა, პუცოლანური აქტივობა, მექანიკური სიმტკიცე და ა.შ. ლაბორატორიულ პირობებში შემუშავებული პუცოლანური დანამატის საფუძველზე მიღებულ იქნა მაღალი ფიზიკურ-მექანიკური თვისებების მქონე ცემენტები.

დასკვნა. საქართველოს კაოლინიზირებული თიხების 600-700°C-ზე თერმული დამუშავებით შესაძლებელია ეფექტური პუცოლანური დანამატის - მეტაკაოლინის მიღება. კაოლინიზებული თიხების ნაცართან ერთად თერმული დამუშავება საშუალებას იძლევა მეტაკაოლინის სინთეზის ტემპერატურა შემცირდეს 550-590°C-მდე, გაუმჯობესდეს მეტაკაოლინის პუცოლანური თვი-სებები და გაიზარდოს ცემენტების მექანიკური სიმტკიცე..

საკვანძო სიტყვები: პუცოლანური დანამატი, კაოლინიზირებული თიხა, მეტაკაოლინი, განატაცი ნაცარი.

UDC 666.3

THERMOELECTRIC PROPERTIES OF GRAPHENE-ADDED $Bi_2Sr_2Co_{1.8}O_y$ CERAMICS

I. Kvartskhava[1], N. Margiani[1], M. Balakhashvili[2], A. Kuzanyan[3]

[1] Georgian Technical University, Institute of Cybernetics, Z. Anjaparidze str., 1st Ln., N6, Tbilisi 0186, Georgia

[2] Georgian Technical University, Institute of Bionanoceramics and Nanocomposites Technology, Kostava Str., N69, Tbilisi 0175, Georgia

[3] Institute for Physical Research of the National Academy of Sciences of Armenia, Ashtarak, Armenia, Ashtarak-2, 0204, Republic of Armenia

E-mail: iakvartskhava@gmail.com

Resume: Goal. The present paper aims to enhance the thermoelectric properties of $Bi_2Sr_2Co_{1.8}O_y$ ceramics by adding graphene (Gr).

Method. Reference (pristine) and Gr-added $Bi_2Sr_2Co_{1.8}O_y$ ceramic materials were prepared by a solid-state reaction method. The phase purity of materials was checked by powder X-ray diffraction analysis. The microstructure was observed by scanning electron microscope. Electrical and thermal transport measurements were carried out.

Results. Based on the experimental results obtained, the power factor (PF) and the figure of merit (ZT) were calculated to evaluate the thermoelectric performance of the prepared composites.

Conclusions. The incorporation of 0.85 wt% Gr into the $Bi_2Sr_2Co_{1.8}O_y$ host matrix leads to an increased density and enhanced electrical conductivity of the material. The Seebeck coefficient of the Gr-added sample shows a similar temperature dependence to that of the reference sample. The thermal conductivity rises with the introduction of Gr. The PF and ZT values of the Gr-added composite are threefold (at 973 K) and twofold (at 573 K) higher, respectively, compared to the reference $Bi_2Sr_2Co_{1.8}O_y$.

Key words: $Bi_2Sr_2Co_{1.8}O_y$ ceramics, graphene additive, microstructure, power factor, figure of merit.

1. INTRODUCTION

Thermoelectric materials have gained significant interest due to their ability to directly convert waste heat into electricity, providing a sustainable and eco-friendly energy solution to address the energy crisis and environmental challenges. The development of highly efficient thermoelectric materials is expected to promote the widespread application of thermoelectric generators for generating electrical power from waste heat discharged by various industrial systems and renewable energy sources [1]. Conventional intermetallic thermoelectric materials contain toxic and rare elements such as Te, Se, Sb, and Pb [2, 3]. Furthermore, intermetallic compounds show poor structural and chemical stability at high temperatures, leading to the evaporation and oxidation of their constituent elements [4-6].

Layered thermoelectric cobaltites, such as Na_xCoO_2, $Bi_2Sr_2Co_{1.8}O_y$, and $Ca_3Co_4O_9$ [7-10] are free from these drawbacks. However, their practical application remains challenging due to relatively low efficiency in converting heat to electricity when compared to conventional materials [11]. The thermoelectric performance is quantified by a dimensionless figure of merit (ZT) represented by the equation [12]: $ZT=\sigma S^2 T/k$, where σ, S, T, and k are electrical conductivity, Seebeck coefficient, absolute temperature, and total thermal conductivity, respectively. Therefore, the thermoelectric conversion efficiency rises with increasing ZT, implying that a high σ, large S, and low k characterize a high-performance thermoelectric material. Additionally, the electrical component of the ZT equation, known as the power factor ($PF=S^2\sigma$), is also used to evaluate the output electrical power [13-14]. The potential of cobaltites for use in thermoelectric generators can be significantly enhanced through doping and/or the introduction of appropriate additives [15-17].

Over the past decade, graphene/ceramic composites have generated significant scientific and technological interest worldwide. Graphene, with its ultrahigh electrical conductivity exceeding 10^6 S/m and its large contact area for building conductive paths, can dramatically enhance the electrical performance of composites and expand the applications of ceramic materials, including energy conversion devices [18-19]. Since 2015, several studies have been conducted to examine the impact of graphene or reduced graphene oxide (RGrO) additives on the thermoelectric properties of p-type $CuAlO_2$, n-type $SrTiO_3$ and ZnO-based materials, WO_3, TiO_2 or $BaTiO_3$ [20–26]. These studies have shown that the optimal amount of Gr/RGrO additive could lead to markedly increased electrical conductivity while effectively lowering the lattice thermal conductivity through phonon scattering. As a result, the thermoelectric conversion efficiency of the prepared materials will be improved. The effect of reduced graphene oxide on the power factor of $Na_xCo_2O_4$ layered cobaltite was reported in [27]. It was found that incorporating RGrO into the $Na_xCo_2O_4$ matrix significantly enhanced the power factor by increasing both electrical conductivity and the Seebeck coefficient.

In our previous paper, we investigated the impact of adding 0.15, 0.35, 0.70, and 1.15 wt% graphene on the power factor of $Bi_2Sr_2Co_{1.8}O_y$ [28]. The results demonstrated that incorporating graphene into this system led to a monotonic decrease in electrical resistivity for the 0.15 to 0.70 wt% % graphene additions, while the Seebeck coefficient of all synthesized samples remained largely unchanged. The addition of 0.70 wt% graphene resulted in about 40% enhancement of the PF value. However, a notable decrease in density was observed in the sample containing 1.15 wt% graphene. This decrease occurred due to the formation of a loose matrix with relatively high porosity and poor texture. As a result, this deterioration adversely affected electrical conductivity and, consequently, the power factor.

The present study aims to investigate the impact of adding 0.85 wt% Gr on the power factor and figure of merit of $Bi_2Sr_2Co_{1.8}O_y$ ceramics.

2. MAIN PART

Reference and 0.85 wt% Gr-added $Bi_2Sr_2Co_{1.8}O_y$ ceramic samples were prepared using solid-state

reaction method from reagent-grade powders of bismuth oxide (Bi_2O_3), strontium carbonate ($SrCO_3$), cobalt (II, III) oxide (Co_3O_4) and graphene nanopowder (www.graphenesupermarket. com, purity: 99.2%, average flake thickness: 12 nm (30–50 monolayers), average particle (lateral) size: ˜ 4.5 µm). The mixtures of these raw powders were homogenized in a planetary mill (Fritsch Pulverisette 7 Premium line) for 1 h at a rotating speed of 120 rpm. After homogenization, the powders were calcined at 1043–1088 K for 18 hours with intermediate grindings in an agate mortar, then pressed into pellets at a hydrostatic pressure of 220 MPa. Finally, the pellets were sintered at 1103–1108 K in air for 20 h, then cooled to room temperature in the furnace. The phase purity of the prepared materials was examined using X-ray diffraction (XRD, Dron–3M diffractometer, CuKα–

radiation) method. The resistivity of the samples as a function of temperature $\rho(T)$ in the temperature range from 293 to 973 K was measured by the standard four-probe method. The temperature dependence of the Seebeck coefficient was determined by a differential method with a Lab-made setup using a KEITHLEY DMM6500 multimeter. Electrical transport measurements were performed on bar-shaped samples with dimensions of $13 \times 7 \times 2.5$ mm^3. Thermal conductivity was measured in the temperature range between 293 and 573 K using the "Hot Disk TPS 500 thermal constants analyzer", coupled with a temperature platform for TPS. Finally, the values of PF and ZT were calculated to evaluate the thermoelectric performance of the synthesized materials.

XRD patterns of the reference and 0.85 wt% Gr-added $Bi_2Sr_2Co_{1.8}O_y$ samples are presented in Fig. 1.
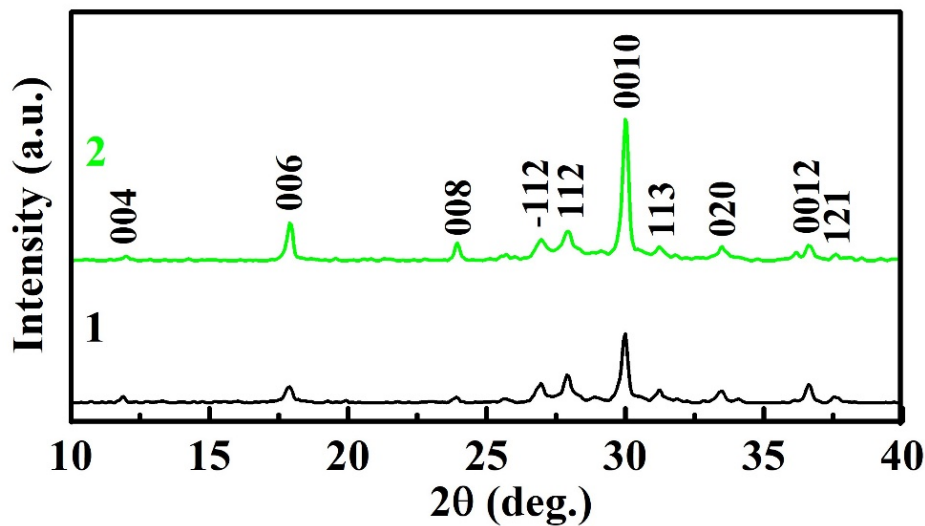
Fig. 1. X-ray diffraction patterns
of reference (1) and 0.85 wt% Gr-added (2) $Bi_2Sr_2Co_{1.8}O_y$ samples

The main peaks align closely with those reported in previous studies [29]. No diffraction peaks of graphene were observed due to its very low content. The XRD patterns indicate that graphene

particles were dispersed along the grain boundaries within the $Bi_2Sr_2Co_{1.8}O_y$ matrix, resulting in the formation of a Gr/ceramic composite.

Fig. 2 shows the surface SEM micrographs of the samples. SEM images show that the addition of Gr improves the sinterability and density of $Bi_2Sr_2Co_{1.8}O_y$ ceramics, which is favorable for lowering electrical resistivity. The apparent density of the reference sample is 4.1 g/cm³, which is 60% of the theoretical value of 6.8 g/cm³ [30]. With the incorporation of Gr, the density of the $Bi_2Sr_2Co_{1.8}O_y$/Gr composite increases to 4.4 g/cm³, representing 65% of the theoretical value.

Fig. 3 illustrates the electrical resistivity of the prepared samples. The addition of 0.85 wt% Gr results in approximately a 3-fold decrease in electrical resistivity in the temperature range of 293 K to 973 K. The lower electrical resistivity of the $Bi_2Sr_2Co_{1.8}O_y$/Gr nanocomposite can be attributed to the highly conductive graphene, which facilitates the formation of a percolation network for easier charge carrier transport across the $Bi_2Sr_2Co_{1.8}O_y$ matrix.

The temperature dependence of the Seebeck coefficient is displayed in Fig. 4. A positive S value is observed in the samples, indicating p-type conduction. The Seebeck coefficient of prepared materials increases as the temperature rises, and its value is not markedly influenced by the graphene additive.

The temperature dependence of the power factor is shown in Fig. 5. Because of the reduced resistivity, the Gr-added sample has a PF value that is more than three times higher at 973 K than that of the reference sample.

Incorporation of graphene leads to a significant increase in thermal conductivity (Fig. 6).

Fig. 7 presents the calculated figure of merit within the temperature range of 293 K to 573 K.
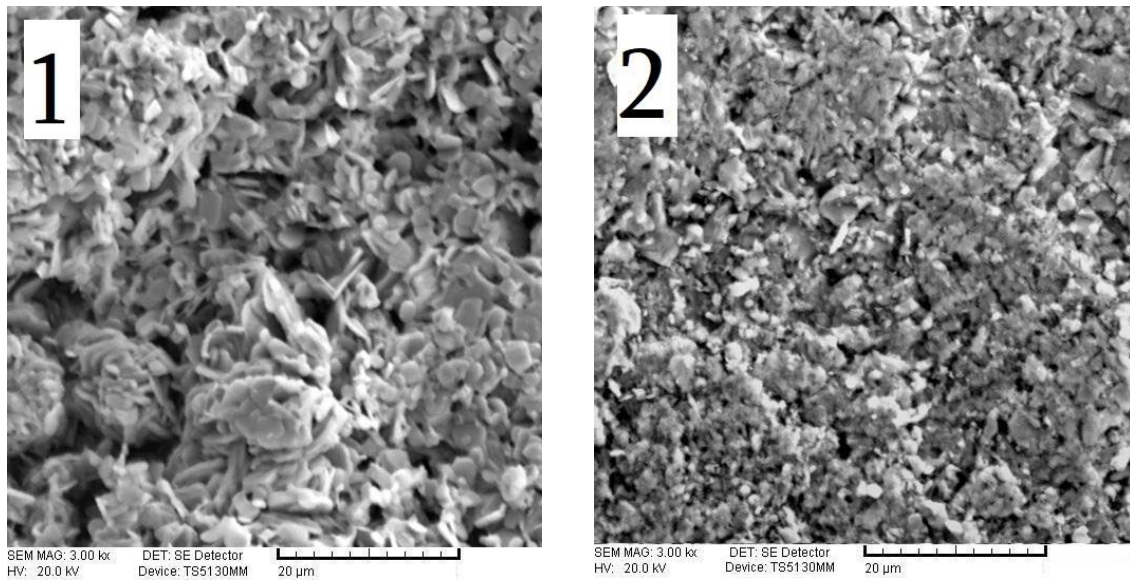
Fig. 2. Surface SEM images of reference (1)
and 0.85 wt. % Gr-added (2) $Bi_2Sr_2Co_{1.8}O_y$ samples
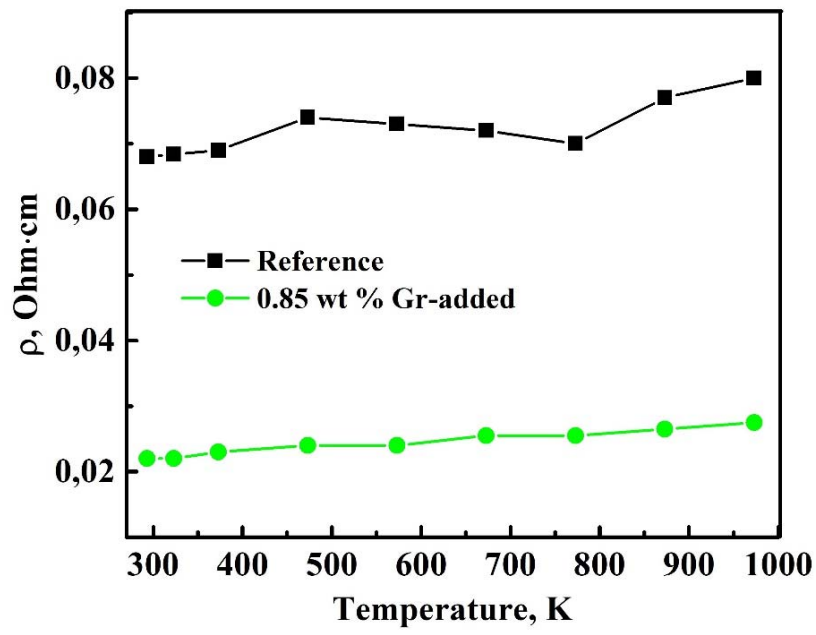
Fig. 3. Temperature dependence of electrical resistivity
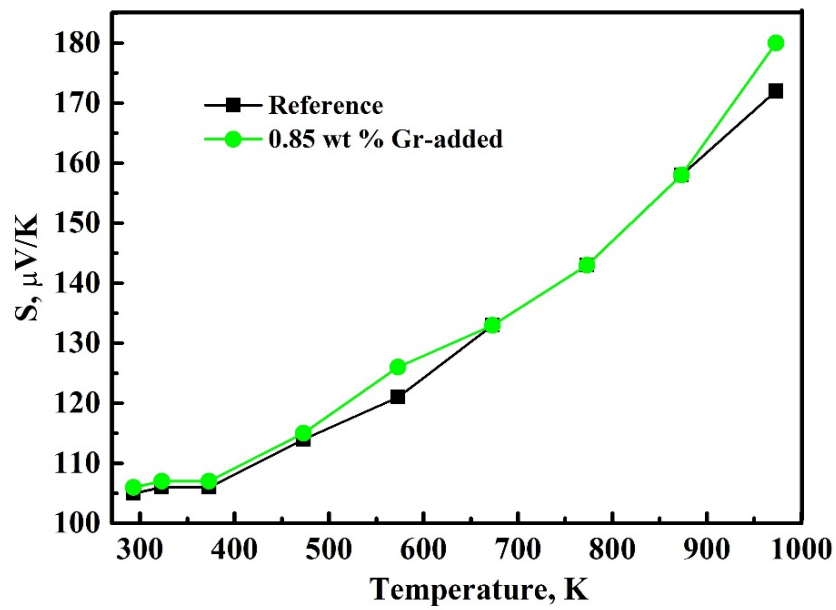
Fig. 4. Temperature dependence of Seebeck coefficient
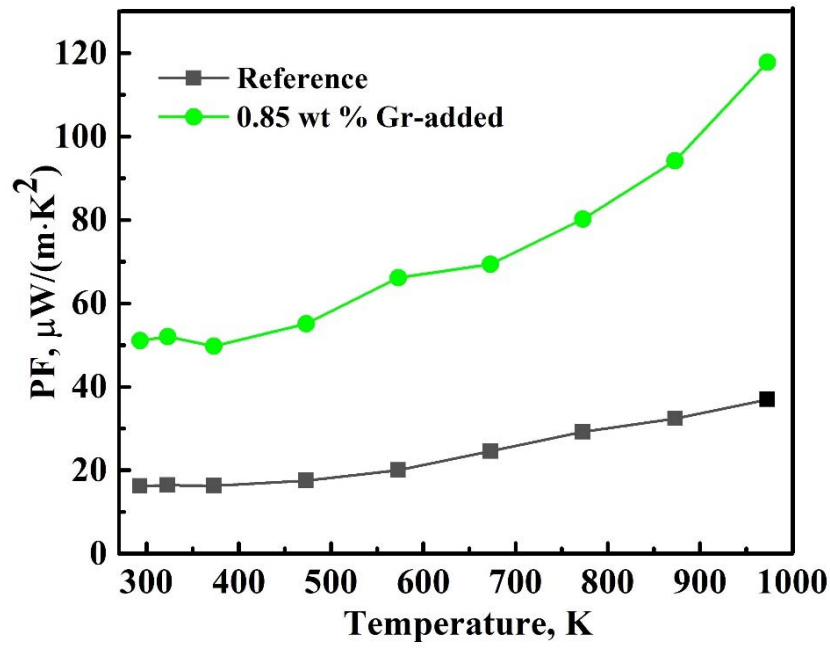
Fig. 5. Temperature dependence of power factor
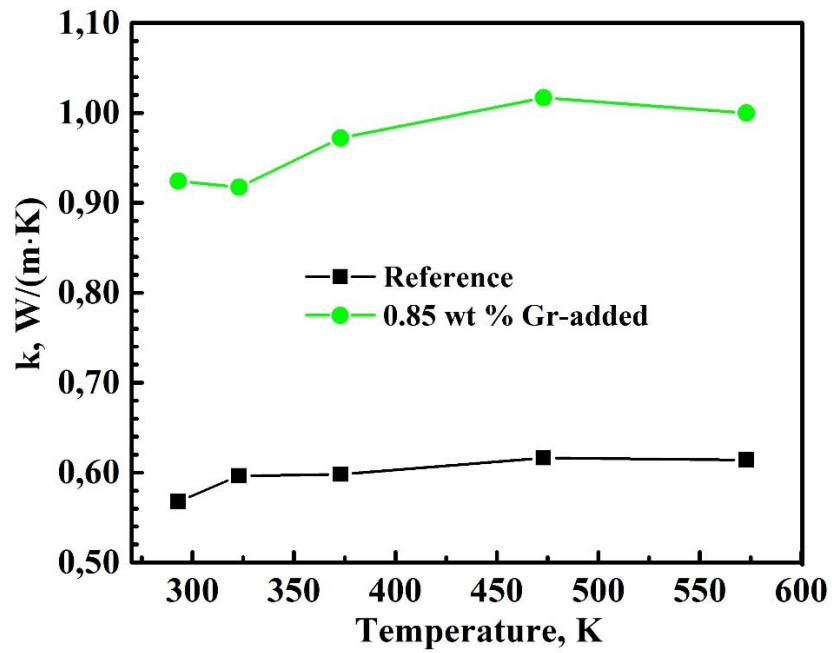
Fig. 6. Temperature dependence of thermal conductivity
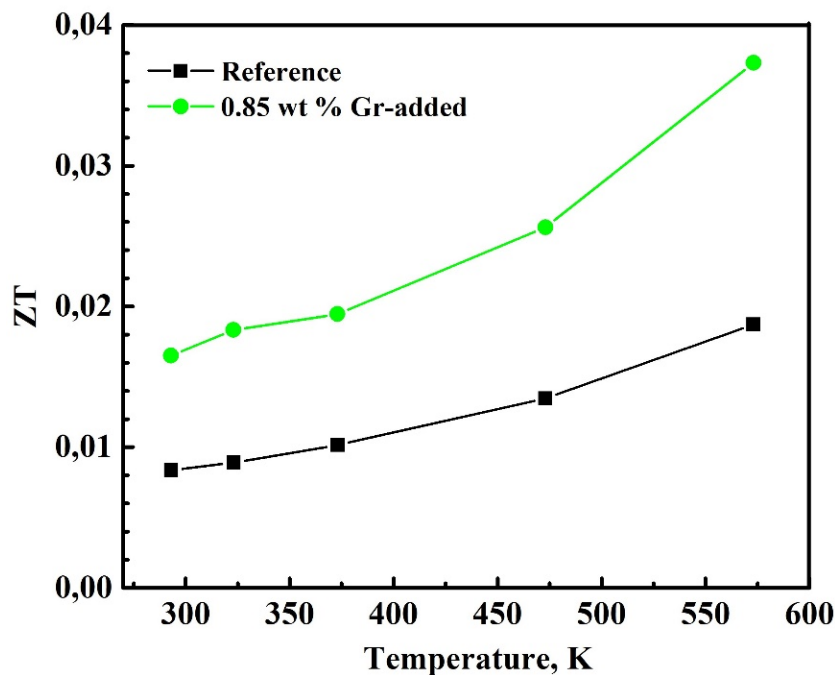
Fig. 7. Temperature dependence of the figure of merit

Incorporation of 0.85 wt% graphene results in a 2-fold rise in the ZT value at 573 K. This is because the reduction in electrical resistivity of the $Bi_2Sr_2Co_{1.8}O_y$/Gr composite dominates the increase in thermal conductivity.

3. CONCLUSION

In summary, reference and 0.85 wt% graphene-added $Bi_2Sr_2Co_{1.8}O_y$ materials have been prepared using a solid-state reaction method. The structure and microstructure of the prepared samples were examined using XRD and SEM techniques. Electrical resistivity, Seebeck coefficient, and thermal conductivity have been measured. Based on the obtained data, the power factor and figure of merit have been calculated. The obtained results show that the incorporation of the Gr additive into the $Bi_2Sr_2Co_{1.8}O_y$ host matrix leads to denser material with improved electrical conductivity. As a result, the graphene-added composite exhibits higher PF and ZT values compared to the reference $Bi_2Sr_2Co_{1.8}O_y$ material.

REFERENCES

1. J. He, Y. Liu, R. Funahashi. Oxide thermoelectrics: the challenges, progress, and outlook, Journal of Materials Research, 2011, vol. 26, pp.1762–1772.

2. K. Koumoto, R. Funahashi, E. Guilmeau, Y. Miyazaki, A. Weidenkaff, Y. Wang, C. Wan. Thermoelectric Ceramics for Energy Harvesting, Journal of the American Ceramic Society. 2013, vol. 96, Issue 1, pp. 1–23.

3. I.V. Matsukevich, A.I. Klyndyuk, E.A. Tugova, A.N. Kovalenko, A.A. Marova, N.S. Krasutskaya. Thermoelectric properties of $Ca_{3-x}Bi_xCo_4O_{9+\delta}$ (0.0 ≤ x ≤ 1.5) ceramics, Inorganic Materials, 2016, vol. 52, Issue 6, pp. 593–599.

4. H. Y. Hong, S. Gwon, D. Kim, K. Park. Influence of sintering temperature and Li^+/Mg^{2+} doping on the thermoelectric properties of $Bi_{2-2x}Li_xMg_xSr_2Co_2O_y$, Advances in Applied Ceramics, 2022, vol. 121, Issue 4, pp. 124-131.

5. S. Bresch, B. Mieller, C. Selleng, T. Stöcker, R. Moos, T. Rabe. Influence of the calcination procedure on the thermoelectric properties of calcium cobaltite $Ca_3Co_4O_9$, J. Electroceram., 2018, vol. 40, pp. 225–234.

6. E. Combe, R. Funahashi, F. Azough, R. Freer. Relationship between microstructure and thermoelectric properties of $Bi_2Sr_2Co_2O_x$ bulk material, Journal of Materials Research, 2014, vol. 29, pp. 1376–1382.

7. Y. Terasaki, Y. Sasago, K. Uchinokura. Large thermoelectric power in $NaCo_2O_4$ single crystals, Phys. Rev. B, 1997, vol. 56, Issue 20, pp. R12685–7.

8. R. Funahashi, I. Matsubara, H. Ikuta, T. Takeuchi, U. Mizutani, S. Sodeoka. An oxide single crystal with high thermoelectric performance in air, Jpn. J. Appl. Phys., 2000, Issue 39, pp. L1127–1129.

9. C. Masset, C. Michel, A. Maignan, M. Hervieu, O. Toulemonde, F.Studer, B. Raveau, J. Hejtmanek. Misfit-layered cobaltite with an anisotropic giant magnetoresistance: $Ca_3Co_4O_9$, Phys. Rev. B, 2000, vol. 62, pp. 166–175.

10. R. Funahashi, I. Matsubara, S. Sodeoka. Thermoelectric Properties of $Bi_2Sr_2Co_{1.8}O_y$ Polycrystalline Materials, Appl. Phys. Lett., 2000, Issue 76, pp. 2385–2387.

11. K. Fujimoto, M. Gibu, Y.Yamaguchi, A. Aimi, K. Nishio, O. Rabin, I. Takeuchi. Thermoelectric properties of bismuth-substituted calcium manganite $Ca_{1-x}Bi_xMnO_{3-\delta}$ prepared via the electrostatic spray deposition method, J. Ceram. Soc. Japan. 2017, vol. 125, Issue 4, pp. 308–312.

12. M.A. Zoui, S. Bentouba, J.G. Stocholm, M. Bourouis. A review on thermoelectric generators: progress and applications, Energies, 2020, vol. 13, Issue 14, article #3606.

13. Y.C. Zhou, C.L. Wang, W.B. Su, J. Liu, H.C. Wang, J.C. Li, Y. Li, J.Z. Zhai, Y.C. Zhang, L.M. Mei. Electrical properties of Dy^{3+}/Na^+ co-doped oxide thermoelectric $[Ca_{1-x}(Na_{1/2}Dy_{1/2})_x]MnO3$ ceramics, Journal of Alloys and Compounds, 2016, vol. 680, pp. 129-132.

14. W. Liu, H.S. Kim, Q. Jie, Z. Ren. Importance of high power factor in thermoelectric materials for power generation application: A perspective, Scripta Materialia, 2016, vol. 111, pp. 3-9.

15. U. Hira, N. Pryds, F. Sher. Thermoelectric properties of dual doped $Bi_2Sr_2Co_2O_y$-based ceramics. J. Electron. Mater. 2019, vol. 48, pp. 4618–4626.

16. X. Liu, M. Fan, X. Zhu, Z. Tian, X.J. Li, H. Song. Optimising the thermoelectric properties of $Bi_2Sr_2Co_2O_y$ using Ag substitution and NanoSiC doping, Ceramics International, 2021, vol. 47, Issue 21, pp. 30657-30664.

17. N.S. Krasutskaya, A.I. Klyndyuk, L.E. Evseeva, N.N. Gundilovich, E.A. Chizhova, A.V. Paspelau. Enhanced thermoelectric performance of $Na_{0.55}CoO_2$ ceramics doped by transition and heavy metal oxides, Solids, 2024, vol. 5, Issue 2, pp. 267-277.

18. Y. Huang, C. Wan. Controllable fabrication and multifunctional applications of graphene / ceramic composites, J. Adv. Ceram., 2020. vol. 9, pp. 271–291.

19. H. Porwal, S. Grasso, M.J. Reece. Review of graphene–ceramic matrix composites, Advances in Applied Ceramics, 2013, vol. 112, pp. 443-454.

20. O. Okhay, A. Tkach. Impact of graphene or reduced graphene oxide on performance of thermoelectric composites, C - Journal of Carbon Research, 2021, vol.7, article no. 37.

21. N. Daichakomphu, R. Sakdanuphab, A. Harnwunggmoung, S. Pinitsoontorn, A. Sakulkalavek. Achieving thermoelectric improvement through the addition of a small amount of graphene to $CuAlO_2$ synthesized by solid-state reaction, Journal of Alloys and Compounds, 2018, vol. 753, pp. 630-635.

22. X. Feng, Y. Fan, N. Nomura, K. Kikuchi, L. Lianjun Wang, W. Jiang, A. Kawasaki. Graphene promoted oxygen vacancies in perovskite for enhanced thermoelectric properties, Carbon, 2017, vol. 112, pp. 169–176.

23. Y. Lin, C. Norman, D. Srivastava, F. Azough, L. Wang, M. Robbins, K. Simpson, R. Freer, I. Kinloch. Thermoelectric power generation from lanthanum strontium titanium oxide at room temperature through the addition of graphene, ACS Appl. Mater. Interfaces, 2015, vol. 7, Issue 29, pp. 15898–15908.

24. C. Mallada, J.L. Menéndez, O.J. Dura, M.A. López de la Torre, R. Menéndez, R. Santamaría. Spark plasma sintered $BaTiO_3$/ graphene composites for thermoelectric applications, Journal of the European Ceramic Society, 2017, vol. 37, Issue 12, pp. 3741–3746.

25. D. Chen, Y. Zhao, Y. Chen, B. Wang, H. Chen, J. Zhou, Z. Liang. One-Step chemical synthesis of ZnO/Graphene oxide molecular hybrids for high-temperature thermoelectric applications, ACS Appl. Mater. Interfaces, 2015, vol. 7, Issue 5, pp. 3224–3230.

26. A.M. Gautam, M. Faraz, N. Khare. Enhanced thermoelectric properties of tungsten oxide-reduced graphene oxide nanocomposites, Ceramics International, 2021, vol. 47, Issue 19, pp. 27885-27889.

27. N. Ronariddh. Effect of reduced graphene oxide on the enhancement of thermoelectric power factor of γ-$Na_xCo_2O_4$, Materials Science and Engineering: B, 2020, vol. 261, article no.114679.

28. N. Margiani, V. Zhghamadze, G. Mumladze, I. Kvartskhava, Z. Adamia, A. Klyndyuk, A. Kuzanyan. Impact of Graphene addition on the microstructure and thermoelectric properties of $Bi_2Sr_2Co_{1.8}O_y$ ceramics, Bulletin of the Georgian National Academy of Sciences, 2022, vol. 16, Issue 1, pp. 17-24.

29. T. Itoh, I. Terasaki. Thermoelectric properties of $Bi_{2.3-x}Pb_xSr_{2.6}Co_2O_y$ single crystals. Jpn. J. Appl. Phys. 2000, vol. 39, Issue 12 R, pp. 6658-6660.

30. K. Rubešová, T. Hlásek, V. Jakeš, Š. Huber, J. Hejtmánek, D. Sedmidubský. Effect of a powder compaction process on the thermoelectric properties of $Bi_2Sr_2Co_{1.8}O_y$ ceramics, J. Eur. Ceram. Soc., 2015, vol. 35, Issue 2, pp. 525-531.

გრაფენის დანამატიანი $Bi_2Sr_2Co_{1.8}O_y$ კერამიკის თერმოელექტრული თვისებები

ი. ქვარცხავა[1], ნ. მარგიანი[1], მ. ბალახაშვილი[2], ა. კუზანიანი[3]

[1] საქართველოს ტექნიკური უნივერსიტეტი, კიბერნეტიკის ინსტიტუტი, ზ. ანჯაფარიძის ქ., 1 შესახვ., N6, თბილისი 0186, საქართველო

[2] საქართველოს ტექნიკური უნივერსიტეტი, ბიონანოკერამიკისა და ნანოკომპოზიტების ტექნოლოგიის ინსტიტუტი. კოსტავას 69, თბილისი 0175, საქართველო

[3] სომხეთის მეცნიერებათა ეროვნული აკადემიის ფიზიკურ კვლევათა ინსტიტუტი, აშტარაკი–2, 0204, სომხეთი

E-MAIL: iakvartskhava@gmail.com

რეზიუმე: მიზანი. წარმოდგენილი ნაშრომი მიზნად ისახავს $Bi_2Sr_2Co_{1.8}O_y$ კერამიკის თერმოელექტრული თვისებების გაუმჯობესებას გრაფენის (Gr) დანამატით.

მეთოდი. მყარფაზური რეაქციის მეთოდით სინთეზირებულ იქნა საწყდენი (უდანამატო) და გრაფენის დანამატიანი $Bi_2Sr_2Co_{1.8}O_y$ კერამიკული მასალები. მასალათა ფაზური სისუფთავე დადგინდა რენტგენოდიფრაქციული ანალიზით. მიკროსტრუქ-ტურის დამზერა განხორციელდა მასკანირებელი ელექტრონული მიკროსკოპით. ჩა-ტარდა ელექტრული და თერმული ტრანსპორტული გაზომვები.

შედეგები. სინთეზირებული კომპოზიტების თერმოელექტრული ეფექტურობის შესაფასებლად, მიღებული ექსპერიმენტული შედეგების საფუძველზე გამოთვლილ იქნა სიმძლავრის ფაქტორი (PF) და ვარგისობის მაჩვენებელი (ZT).

დასკვნები. $Bi_2Sr_2Co_{1.8}O_y$ საწყდენ მასალაში 0.85 წონითი % გრაფენის დანამატის შეტანა განაპირობებს მასალის სიმკვრივის ზრდასა და ელექტროგამტარობის გაუმ-ჯობესებას. Gr-ის დანამატიანი ნიმუშის ზეებეკის კოეფიციენტი ავლენს საწყდენი ნიმუშის მსგავს ტემპერატურულ დამოკიდებულებას. გრაფენის დანამატი ამაღლებს თბოგამტარობას. გრაფენის შემცველი კომპოზიტის სიმძლავრის ფაქტორისა და ვარგისობის მაჩვენებლის მნიშვნელობები, შესაბამისად, 3–ჯერ (973 K–ზე) და 2-ჯერ (573 K–ზე) იზრდება საწყდენ $Bi_2Sr_2Co_{1.8}O_y$–თან შედარებით.

საკვანძო სიტყვები: $Bi_2Sr_2Co_{1.8}O_y$ კერამიკა, გრაფენის დანამატი, მიკროსტრუქტურა, სიმძლავრის ფაქტორი, ვარგისობის მაჩვენებელი.

UDC 691.5.01

DETERMINATION OF THE POSSIBILITY OF LIGHTWEIGHT EXPANDED CLAY AGGREGATE (LECA)   FROM GEORGIAN MINERAL SILICATE RAW MATERIALS

T. Cheishvili, R. Skhvitaridze, N. Mukhatgverdeli, G. Loladze, A. Skhvitaridze, M. Zakaraia

Georgian Technical University, Faculty of Chemical Technology and Metallurgy, 69 Kostava St., Tbilisi 0175, Georgia

E-mail: t.cheishvili@gtu.ge

Resume: Objective: Study of mineral silicate raw materials of Georgia with the aim of determining the possibility of obtaining from it Lightweight Expanded Clay Aggregate (LECA) by heat treatment.

Method: Evaluation of transformations of six types of mineral raw materials during high-temperature heat treatment (900 – 1250^{0}C) and identification of rocks prone to intumescent/ transition to a porous substance. Study of the required standard properties of the obtained porous materials and their classification.

Result: The ability of clay slate and obsidian to expand over a wide temperature range was determined, and their properties were studied and classified.

Conclusion: two types of raw materials materials– clay slate and obsidian (in the form of mono charge) out of the six units selected for study – exhibit a high degree of foaming after heat treatment at 1100-1250^{0}C and, according to the studied characteristics/properties required by the standards, are classified as LECA expanded clay and foam glass materials.

1. INTRODUCTION

It is known that various types, but especially artificial, (LECA – lightweit expanded clay aggreqete) are widely used in technology and many industries. The traditional technology of their production is based on the thermal treatment of clay rocks of various nature or man-made raw materials and their expansion. The porous materials obtained by this method are characterized by a closed-pore structure, lightness, environmental friendliness, heat and sound insulation properties, as well as other, often unique, physical and chemical characteristics [1] [2] [3].

The most commonly used products made from lightweight porous inorganic materials are of two types: the so-called "expanded clay" and foam glass. Their identity is determined by the method of production – high-temperature, but different foaming process regime, high porosity of structures and low bulk/specific density, while the main areas of their application differ significantly. In particular, expanded clay is known as a granular filler for lightweight concrete or an invariable

component of thermal insulation, water- and frost-resistant coatings, when expanded clay is used to make thermal insulation products of various shapes and purposes [4] [5] [6].

It is worth noting that the types of operating parameters and a number of physical and chemical characteristics regulated by the relevant standards for both highly efficient energy-saving porous inorganic materials are different depending on the various areas of their application [7] [8].

It should be noted that both known types of LECA (expanded clay and foam glass) are obtained using different raw materials. To obtain expanded clay (oval-shaped granules), natural rocks are used – easily soluble clays, shales and other types of clay minerals, the type and composition of which are regulated by standards [9] and are generally characterized in a number of works [10] 11]. The technological process of obtaining expanded clay from clay rocks requires processing raw materials at a temperature of $1100-1250^0C$, and for by intumescent firing it is recommended to use frit of approximately the same size as crushed stone, or artificially obtained granules (5-10; 10-15; 15-20 mm). When the raw material is difficult to intumescent (due to its composition), they resort to creating mixtures of "main raw material – fermentive". Man-made (mainly organic) materials are often used as fermentive agent – waste oils, coal dust, etc., which increases the environmental risk – the level of environmental pollution with carbon dioxide [12][13].

Modern technology for the production of foam glass and foam glass products is based on the use of two types of raw materials in the technological process: secondary (collected) glass products

(bottles, jars, window and other types of glass) and granules/frits made from specially welded glass. The inclusion of both types of raw materials in the glass manufacturing process requires multi-stage preparation: in the case of using smashed glass – collection, sorting by assortment, washing, crushing, fine grinding in a special mill, and in the case of using fritted granules – preparation of a multi-component mixture, its heating at a temperature of $1450-1500^0C$. Granulation (fritting) on water, combined pure grinding of frit and filler. Finally, heating pure fractional mixtures obtained by both methods at $850-1000^0C$, a foam glass product is obtained [14] [15].

The technology of foam glass production from the above-mentioned raw material base is characterized by high energy and material intensity. Ensuring the competitiveness of glass as a unique energy-saving material necessitates the search for a new non-traditional raw material base. In this direction, research is being conducted in many countries around the world to identify and study natural rocks and man-made waste suitable for foam glass production [16] [17].

Therefore, our research was aimed at expanding the acceptable raw material base of two porous materials presented in the expanded clay nomenclature - expanded clay and foam glass, by reducing material consumption and simplifying the technological process of their production.

2. MAIN PART

In order to expand the acceptable resource base of two types of multifunctional (expanded clay: foam glass) LECA – lightweit expanded clay aggreqete and to comprehensively address envi-

ronmental and technological issues within the framework of research related to their implementation, an alternative resource base was selected: mineral-bearing rocks available on the territory of Georgia. In particular, silicate rocks were selected for the study: zeolite, obsidian, clay slate, argillite, volcanic ash and trachyte (the main raw material). As a result of studying and analyzing their chemical composition, it was established that these materials are promising for use in the technological process of obtaining LECA [18].

At the current stage of the work, an experimental study was conducted, the purpose of which was to study the behavior of six main types of selected raw materials during their high-temperature processing. The heat treatment interval was defined as $1000–1250^0C$, and the holding time at the selected temperatures was 20–25 min, the results of heat treatment of the studied raw materials are presented in the form of photographs in Figure 1.
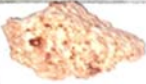
Fig. 1. Photographs demonstrating the results of heat treatment
of the studied raw materials

Based on the results obtained for all six materials, the following general conclusion can be drawn:

– **Trachyte and volcanic ash** are less prone to swelling. However, an increase in temperature causes: a change in the color of trachyte fragments, and at 1250^0C their slight porosity is observed, while volcanic ash is calcined only at 1200 and 1250^0C;

– **Argolite** remains practically unchanged up to 1200^0C, and at 1250^0C it melts completely, forming a black glassy mass;

- The transformation of **zeolite** is manifested in a gradual change of color: 1000^0C – pink; 1200^0C – milky. Melting of its grains, with the formation of a heterogeneous melt (a combination of black and milky parts), occurs at 1250^0C;
- In the case of **clay slate**, swelling of raw material fragments was clearly observed in the temperature range of $1100 – 1200^0$C; at 1250^0C, melting and "shrinkage" of the swelling material already occurs;
- Thermal treatment of **obsidian** fragments at a temperature of 1100^0C already causes their swelling. A further increase in temperature ($1100-1250^0$C) proportionally increases the degree of their swelling.

The swelling coefficient (K_α) was determined for materials processed at temperatures corresponding to maximum swelling, which was calculated using the formula $K_\alpha = \gamma/\gamma'$ (kg/m3), where γ and γ' respectively, are the bulk densities of the initial raw materials (shale and obsidian) with a fraction of 10-15 mm and materials obtained by swelling (temperatures corresponding to the maximum). It has been experimentally established that K_α the value for obsidian is 4.1, and for slate - 3.9. That is, obsidian is characterized by a greater tendency to swelling than slate.

Table 1

Characteristics/properties of LECA type materials obtained from obsidian and slate and the characteristics required by the relevant standards

| N | Main characteristics required by GOST | Design. And unit | Meaning of properties | | | |
| | | | Foam glass | | Expanded clay | |
			GOST 33949 -2016 req.	Foam glass from obsidian-	GOST 32496-2013 req.	Expanded clay from foam glass
1	Specific gravity[2]	D kg/m³	$8 \le d \le 200$	190	X[3]	-
2	Bulk density [1]	γ' kg/m³	X[3]	-	$100 \le \gamma' \le 1200$	650
3	Compression strength	P(MPa)	$0,3 \le P \le 2,0$[2]	0,81	$0,5 \le P \le 10$[1]	4,8
4	Water absorption [1]	W(%)	X[3]	-	$W \le 20$	16
5	Sorption capacity [1]	S (%)	$S \le 0,7$	0,42	X[3]	-
6	Water resistance (softening coefficient) [1]	ξ	X[3]	-	$\xi \le 1,8$	0,76
7	Thermal conductivity coefficient [2]	λ_{25^0C} (W/m· K)	$\lambda \le 0,065$	0,055	$\lambda \le 1,8$	1,45

[1]   For granular materials with the particle size distribution required by the standard

[2]   For geometric figured patterns

[3]   This type of material is not required by the standard.

Based on the experimental results, it was confirmed that of the six types of raw materials studied, two types clearly showed a tendency to swell (transform into a porous material): the temperature range for clay swells is 1100-1200^{0}C (maximum 1200^{0}C), and for obsidian - 1100-1250^{0}C (maximum 1250^{0}C). The difference between them, which is noticeable visually, is in color and texture. Expanded slate is a brownish-brown layered material, while expanded obsidian is a milky-gray, completely glassy, homogeneous material. The first of them is similar to expanded clay, the second to foam glass. This assumption was confirmed by establishing the required characteristics in the relevant standards (GOST 32496-2013 for expanded clay and GOST 33949-2016 for foam glass) [7] [8].

For porous materials obtained from obsidian and slate, the values of a number of characteristic properties required by the relevant standards were determined. The results of the study are presented in Table 1.

The seven quality characteristics specified in the table for colored grains and defined by the standards for porous materials, four must correspond to foam glass and five to obsidian. Since the product obtained from obsidian and slate has characteristics that are within the limits set by the relevant standards. It became possible to combine porous materials obtained from shale with expanded clay, and porous materials obtained from obsidian with materials such as foam glass.

3. CONCLUSION

For six silicate raw materials of different types and compositions, their transformation into porous materials during heat treatment at a temperature of 900-1250^{0}C was determined. In this temperature range, two types of raw materials - slate and obsidian - clearly demonstrate the ability to transform into highly porous materials: slate at 1200^{0}C, and obsidian at 1250^{0}C, with an increase in volume of approximately four times. A comprehensive comparative analysis of the properties of two main types of artificially obtained porous materials (expanded clay and foam glass), required by the standard and obtained from the raw materials taken for research, showed that by high-temperature firing of clay shale and obsidian, it is possible to obtain two different types and grades of porous expanded clay materials – expanded clay grade M700 from clay slate and expanded clay grade D200 from foam glass.

REFERENCES

1. Kudryavtsev P. (2020). The main ways of creating porous composite materials. Nanotechnology in Construction. 12(5), 256-269 (in Russian);

2. Lin X.(2021) Porous Inorganic Materials. ACS publications
https://porous.acs.orga>dei>aesbiomaterials.1c00733;

3. Wang X.(2011) Porous Inorganic Materials. Wiley Online Library
https://onlinelibrary.willey com.

4. LECA Lightweght Agregatic (LWA) rusulad unda aq LECA-LWAC.
   https:www.leca.co.uk>products;

5. LECA Technical Manual, Expanded Clay https://www.keramzit.by/articls; (in Russian)

6. Aaboe R. Fiam glass=an alternative lightweight and insulatin.
   https:www.vegvesen no>an>foku somrader;

7. GOST 32496-13 (2014) Porous fillers for lightweight concrete. Technical conditions. M. Standartinform. (in Russian);

8. GOST 33949-2016 (EN 13167-2012, NEQ) Cellural glass thermal insulating product for buceding and counstracions (in Russian);

9. GOST 32026-2012 (2014). Clay raw materials for the production of expanded clay gravel, crushed stone and sand. Technical conditions. M. GosExpert.ru (in Russian)

10. Augustnik A. (1975) Ceramics. 2nd edition; Leningrad; (in Russian)

11. Cheishvili T., Skvitaridze A (2019) Thermal Moifying and Pprofical Application of Argieous Raus Materials, journal of the Georgian Ceramic Association. V.21,1(41);

12. Goryainov K., Goryainova S. (1982). Technology of thermal insulation materials and products: textbook - M. Stroyizdat (in Russian),
    https://library.tou.edu.kz>fulltext>buuk

13. Guraspeishvili A., Mshvildadze N., Cheishvili T. (2023). Clayey Rocks Expansion Process Confral Using Technoqenic Additives. Chemistry-achievements and prospeets . Gtu. 1SB 978-9941-28-970-5.
    https://www.gtu.ge;

14. Demidovich K. (1975) Framglass nayka u Tchnical. Minsk (in Russian);

15. Preparation and characteristics of glass foam (2019). Aalborg Universitets forsrningspartal.
    https://w.b.n.aan.dk>fiees>PMD_Martin_Bondere;

16. Malkonyan R., Suvorova D., Manakova N. (2018) Vitreus Foamed Materials. Chalenpes of Production and Solutions. Doi:10. 25702| ksc.2307-5228-2018-10-1-133-156 (in Russian);

17. Manakova N, Seneta A. (2020). USE OF TECHNOGENIC RAW MATERIALS IN PRODUCING POROUS MATERIAL; DOI: 10.37614/2307-5252.2020.3.4.023 (in Russian)

18. Cheishvili T., Skvitaridze R., Loladze G., Zakaraia M, Mukhatgverdeli N., kvitardze A., Guraspashvili A. (2024). Sselection of Local Silicate Ray Materials nd Evolution of Technological Feasibility to Expaned of Ray Base for Obtaining Leca.Georgian Engineering News.V,2. Doi:https:/doi.org/10.36073/15312-028.

საქართველოს მინერალური სილიკატური ნედლეულიდან მსუბუქი ფორიანი მასალების (LECA) მიღების შესაძლებლობის დადგენა

თ. ჭეიშვილი, რ. სხვიტარიძე, ნ. მუხათგვერდელი, გ. ლოლაძე, ა. სხვიტარიძე, მ. ზაქარაია

საქართველოს ტექნიკური უნივერსიტეტი, ქიმიური ტექნოლოგიისა და მეტალურგიის ფაკულ-ტეტი, კოსტავას ქ. 69, თბილისი 0175, საქართველო

E-MAIL: t.cheishvili@gtu.ge

რეზიუმე: მიზანი: საქართველოს მინერალური სილიკატური ნედლეულის შესწავლა, მათგან მსუბუქი ფორიანი არაორგანული მასალის (LECA) თერმული დამუშავებით მიღების შესაძ-ლებლობის დადგენის მიზნით. **მეთოდი:** მაღალტემპერატურული თერმული დამუშავების (900–1250⁰C) ექვსი სახის მინერალური ნედლეულის გარდაქმნათა შეფასება და აფუე-ბისადმი/ფორიან მასალაში გადასვლისადმი მიდრეკილი ქანების გამოვლენა. მიღებული ფორიანი მასალების სტანდარტით მოთხოვნადი თვისებათა შესწავლა და მათი კლასი-ფიცირება. **შედეგი:** დადგინდა თიხაფიქლის და ობსიდიანის აფუების უნარი ფართო ტემ-პერატურულ ინტერვალში, ხოლო თვისებების შეფასებით მოხდა მათი კლასიფიცირება. **დასკვნა:** ექვსი ერთეული საკვლევად აღებული ნედლეიდან ორი სახეობა-თიხაფიქალი და ობსიდიანი (მონოკაზმების სახით) ავლენენ, მათი თერმული დამუშავებით 1100-1250⁰C, აფუების მაღალ ხარისხს და შესწავლილი მახასიათებელი/სტანდარტებით მოთხოვნადი თვისებების საფუძველზე მიეკუთვნებიან LECA-ს კერამზიტის და ქაფმინის ტიპის მასალებს..

საკვანძო სიტყვები: მინერალური ნედლეული, თერმული დამუშავება, ფორიანი მასალა, მახასიათებელი თვისებები, სტანდარტებით კლასიფიკაცია.

THE GEORGIAN CERAMISTS ASSOCIATION JOINED
THE INTERATIONAL CERAMIC FEDERATION SINCE 2008

THE GEORGIAN CERAMISTS ASSOCIATION HAS BEEN A MEMBER
OF THE EUROPEAN CERAMIC SOCIETY SINCE 2002

THE GEORGIAN CERAMIC ASSOCIATION WAS FOUNDED IN 1998
THE MAGAZINE WAS FOUNDED IN 1998